NAVAL POSTGRADUATE SCHOOL

MONTEREY, CALIFORNIA

THESIS

EVALUATION OF WIDEBAND LEAKAGE CANCELLATION CIRCUIT FOR IMPROVED TRANSMIT-RECEIVE ISOLATION

by

Pek, Wee Kok

December 2011

Thesis Advisor:	David C. Jenn
Second Reader:	Ric Romero

Approved for public release; distribution is unlimited

THIS PAGE INTENTIONALLY LEFT BLANK

REPORT DOCUMENTATION PAGE			Form Approved OMB No. 0704-0188
Public reporting burden for this collection of information is estimated to average 1 hour per response, including the time for reviewing instruction, searching existing data sources, gathering and maintaining the data needed, and completing and reviewing the collection of information. Send comments regarding this burden estimate or any other aspect of this collection of information, including suggestions for reducing this burden, to Washington headquarters Services, Directorate for Information Operations and Reports, 1215 Jefferson Davis Highway, Suite 1204, Arlington, VA 22202-4302, and to the Office of Management and Budget, Paperwork Reduction Project (0704-0188) Washington DC 20503.			
1. AGENCY USE ONLY *(Leave blank)*	**2. REPORT DATE** December 2011	**3. REPORT TYPE AND DATES COVERED** Master's Thesis	
4. TITLE AND SUBTITLE Evaluation of Wideband Leakage Cancellation Circuit for Improved Transmit-Receive Isolation		**5. FUNDING NUMBERS**	
6. AUTHOR(S) Pek, Wee Kok			
7. PERFORMING ORGANIZATION NAME(S) AND ADDRESS(ES) Naval Postgraduate School Monterey, CA 93943-5000		**8. PERFORMING ORGANIZATION REPORT NUMBER**	
9. SPONSORING /MONITORING AGENCY NAME(S) AND ADDRESS(ES) N/A		**10. SPONSORING/MONITORING AGENCY REPORT NUMBER**	
11. SUPPLEMENTARY NOTES The views expressed in this thesis are those of the author and do not reflect the official policy or position of the Department of Defense or the U.S. Government. IRB Protocol number _____N/A_____.			
12a. DISTRIBUTION / AVAILABILITY STATEMENT Approved for public release; distribution is unlimited		**12b. DISTRIBUTION CODE** A	

13. ABSTRACT (maximum 200 words)

The objective of this thesis is to improve the cancellation performance of a wideband leakage cancellation circuit (WLCC). The results of this thesis can be applied to any sensor or communication system that simultaneously transmits and receives, for example, continuous wave (CW) radar, frequency modulated continuous wave (FMCW) radar, or a wirelessly networked distributed digital phased array (WNDDPA), where the isolation is required between the transmit and receive paths.

The approach is to investigate leakage cancellation circuit (LCC) techniques in the analog domain. A frequency demultiplexing and multiplexing circuit (FDMC) is adopted for the analog study and is simulated using Advanced Design System 2011.05 (ADS). Both narrowband and wideband LCC models are simulated in ADS to investigate their phase and amplitude balance properties. Methods such as applying grounded stubs to match the phase slopes of the cancellation and leakage paths are also investigated.

Two sets of grounded shunt stubs with different characteristics are applied on the leakage and cancellation paths to achieve near coherent cancellation. Using this configuration, the maximum cancellation power of the LCC is about 87 dB, and the 3.0 dB bandwidth of the cancellation is about 56 MHz.

14. SUBJECT TERMS Transmit Receive Isolation, wideband, leakage cancellation			**15. NUMBER OF PAGES** 101
			16. PRICE CODE
17. SECURITY CLASSIFICATION OF REPORT Unclassified	**18. SECURITY CLASSIFICATION OF THIS PAGE** Unclassified	**19. SECURITY CLASSIFICATION OF ABSTRACT** Unclassified	**20. LIMITATION OF ABSTRACT** UU

NSN 7540-01-280-5500

Standard Form 298 (Rev. 2-89)
Prescribed by ANSI Std. 239-18

THIS PAGE INTENTIONALLY LEFT BLANK

Approved for public release; distribution is unlimited

EVALUATION OF WIDEBAND LEAKAGE CANCELLATION CIRCUIT FOR IMPROVED TRANSMIT-RECEIVE ISOLATION

Pek, Wee Kok
Civilian, Singapore Technologies Dynamics Pte Ltd
B.Eng, National University of Singapore, 1998

Submitted in partial fulfillment of the
requirements for the degree of

MASTER OF SCIENCE IN ELECTRICAL ENGINEERING

from the

NAVAL POSTGRADUATE SCHOOL
December 2011

Author: Pek, Wee Kok

Approved by: David C. Jenn
Thesis Advisor

Ric Romero
Second Reader

R. Clark Robertson
Chair, Department of Electrical and Computer Engineering

THIS PAGE INTENTIONALLY LEFT BLANK

ABSTRACT

The objective of this thesis is to improve the cancellation performance of a wideband leakage cancellation circuit (WLCC). The results of this thesis can be applied to any sensor or communication system that simultaneously transmits and receives, for example, continuous wave (CW) radar, a frequency modulated continuous wave (FMCW) radar, or a wirelessly networked distributed digital phased array (WNDDPA), where isolation is required between the transmit and receive paths.

The approach is to investigate leakage cancellation circuit (LCC) techniques in the analog domain. A frequency demultiplexing and multiplexing circuit (FDMC) is adopted for the analog study and is simulated using Advanced Design System 2011.05 (ADS). Both narrowband and wideband LCC models are simulated in ADS to investigate their phase and amplitude balance properties. Methods such as applying grounded stubs to match the phase slopes of the cancellation and leakage paths are also investigated.

Two sets of grounded shunt stubs with different characteristics are applied on the leakage and cancellation paths to achieve near coherent cancellation. Using this configuration, the maximum cancellation power of the LCC is about 87 dB, and the 3.0 dB bandwidth of the cancellation is about 56 MHz.

THIS PAGE INTENTIONALLY LEFT BLANK

TABLE OF CONTENTS

I. INTRODUCTION....1
A. BACKGROUND....1
1. Leakage Problem in CW and FMCW Radars....2
2. Isolation of Transmit and Receive Signals....2
3. Amplitude and Phase Imbalance in LCC....4
4. Wideband Leakage Cancellation Circuit....7
B OBJECTIVE....8
C. SCOPE AND ORGANIZATION....9

II. IDEAL LCC SIMULATION....11
A. INTRODUCTION....11
B. IDEAL LCC SIMULATION....11
C. EFFECTS OF ANTENNA MISMATCH....15
D. EFFECTS OF SIGNAL POWER....18
E. EFFECTS OF NON-IDEAL COMPONENTS....20
1. Non-ideal Power Splitter....21
2. Non-ideal Circulator....23
3. Non-ideal Phase Shifter....24
F. SUMMARY....29

III. WIDEBAND LCC....31
A. INTRODUCTION....31
B. RESPONSE OF WLCC....33
1. Magnitude Response of the Residual Signal....33
2. Effects of Phase Imbalance....37
C. PHASE SLOPE ALIGNMENT....39
1. Concept of Phase Slope Alignment....39
2. Shunt Stub Circuit for Phase Slope Alignment....40
3. Application of Shunt Stub Circuit to the Leakage Path....45
4. Application of Shunt Stub Circuit to the Cancellation and Leakage Paths....48
5. Mismatch Effects of a Dipole Antenna....54
6. Application of Spiral Antenna....59
D. SUMMARY....68

IV. SUMMARY, CONCLUSIONS, AND RECOMMENDATIONS....71
A. SUMMARY....71
B. CONCLUSIONS....72
C. RECOMMENDATIONS....73
1. Broadbanding Techniques for Antenna Impedance Matching....73
2. Modeling of Transmit and Receive Module....73
3. Modeling with ADS Transient Simulator....73
4. Hardware Prototype....73

LIST OF REFERENCES **75**
INITIAL DISTRIBUTION LIST **77**

LIST OF FIGURES

Figure 1. Basic principle of range computation in FMCW radar (From [1]).....1
Figure 2. Operation of LCC (From [9]). 4
Figure 3. Basic LCC configuration model (From [9]). 4
Figure 4. Effects of phase and amplitude imbalance (From [9]).....6
Figure 5. Frequency response of LCC (From [11]).....6
Figure 6. Block diagram of WLCC (From [9]). 7
Figure 7. Conceptual frequency response of WLCC versus LCC (From [9]). 8
Figure 8. Ideal LCC model in ADS (After [9], [11]). 12
Figure 9. Scattering parameter S_{31} versus that variation of attenuation sweep variable X. 13
Figure 10. Magnitude of transmission coefficient from *Port* 1 to *Port* 3 versus frequency.....14
Figure 11. Phase of transmission coefficient from *Port* 1 to *Port* 3 versus frequency. 14
Figure 12. LCC model for load mismatch simulation. 15
Figure 13. Magnitude of S_{31} versus LCC attenuation X at various load impedance (After [9]). 16
Figure 14. Magnitude of S_{31} versus frequency for impedance mismatch case. 17
Figure 15. Phase of S_{31} versus frequency for impedance mismatch case. 17
Figure 16. Simulation model for receiver power study (After [9]). 19
Figure 17. Variation of residual power versus received power. 20
Figure 18. Settings for a realistic power splitter modeling. 22
Figure 19. Magnitude of S_{31} under the influence of non-ideal power splitter.....22
Figure 20. Setting for more realistic circulator modeling. 23
Figure 21. Magnitude of S_{31} under the influence of non-ideal circulator and power splitter. 24
Figure 22. Settings for non-ideal phase shifter.....25
Figure 23. Simulation model for non-ideal components. 26
Figure 24. Effects of non-ideal components on magnitude of S_{31}. 27
Figure 25. Magnitude of S_{31} parameter versus frequency with non-ideal components. ...28
Figure 26. Phase of S_{31} versus frequency with non-ideal components. 28
Figure 27. ADS model of WLCC with FDMC using power splitters (After [11]). 32
Figure 28. ADS model of WLCC with FDMC using circulators (After [11]). 33
Figure 29. Amplitude of residual using FDMC with power splitters (After [11]). 34
Figure 30. Amplitude of residual signal using FDMC with circulators (After [11]). 34
Figure 31. Cancellation signal using FDMC with power splitters (After [11]). 35
Figure 32. Cancellation signal using FDMC with circulators (After [11]). 36
Figure 33. Phase change of signal through WLCC using FDMC with power splitter versus frequency. 37
Figure 34. Phase change of signal through WLCC using FDMC with circulator versus frequency. 38
Figure 35. Model of LCC with phase slope alignment. 39

Figure 36. Magnitude of residual power versus attenuation in LCC over frequency of 2.36 GHz and 2.44 GHz. 40
Figure 37. Phase slope alignment circuits consisting of quarter wave length stubs connected in series and parallel. 41
Figure 38. Phase response of the quarter wavelength stub phase slope alignment circuit. 42
Figure 39. Application of phase slope alignment circuit on LCC with non-ideal circulator. 46
Figure 40. Plot of residual power versus LCC attenuation. 47
Figure 41. Application of shunt stub circuits on both cancellation and leakage paths. 48
Figure 42. Plot of residual power versus LCC attenuation with 2 sets of shunt stubs circuits. 49
Figure 43. Phase angles of the leakage and cancellation paths versus frequency. 50
Figure 44. Magnitude of residual signal versus frequency. 51
Figure 45. Magnitude responses of phase slope alignment circuits with three quarter wavelength shunt stubs and quarter wavelength series stubs applied to leakage path. 52
Figure 46. Magnitude responses of WLCC with phase slope alignment circuits with quarter wavelength shunt stubs and three quarter wavelength series stub....53
Figure 47. Cancellation *C* versus frequency. 53
Figure 48. Calculated VSWR as a function of frequency for dipoles of different wire diameter (From [18])....54
Figure 49. ADS model of LCC with a dipole antenna. 55
Figure 50. Residual signal level with dipole antenna, LCC attenuation of 20 dB. 56
Figure 51. Residual signal level with dipole antenna, LCC attenuation of 21.8 dB. 57
Figure 52. Signal level at the *Port* 2 of circulator along the antenna path. 57
Figure 53. Magnitude of the leakage and cancellation signals with source of 6.0 dBm. ..58
Figure 54. Phase of the leakage and cancellation signals. 58
Figure 55. Magnitude of S_{11} parameter of spiral antenna with frequency. 60
Figure 56. Phase responses of the S_{11} parameter of spiral antenna with frequency. 61
Figure 57. ADS model of WLCC with spiral antenna. 61
Figure 58. ADS simulation setting for the spiral antenna model. 62
Figure 59. Syntax of spiral antenna S_{11} parameter file. 63
Figure 60. Magnitude of residual signal in dBm with frequency at source power of 6.0 dBm. 63
Figure 61. Magnitude of the cancellation and leakage signals. 64
Figure 62. Phase of cancellation and leakage signals. 65
Figure 63. ADS model of modified WLCC with spiral antenna. 66
Figure 64. Magnitude of cancellation and leakage signal with frequency at source power of 6.0 dBm. 67
Figure 65. Phase of the cancellation and leakage signals with frequency. 67
Figure 66. Magnitude of residual signal with frequency. 68

LIST OF TABLES

Table 1. Component specification (After [11]).....21
Table 2. Variations of phase slope with stub length. 43
Table 3. Phase slope introduced by various WLCC configurations. 44
Table 4. Length of shunt stubs for LCC design. 45
Table 5. S_{11} parameters of spiral antenna used for simulation.....60

THIS PAGE INTENTIONALLY LEFT BLANK

LIST OF ACRONYMS AND ABBREVIATIONS

ADS	Advanced System Design
ATTEN	Attenuator or Attenuation
CW	Continuous Wave
ESM	Electronic Support Measures
FDMC	Frequency Demultiplexing and Multiplexing Circuit
FMCW	Frequency Modulated Continuous Wave
LCC	Leakage Cancellation Circuit
RF	Radio Frequency
TRM	Transmit-Receive Module
TERM	Termination
WLAN	Wireless Local Area Network
WLCC	Wideband Leakage Cancellation Circuit
WNDDPA	Wireless Network Distributed Digital Phase Array

THIS PAGE INTENTIONALLY LEFT BLANK

EXECUTIVE SUMMARY

Radar with continuous transmit and receive capability has attractive features such as low transmit power levels. The low transmit power characteristics not only lower the cost of production but, more importantly, make it difficult for electronic support measures (ESM) to detect the radar signals. Typically, a circulator is used to isolate the transmit signal from the receive signal for such radar. Due to manufacturing limitations, a circulator can only provide for isolation of around 20–30 dB. In some applications, such a level of isolation is insufficient. The consequence of imperfect transmit receive isolation is that the power detector in the receive path is overwhelmed, thus degrading the receiver's sensitivity. One of the techniques to isolate the transmit signal from the receive signal is through the use of a leakage cancellation circuit (LCC).

The object of this thesis is to improve the cancellation performance of a wideband leakage cancellation circuit (WLCC). The approach is to evaluate WLCC performance through simulation using Advanced Design System 2011.05 (ADS) from Agilent. The concept of the LCC is to apply attenuation and phase shift on a copy of the transmit signal and coherently subtract leakage with this cancellation signal. A basic LCC consists of an attenuator and a phase shifter as shown in Figure 1.

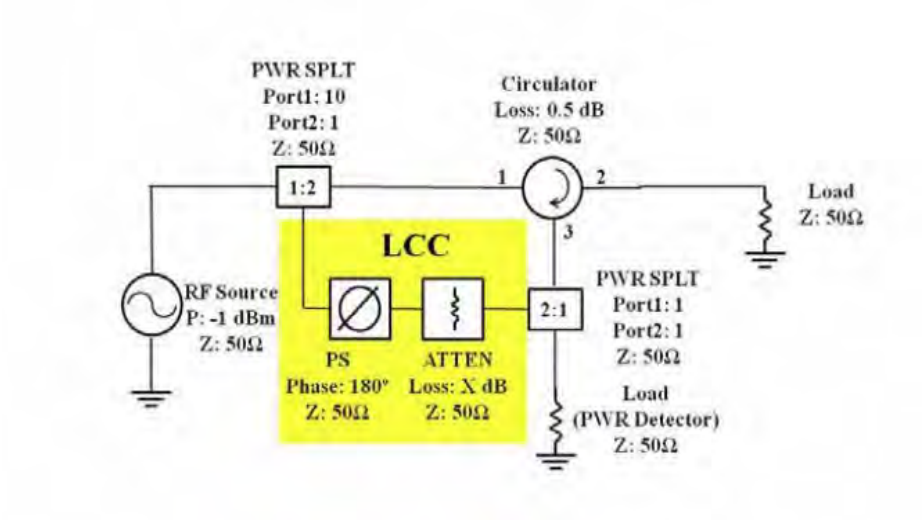

Figure 1. Basic LCC design (From [1]).

It is found that hardware limitations degrade the performance of the LCC significantly. For instance, the phase slope of a phase shifter can narrow the LCC cancellation bandwidth. When operating beyond the designed center frequency, the cancellation decreases rapidly, as shown in Figure 2.

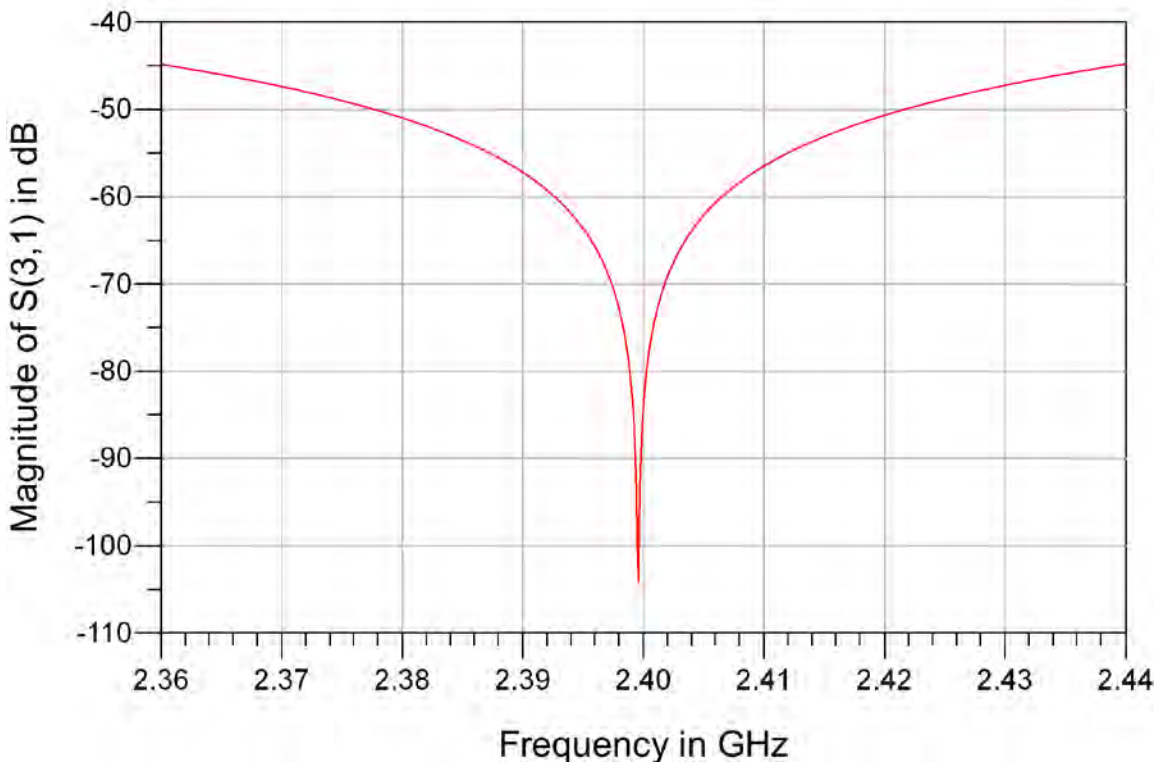

Figure 2. Degradation of cancellation with non-ideal components.

In the frequency demultiplexing multiplexing circuit (FDMC) design of WLCC, the signal is divided into multiple frequency sub-bands and, subsequently, a narrowband LCC is applied to each frequency sub-band [2]. Elliptic band-pass filters that are applied in the FDMC WLCC have frequency dependent magnitude and phase responses that are undesirable. The elliptic band-pass filters introduce amplitude and phase imbalance between the cancellation and leakage signal. As a result, coherent cancellation cannot be achieved.

The use of grounded shunt and series stubs as a phase slope alignment circuit is investigated through simulation. It is proposed to apply shunt and series stubs circuits on both cancellation and leakage paths, as shown in Figure 3.

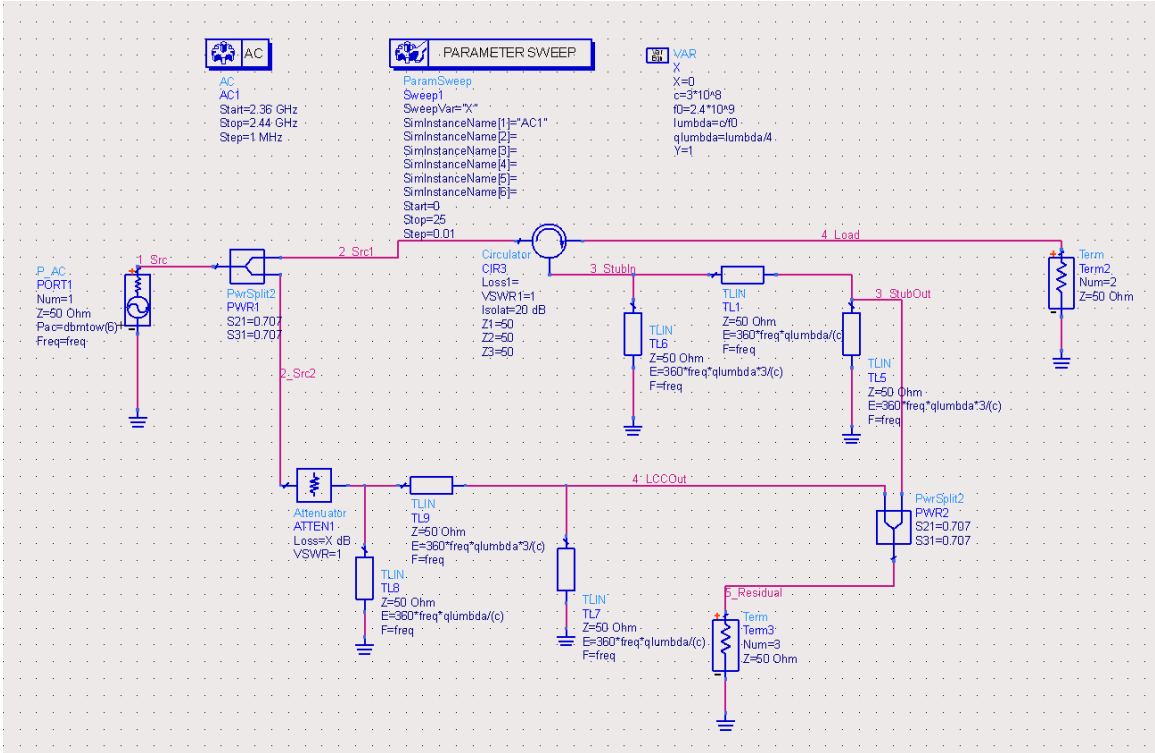

Figure 3. Application of shunt stub circuits on both cancellation and leakage paths for coherent cancellation.

In order to maintain the magnitude and phase balance, the input signal in the cancellation path is phase shifted by -270^{o}, and the leakage signal is phase shifted by -90^{o}. The reason for this configuration is that the phase change and phase slope of stub circuits follow a discrete form. The cancellation power characteristic of this LCC configuration is shown in Figure 4.

The maximum cancellation is about 87 dB at 2.38 GHz and 2.42 GHz as shown in Figure 4, and the 3 dB bandwidth of the cancellation circuit is about 56 MHz. Ideal coherent cancellation is not achieved due to the slight difference in the magnitude and phase responses between the stubs circuits used in the two paths.

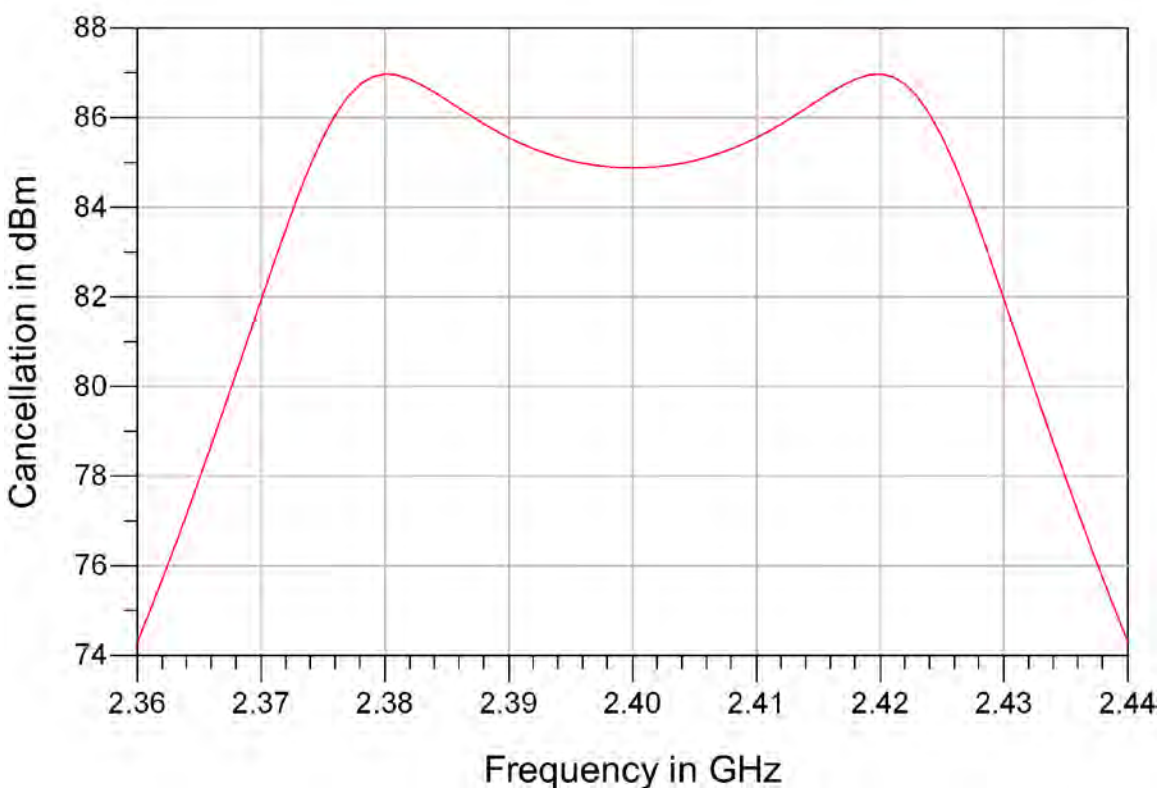

Figure 4. Cancellation versus frequency (source power of 6.0 dBm).

The new circuit design increases the cancellation bandwidth. However, it was found that antenna mismatch can significantly degrade the cancellation circuit performance. The results of this thesis can be applied to any sensor or communication system that simultaneously transmits and receives, such as continuous wave (CW) radar, frequency modulated continuous wave (FMCW) radar or a wirelessly networked distributed digital phased array (WNDDPA), where isolation and cancellation are required between the transmit and receive paths.

LIST OF REFERENCES

[1] Wei-Han Cheng, "Cancellation circuit for transmit-receive isolation," Naval Postgraduate School Master's Thesis, September 2010.

[2] T. H. Ang, "Conceptual design and software simulation of a wideband leakage cancellation circuit," Naval Postgraduate School Master's Thesis, December 2010.

THIS PAGE INTENTIONALLY LEFT BLANK

ACKNOWLEDGMENTS

I would like to express my gratitude to my thesis advisor, Professor David Jenn for his valuable time and guidance. I would also like to thank Professor Ric Romero for his technical expertise and insights as a second reader. I would like to thank Mr. Robert Broadston for providing his technical expertise and valuable suggestions. I would like to thank Singapore Technologies Dynamics Pte Ltd for sponsoring me on this master program. Last, but not least, I thank my wife, Pauline, for her understanding throughout the master program.

THIS PAGE INTENTIONALLY LEFT BLANK

I. INTRODUCTION

A. BACKGROUND

Radar systems typically illuminate a target with a microwave signal, which is then reflected and received by a receiving antenna. The radar systems exploit the temporal, spatial and frequency characteristics of the reflected signal to determine target attributes such as velocity, range and radar cross section. Signals emitted by radar systems can be either pulsed or continuous wave. In the case of continuous wave (CW) radar, a continuous frequency is transmitted. The CW radar makes use of the Doppler shift between the transmitted and received signal to determine the speed of the target. Since only a single frequency is transmitted, CW radar is capable of determining the speed of the target but not its range.

Another class of CW radar is the frequency modulated continuous wave (FMCW) radar [1]. The FMCW radar transmits a continuous wideband signal over a radio frequency (RF) band to determine the range of the target. In Figure 1, the basic working principle of FMCW radar is shown.

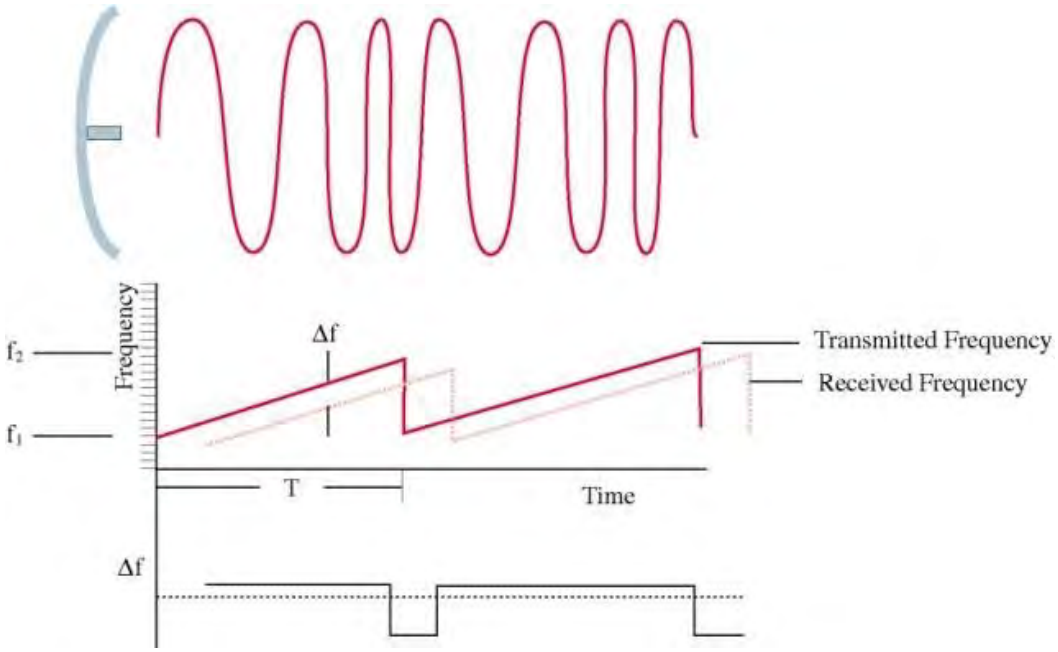

Figure 1. Basic principle of range computation in FMCW radar (From [1]).

As illustrated in Figure 1, the FMCW radar transmits a frequency modulated signal that is incident on the target. Part of this RF signal is reflected by the surface of target. The frequency is swept linearly from f_1 to f_2. The frequency shift between the transmitted signal and the received reflected signal is used to compute the range of the target. As shown in Figure 1, Δf represents the change in frequency between the transmitted and received signal and T is the duration of the frequency sweep. The range of the target can be determined from

$$R = \frac{\Delta f T c}{2\left(f_2 - f_1\right)} \tag{1}$$

where $c = 3\text{x}10^8$ ms^{-1} is the velocity of light in free space. As it can be seen in Equation (1), it is generally desirable to implement a radar system with a frequency band that is as wide as possible for better range resolution. Such attributes are difficult to implement in practice due to the limitation in hardware components.

1. Leakage Problem in CW and FMCW Radars

CW and FMCW radars typically do not emit distinct pulses of microwave energy compared to pulsed radar. As a result, the low transmit power levels make it difficult for electronic support measures (ESM) to detect the radar's signal [2]. A disadvantage is that the continuous transmit and receive nature of the CW and FMCW radar allows undesired leakage of the transmitted signal directly to the receiver since there is no temporal separation between the two signals. This direct leakage of the transmitter power onto the receiver input reduces the performance of the CW radar as the receiver is desensitized.

2. Isolation of Transmit and Receive Signals

For CW radar with a single antenna configuration, isolation can be obtained by using a hybrid junction, circulator, turnstile junction, or with separate polarizations [3]. As explained in [3], typical isolation through hybrid junction is of the order of 20 to 30 dB and perhaps 60 dB or more with extreme precision. One of the limitations of a hybrid junction is the inherent loss of half of the transmit power and half of the receive power.

In [4], a circulator is designed to minimize return losses and achieve isolation of 20 to 30 dB between the three terminals of the circulator.

Use of separate antennas for transmit and receive is proposed in [5]. Two cylindrical spiral antennas with oppositely directed windings are used by the authors so that the transmitted channel is orthogonal to that of the received channel. The two antennas are physically separated and their separation is comparable to the wavelength of the transmission. Such technique is only applicable in cases where a two antenna configuration can be deployed.

An analog leakage cancellation circuit can be added to suppress leakage [6]. This technique involves continuous tracking of the amplitude and the phase of leakage signal. In order to suppress the leakage signal, a cancellation signal that has equal amplitude but opposite phase is added. Digital leakage cancellation circuits that exploit the similarity or correlation between the transmitted and leakage signals are proposed in [7], [8]. Such digital cancellation techniques usually require low distortion in quantization for controlling component, digital linear correction and minimal delay between digital processing and analog-to-digital (ADC) conversion, as suggested in [6].

In the previous work [9], a narrowband leakage cancellation circuit (LCC), as shown in Figure 2, was designed to improve transmit/receive isolation in the synchronization of a wirelessly distributed digital phase array [10]. The goal of the cancellation branch is to coherently cancel the leakage L and mismatch M, so that only the desired signal S remains. The basic operation of the LCC is as shown in Figure 2.

As shown in Figure 3, the LCC can be represented by an attenuator and phase shifter. The source signal is divided by a power splitter. Some of the source power is circulated through a circulator to a 50 Ω load which represents the antenna. The other part of the source power is fed into the LCC. As illustrated in Figure 2, the output of the LCC is the cancellation signal C designed to cancel leakage signal L from the circulator. Ideally, the load antenna is perfectly matched and mismatch M from the load antenna is zero. For the case of complete cancellation, only the received signal S arrives at power detector, which is shown as a load in Figure 2.

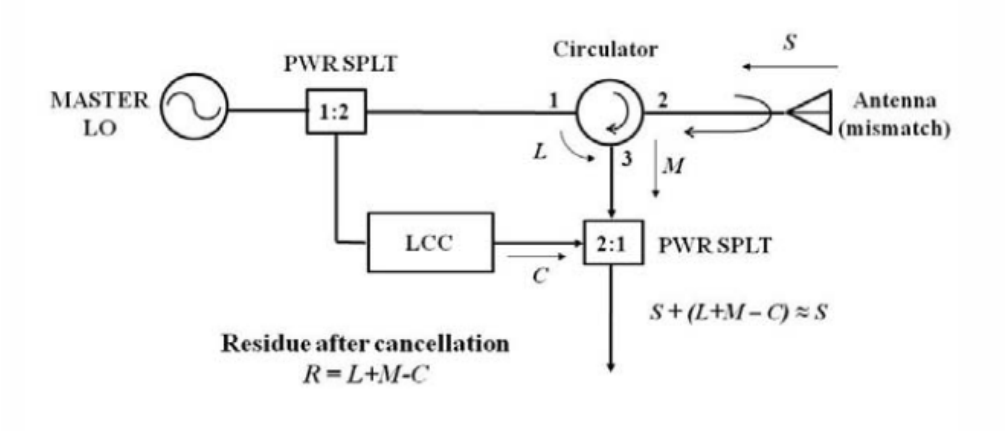

Figure 2. Operation of LCC (From [9]).

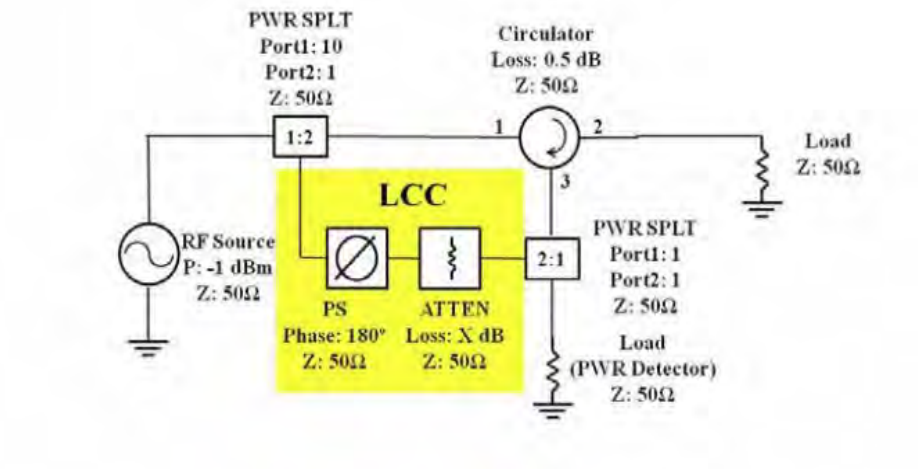

Figure 3. Basic LCC configuration model (From [9]).

3. Amplitude and Phase Imbalance in LCC

For the analysis of a LCC with coherent cancellation, the complex voltage at the input of the power detector is given by,

$$S+\left(L+M-C\right)=S+R\approx S \tag{2}$$

where R is the residue signal after cancellation, as shown in Figure 2. The cancellation improvement CI in dB is given by,

$$CI = 20\log_{10}\left(\frac{R}{L+M}\right) = 20\log_{10}\left(1-\frac{C}{L+M}\right). \quad (3)$$

From Equation (2), it can be seen that the LCC output L has to be 180^{o} out of phase compared with $L+M$. In practice, it is generally difficult to match both phase and amplitude of leakage and LCC output to achieve ideal cancellation; that is, a residual R = 0.

The sum of the leakage term $L+M$ and LCC output C can be expressed by

$$V = V_1 + V_2 = 1 + \alpha e^{j\varphi} \quad (4)$$

where, V_1 represents $L+M$ and V_2 represents C. The voltage V_1 is used as a reference signal and is set to unity; α and φ represent the amplitude and phase of the cancellation signal relative to the reference.

In Figure 4, the effects of phase and amplitude imbalance between the leakage and cancellation signals are shown. It can be seen from Figure 4 that, with a slight phase imbalance of two degrees, the performance of the LCC degrades significantly by decreasing the suppression to about 35 dB.

The simple LCC configuration as shown in Figure 3 has a limited bandwidth [11] as evident from the plot in Figure 5. The 60 dB cancellation bandwidth of the LCC is 4 MHz or 0.1667 % of the carrier frequency. Increasing the bandwidth to 50 MHz or 2.083 % of the carrier frequency, we observe that the cancellation bandwidth of the LCC is only 40 dB.

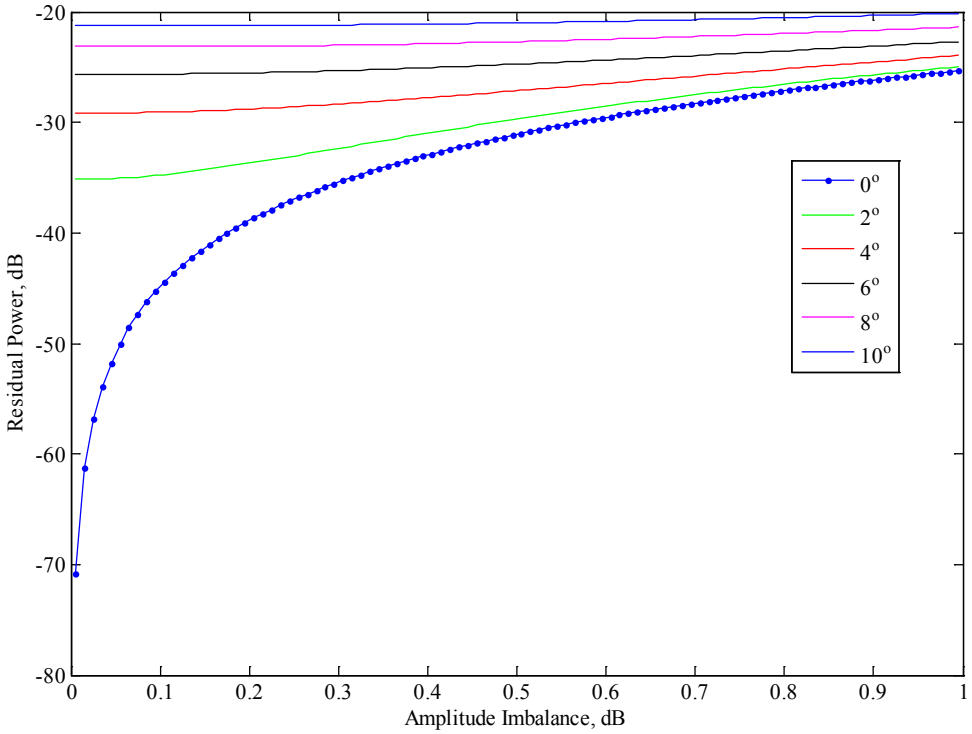

Figure 4. Effects of phase and amplitude imbalance (From [9]).

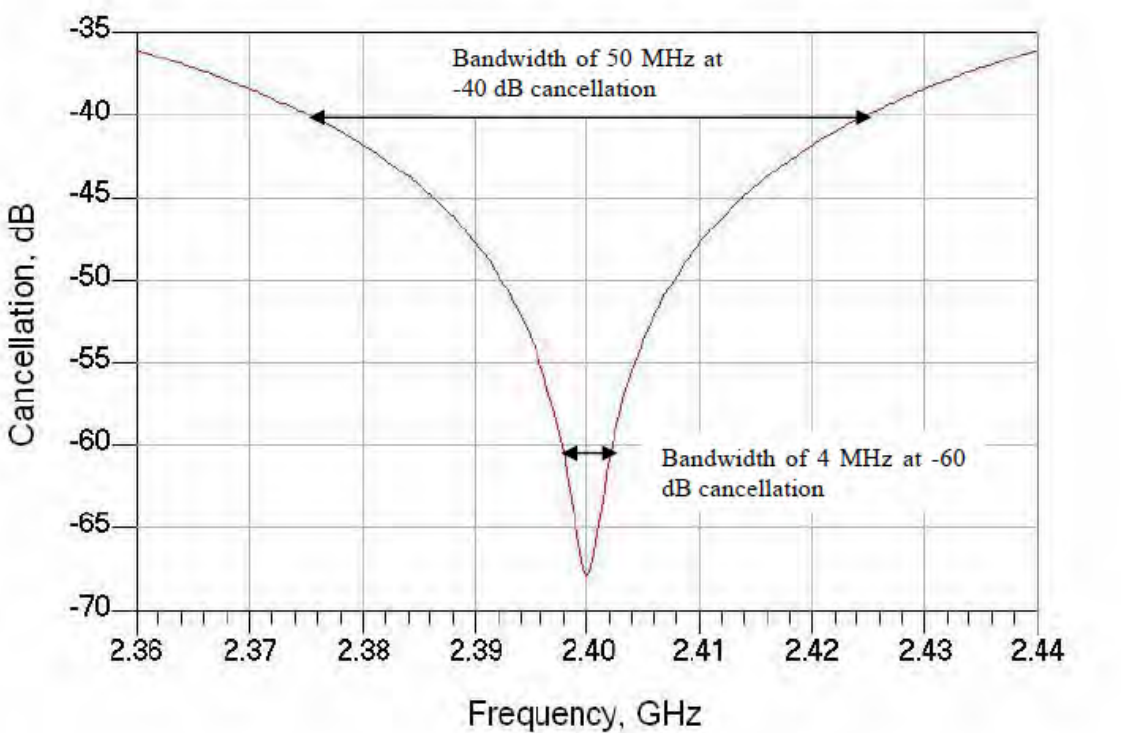

Figure 5. Frequency response of LCC (From [11]).

4. Wideband Leakage Cancellation Circuit

The application of a frequency demultiplexing and multiplexing circuit (FDMC) is proposed in [11] to implement a wideband LCC (WLCC) structure. The structure of the WLCC is shown in Figure 6.

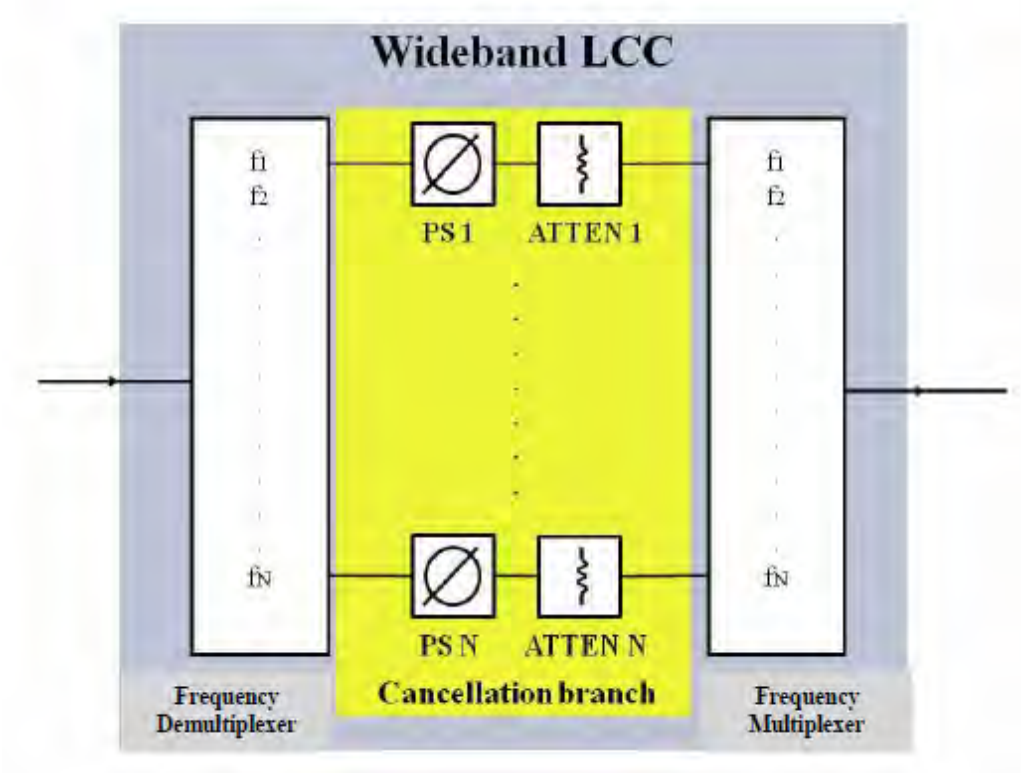

Figure 6. Block diagram of WLCC (From [9]).

The WLCC consists of a bank of multiple narrowband LCCs where each channel is tuned to work in a specific center frequency. The incoming wideband signal is divided into multiple narrowband signals. Each of these narrowband signals is then attenuated and phase shifted by a specific LCC. The output of the narrowband LCC is recombined to produce a wideband cancellation signal. The goal of the WLCC is to achieve a frequency response as shown in Figure 7.

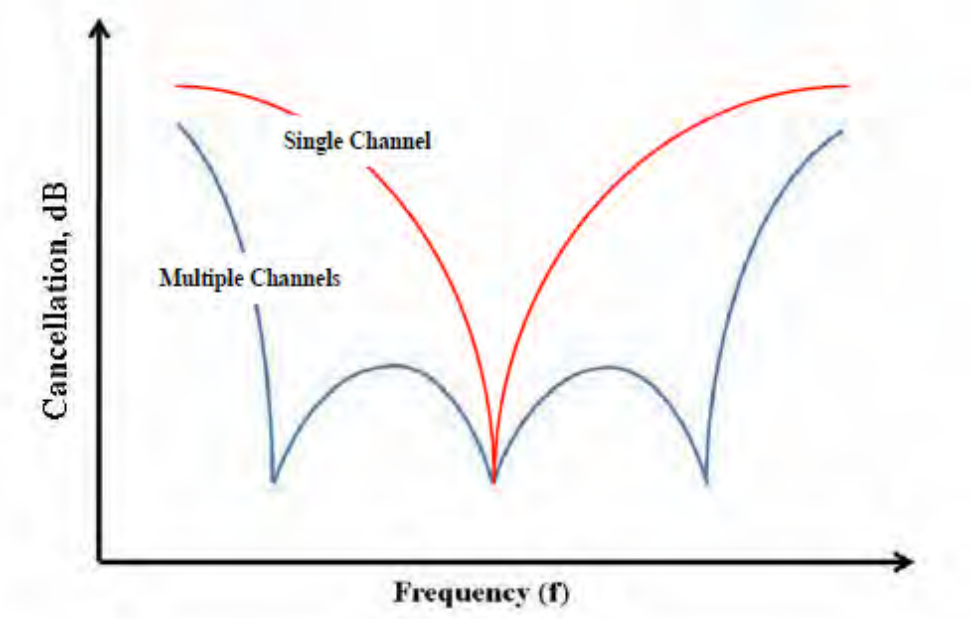

Figure 7. Conceptual frequency response of WLCC versus LCC (From [9]).

The plot in Figure 7 shows the desired response of a WLCC that is constructed by superimposing multiple LCCs. The challenge of implementing the WLCC with a FDMC not only lies with matching the amplitude responses of LCC banks but, more importantly, tuning the phase responses so that they cancel out the leakage coherently.

B OBJECTIVE

The objective of this research is to improve the cancellation performance of a WLCC. The results of this thesis can be applied to any sensor or communication system that simultaneously transmits and receives, for example, CW or FMCW radar, or a wirelessly networked distributed digital phased array (WNDDPA), where isolation and cancellation are required between the transmitted and received signals.

The approach is to investigate LCC techniques in the analog domain. A FDMC structure is adopted for the analog study and is simulated using Advanced Design System 2011.05 (ADS) from Agilent Technologies. Both narrowband and wideband LCC models are simulated in ADS to investigate their phase and amplitude balance properties.

Methods such as applying grounded shunt stubs to align the phase slopes of the cancellation and leakage signals are also investigated.

C. SCOPE AND ORGANIZATION

This thesis is organized into four chapters. In Chapter I, background information such as the isolation problem of CW and FMCW radar and its improvement using cancellation circuits was covered.

In Chapter II, the ideal LCC model used for simulation is presented. The results and analysis of the ideal LCC model are used as a reference for comparison of results obtained from the WLCC.

In Chapter III, the results of a WLCC based on a FDMC model are simulated in ADS. The results and analysis on different scenarios such as mismatched load impedance, power efficiency and phase slope characteristics are presented. The use of grounded shunt stubs for phase slope alignment between paths and its effects on the WLCC performance are shown in Chapter III.

In Chapter IV, a summary of the work carried out in this thesis is provided. Recommendations for future research are also proposed.

THIS PAGE INTENTIONALLY LEFT BLANK

II. IDEAL LCC SIMULATION

In this chapter, analysis of the narrowband LCC is carried out. The findings serve as the basis for our comparison with the case of the WLCC. The study of the narrowband LCC is carried out using ADS from Agilent Technologies.

A. INTRODUCTION

An accurate simulation model allows understanding of the system behavior prior to its implementation. Simulation also helps to reduce risk and uncertainty before the actual development since designers are able to eliminate some or most design problems. ADS is used in the study of the LCC in this thesis because it supports the design of RF microwave modules and systems with accurate models.

ADS is an electronic design automation software system. ADS uses a complete set of simulation technologies ranging from frequency and time-domain circuit simulation to electromagnetic field simulation to provide a single, integrated design environment. Some of the ADS features used in the study of this thesis are AC simulator, S-parameter simulator, and parameter sweep controller. These features are used to investigate circuit behavior when a parameter is varied over a range of values.

B. IDEAL LCC SIMULATION

A ideal LCC simulation model using an AC power source, attenuator, phase shifter, circulator and two power splitters can be built in ADS as shown in Figure 8. The S-parameters simulator together with the parameter sweep controller is used in this LCC model. In this model, we assume that the components used are close to ideal and the impedances are matched to that of the power source (all 50 Ω). The power source frequency is swept from 2.36 GHz to 2.44 GHz in steps of 1.0 MHz. The output power of the source is set at 6.0 dBm for convenience.

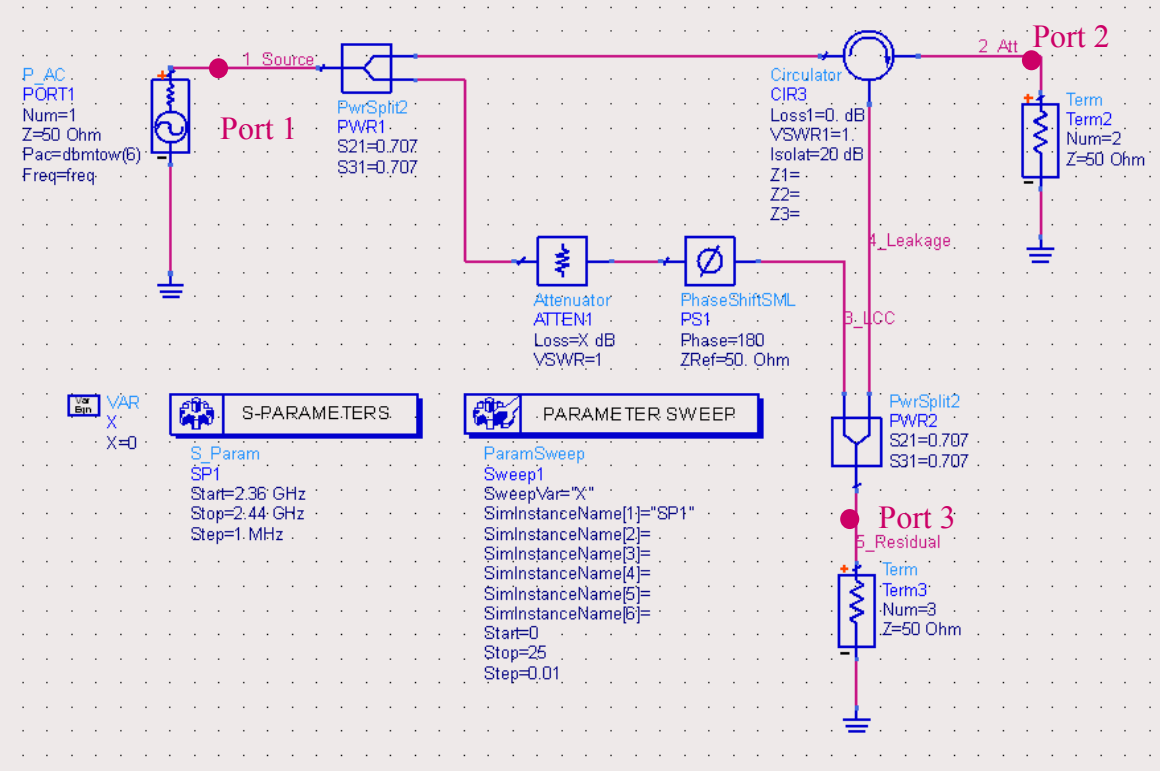

Figure 8. Ideal LCC model in ADS (After [9], [11]).

The circulator used in this model is ideal with a voltage standing wave ratio (VSWR) of 1.0. This implies that there is no reflection when a signal is circulated from *Port* 1 to 2, or 2 to 3, or 3 to 1 of the circulator. The isolation of the circulator is set to 20 dB for a realistic simulation. The circuit is terminated with a matched load so that there is no reflected signal from the load antenna back to the circulator and, subsequently, into *Port* 3 of the circulator. Therefore, the leakage signal is due entirely from non-ideal circulator isolation.

The phase shifter is set at 180° so that the output of the LCC, labeled as *3_LCC* in Figure 8, is 180° with respect to the leakage signal, labeled as *4_Leakage* in Figure 8. Using the parameter sweep controller, we swept the attenuation on the LCC from 0 to 25 dB in steps of 0.01 dB as shown in Figure 8.

The resultant plot of the scattering parameter S_{31} versus the change in attenuation is shown in Figure 9. Scattering parameter S_{31} represents the transmission coefficient

from *Port* 1 (source) to *Port* 3 (residual signal) when all other ports are terminated in matched loads [12]. Therefore, the S_{31} parameter is used for the analysis as it represents the residual signal power level with respect to the source power level.

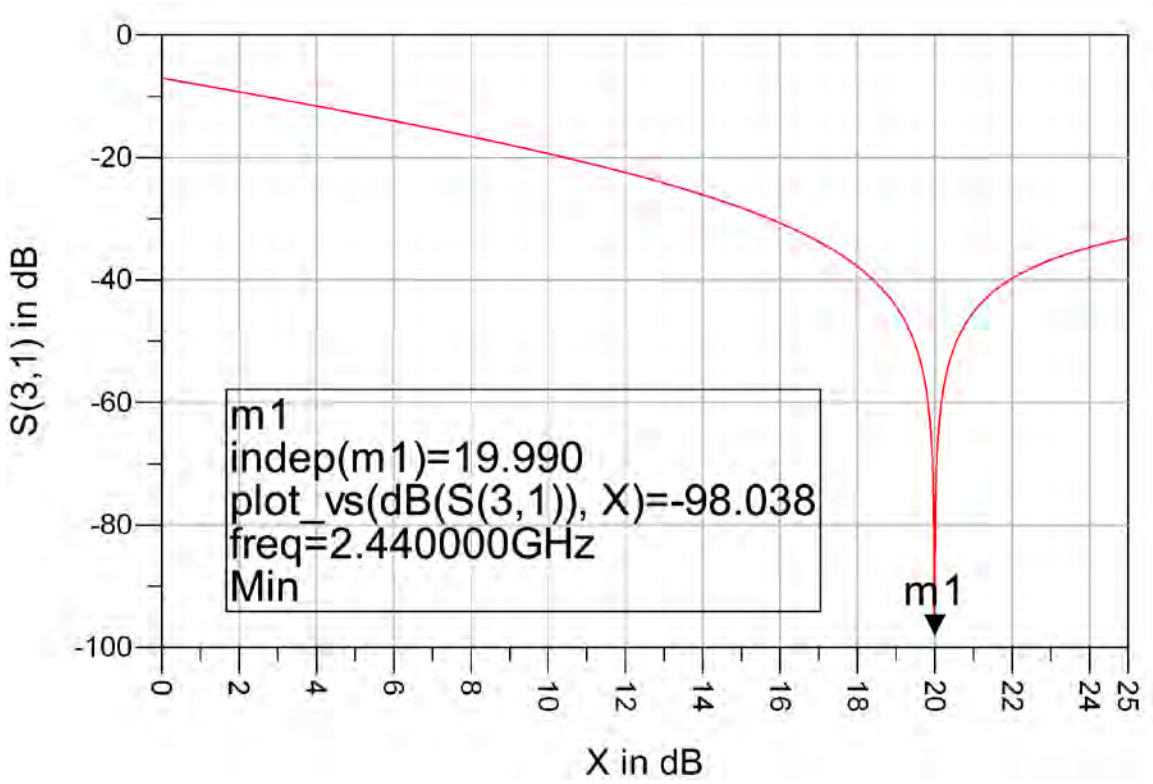

Figure 9. Scattering parameter S_{31} versus that variation of attenuation sweep variable X.

As can be seen in Figure 9, the transmission coefficient is notched at −98.038 dB when the attenuation is set to 19.990 dB. This occurs when there is almost perfect cancelation between the leakage and the LCC output.

The attenuation of the LCC is set at 19.990, and the simulation is repeated. The magnitude and phase of S_{31} or transmission coefficient from *Port* 1 to *Port* 3 are shown in Figure 10 and Figure 11, respectively.

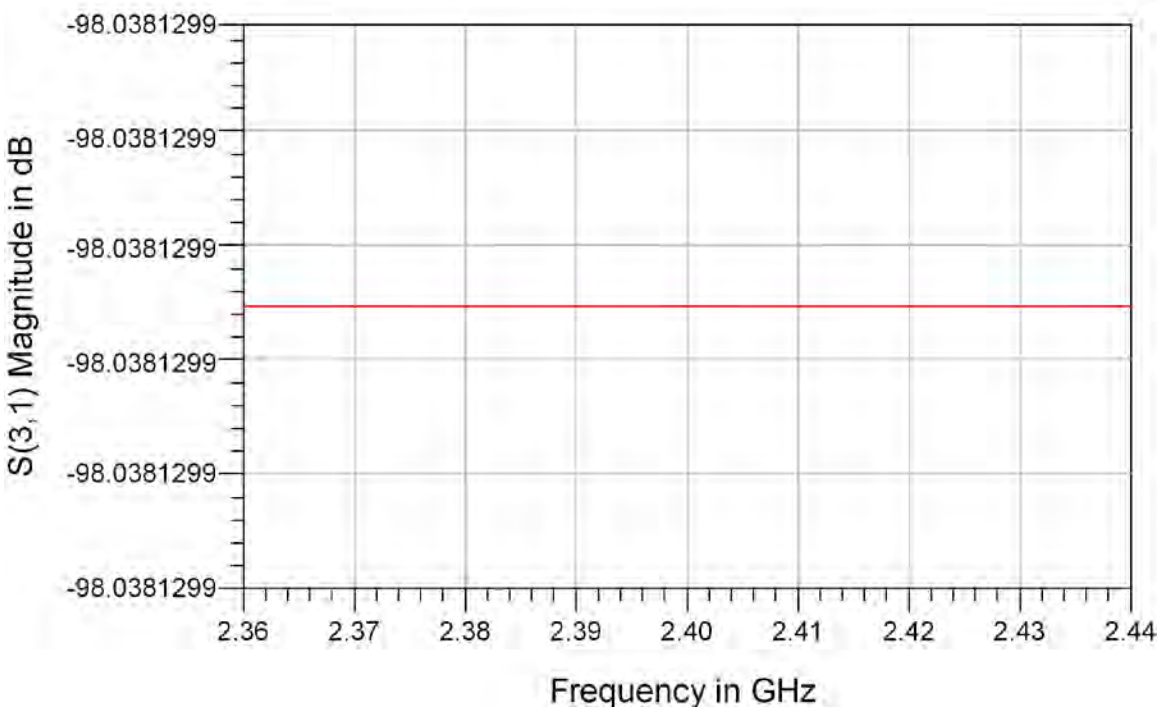

Figure 10. Magnitude of transmission coefficient from *Port* 1 to *Port* 3 versus frequency.

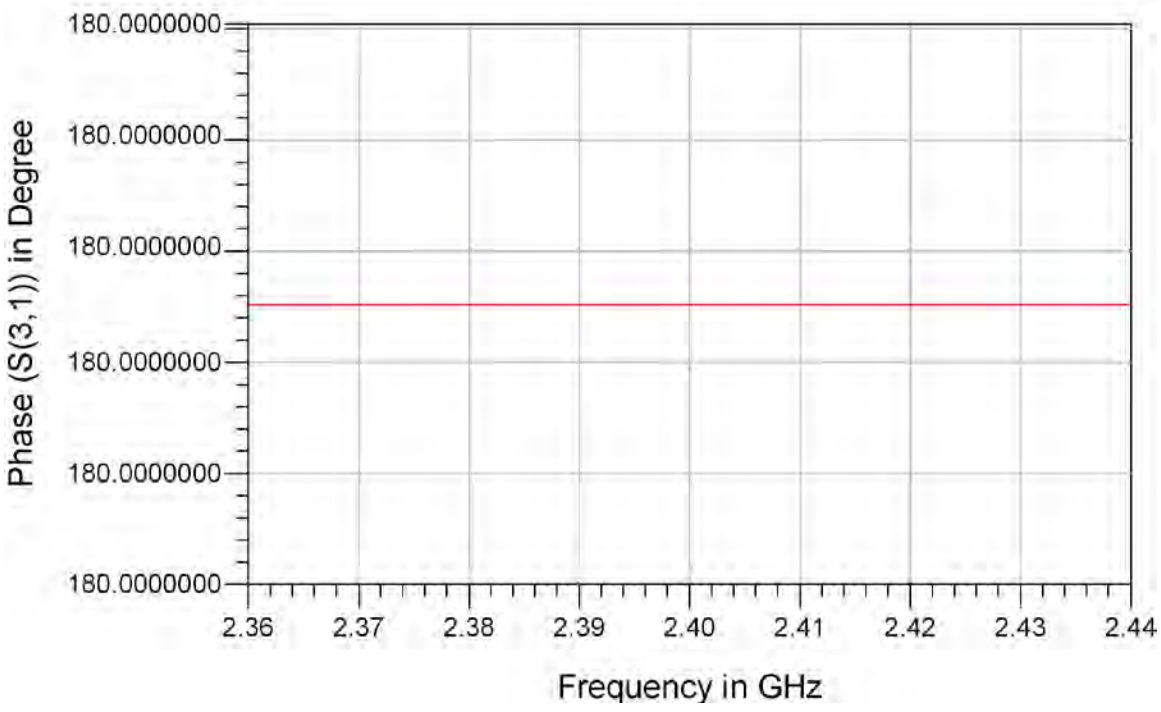

Figure 11. Phase of transmission coefficient from *Port* 1 to *Port* 3 versus frequency.

From Figure 10 and Figure 11, we see that the ideal LCC has a flat magnitude response of −98.038 dB and constant phase change of 180° over the entire frequency range of interest. This is because the device characteristics were assumed independent of frequency. In practice, the components used in the construction of LCC are far from ideal, and the behavior of the cancellation circuit deviates significantly from what is shown in Figure 10 and Figure 11. This is discussed in the next section.

C. EFFECTS OF ANTENNA MISMATCH

In the reality, the precision of components is limited by the materials and manufacturing processes. As a result, load impedance is not perfectly matched. This mismatch in impedance causes undesired reflections that can lead to reduction in amplitude and additional phase error. An impedance matching network is usually introduced between the load impedance and a transmission line for impedance matching proposes. The model used for the study of the effects of antenna mismatch is shown in Figure 12.

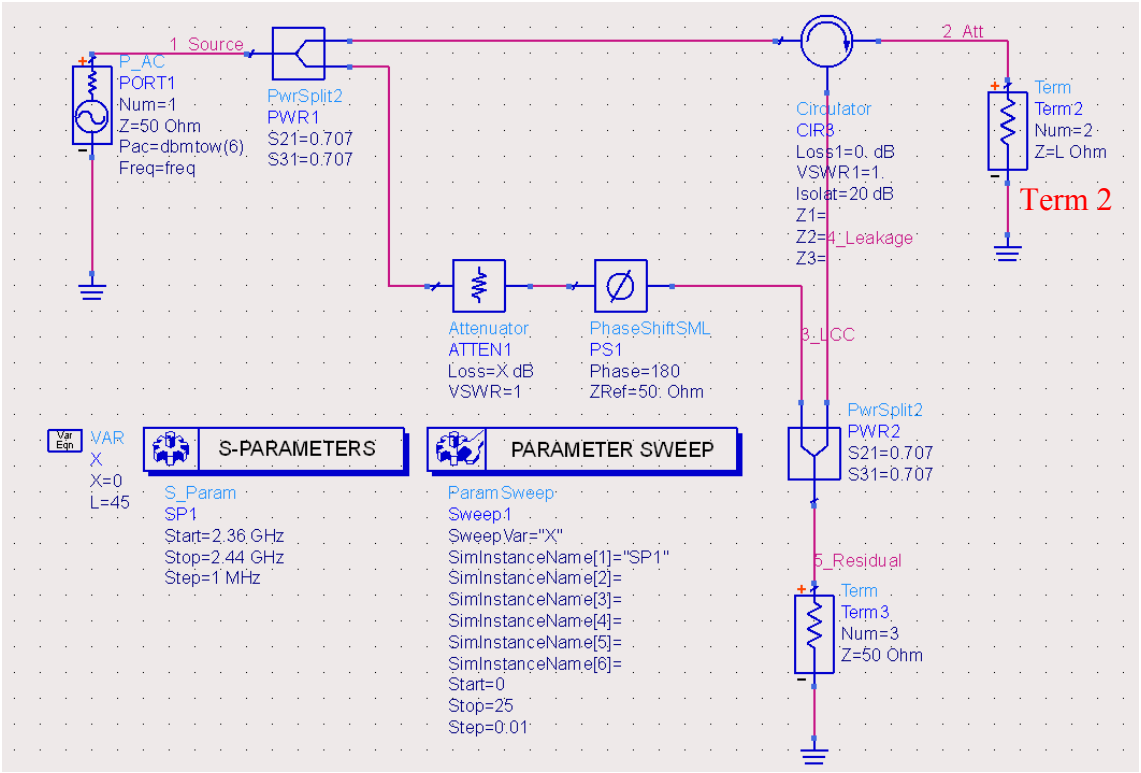

Figure 12. LCC model for load mismatch simulation.

In order to study the effects of load impedance mismatch, the load impedance (*Term* 2 in Figure 12) is varied from 45 to 60 Ω in steps of 5.0 Ω. The phase shifter is fixed at 180°, and the attenuation of the LCC is varied from 0 to 30 dB in steps of 0.01 dB. The effects of load impedance mismatch on the leakage power are shown in Figure 13.

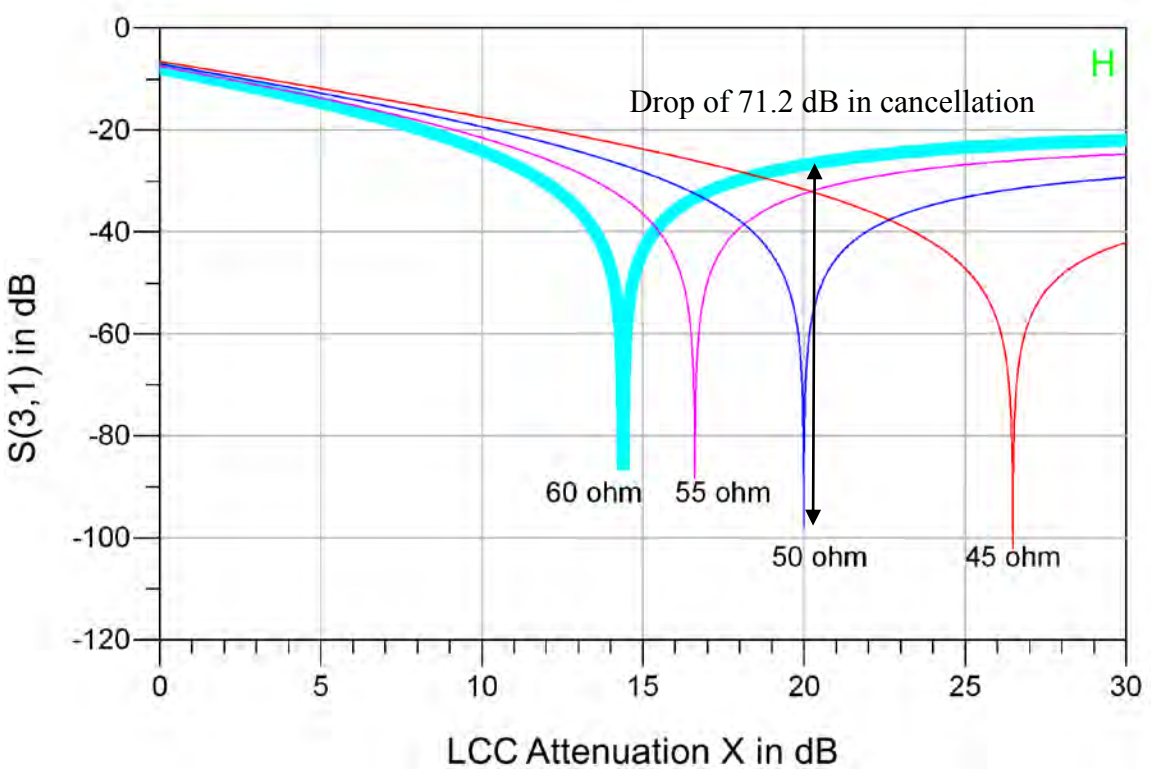

Figure 13. Magnitude of S_{31} versus LCC attenuation X at various load impedance (After [9]).

As shown in Figure 13, mismatch variation in the load impedance causes a change in the leakage signal. Tuning the LCC reduces the residual signal to very low levels as shown in Figure 9, but if the leakage changes due to a mismatch change and the LCC is not tuned, the effectiveness of the LCC can be reduced by over 70 dB as shown in Figure 13. The distortion in the magnitude and phase of the transmission coefficient S_{31} can be seen in Figure 14 and Figure 15, respectively. Again, these results are independent of frequency because the parameters of devices in the circuit are modeled as being independent of frequency.

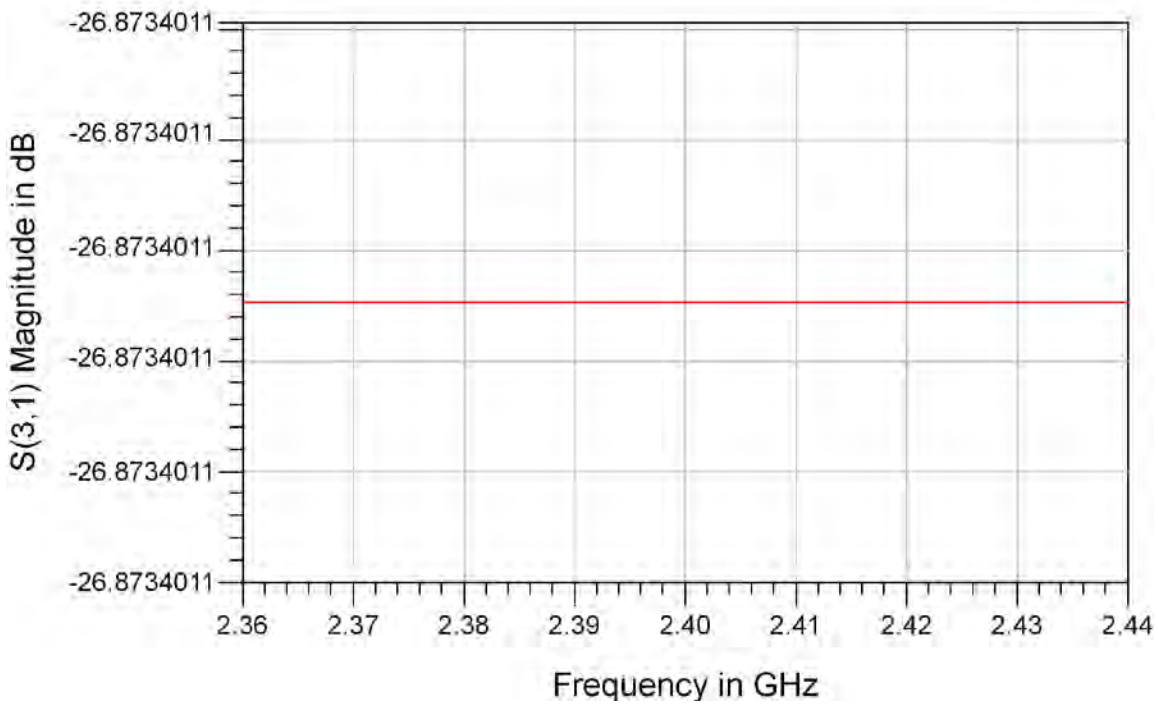

Figure 14. Magnitude of S_{31} versus frequency for impedance mismatch case.

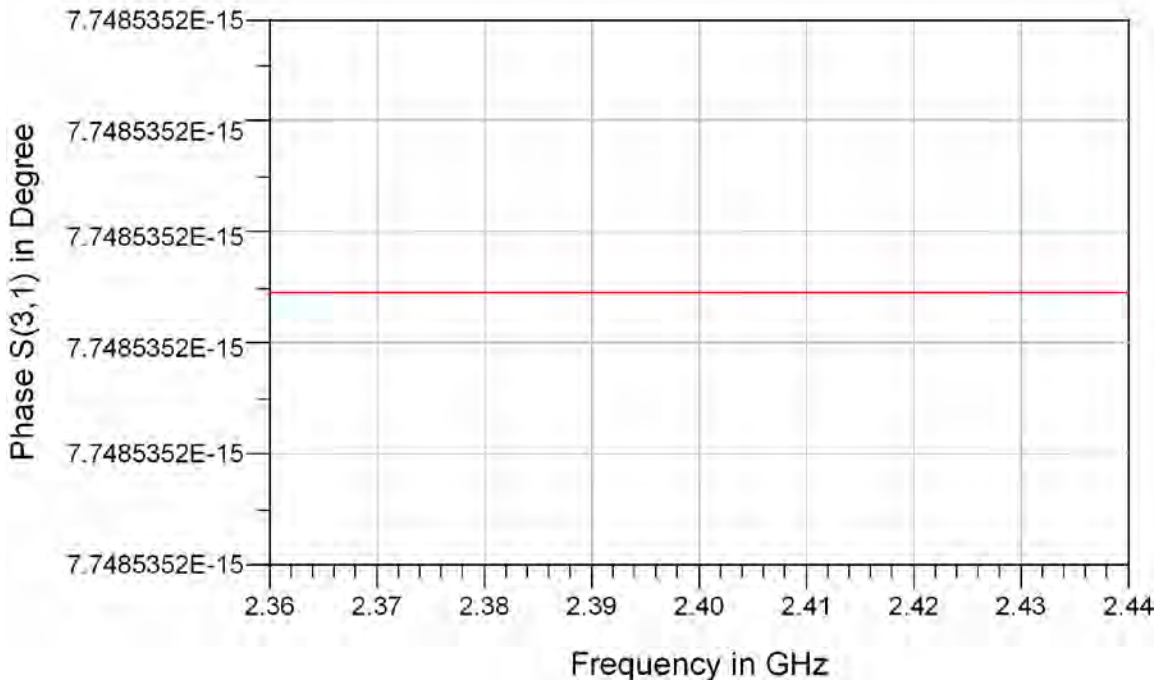

Figure 15. Phase of S_{31} versus frequency for impedance mismatch case.

The extent of distortion in amplitude and phase is shown in Figure 14 and Figure 15, respectively, for the case where the LCC is tuned for a 50 Ω load but actually terminated with a 60 Ω antenna load. The residual increases from −98.038 dB in Figure 10 to −26.873 dB in Figure 14 due to the amplitude imbalance. It can be seen in Figure 15 that the impedance mismatch causes a drastic change in the phase response of the S_{31} parameter.

Matching of the antenna impedance is important in maintaining the low residual power level in the design of a LCC. Mismatch in the antenna impedance reduces the cancellation level. Retuning of the LCC circuit reduces the impact of the load mismatch; however, there are limitations to the tuning procedure, such as variation of VSWR of an adjustable attenuator as the attenuation changes [9].

D. EFFECTS OF SIGNAL POWER

The impact of the signal power level from the antenna is presented in this section. The variation of the signal power level is modeled by an attenuator (*ATTEN*2), a phase shifter (*PS*2) and a shorted component (*Short*1) as shown in Figure 16. The received signal is generated from the transmit signal modified by a phase shifter, and an attenuator with a shorted line attached. The attenuator can be adjusted to vary the simulated signal's strength. This arrangement was used in the laboratory as well. It avoids the problem of trying to synchronize the frequencies of the two signal generators. The power level of the received signal is modeled by varying the attenuation *ATTEN*2. The phase difference (path delay) between transmit and receive signals is modeled by a phase shifter. The simulation is conducted by varying *ATTEN*2 from 0 to 100 dB in steps of 0.1 dB. This represents receive signal power level at various amplitudes.

In Figure 17, the variation of the residual power with increasing attenuation *ATTEN*2 is shown. It can be observed from Figure 17 that as the attenuation drops from 0 to 30 dB the residual power decreases linearly. A deep notch of −126.272 dB on the residual power level occurs when the attenuation is set at 40.1 dB. For attenuations greater than about 55 dB, the residual power remains at about −87 dB. As explained in [9], the linear decrease of residual power is dominated by the received signal since the

LCC cancels out more than 90 dB of leakage signals as shown in Figure 10. The deep notch occurs as the received signal is 180^{o} out of phase compared to the leakage signal providing further cancellation. The tail end of the plot in Figure 17 shows the limitation of the LCC based on the precision of the attenuator used in the model. Therefore, by increasing the precision of the components used in the LCC, the performance of the cancellation can be further enhanced. However, this may not be possible with realistic hardware.

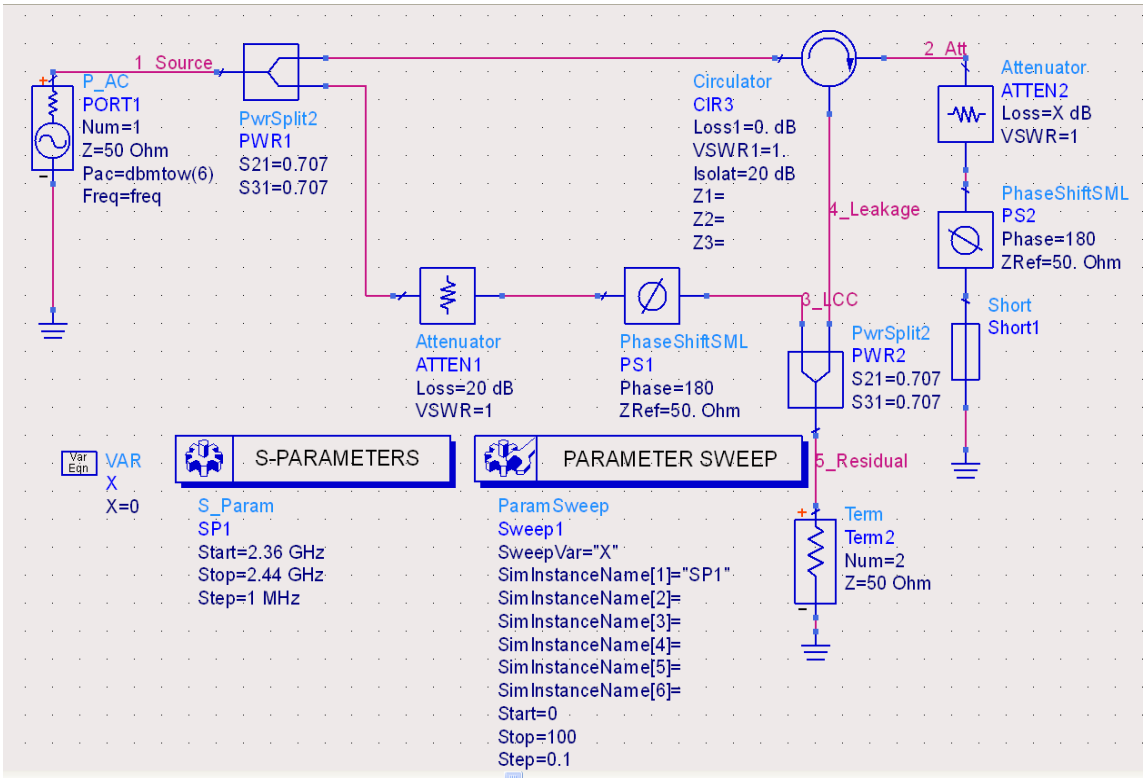

Figure 16. Simulation model for receiver power study (After [9]).

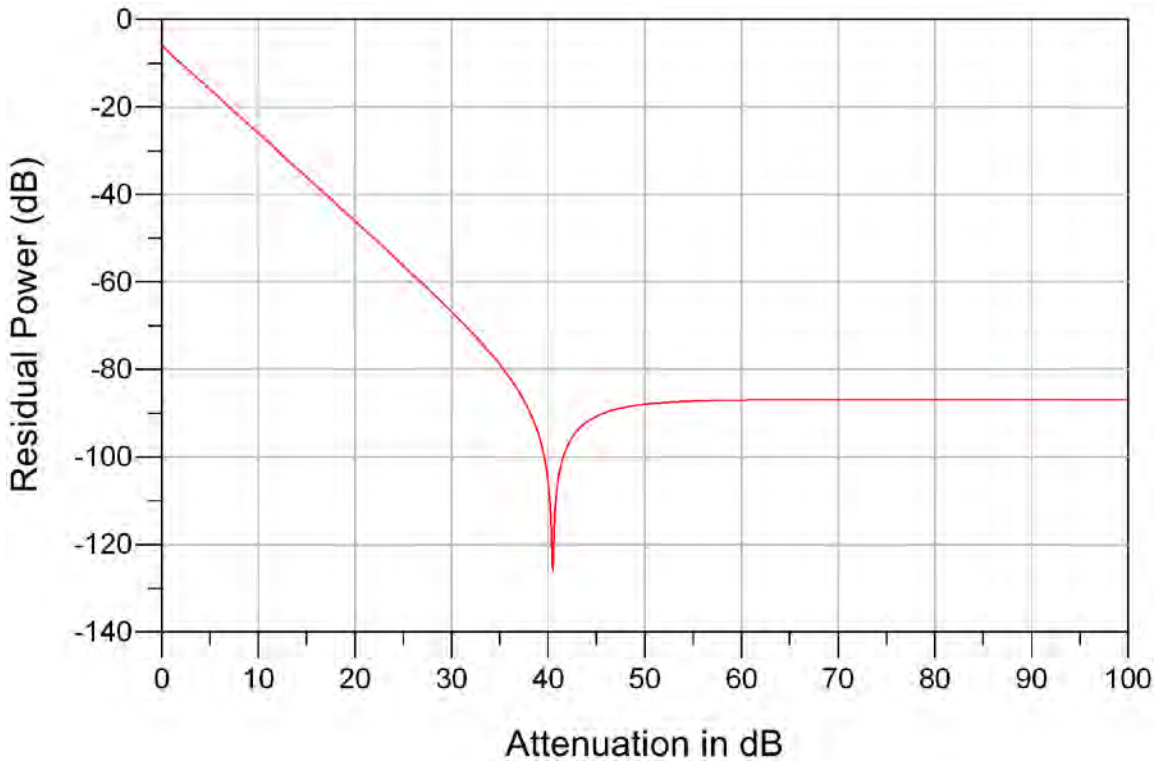

Figure 17. Variation of residual power versus received power.

E. EFFECTS OF NON-IDEAL COMPONENTS

In this section, the effects of non-ideal components in the LCC are investigated. The study of the LCC so far is based on the ideal component models provided by ADS; however, in a real implementation, the component characteristics vary from those of an ideal component. As a result, the performance of the LCC is greatly affected due to the sensitivity of the residual signal to amplitude and phase imbalance as reported in [9].

The parameters of the components used in this section are based on the components available in the Microwave Laboratory of Electrical and Computer Engineering Department at the Naval Postgraduate School. The specifications of the components used for the study are shown in Table 1.

Table 1. Component specification (After [11]).

Component	Manufacturer and Model	Specifications
3 dB Power Splitter	Pasternack PE2014	Frequency range 2 to 4 GHz Minimum Isolation 20 dB VSWR 1.3 Maximum insertion loss 0.30 dB [13]
Circulator	CITOM D3C2040	Frequency range 2 to 4 GHz Impedance 50 Ω Isolation 20 dB Insertion loss 0.4 to 0.5 dB VSWR 1.25 to 1.30
Phase Shifter	SAGE LABORATORIES INC 6708	Frequency Range DC to 8 GHz Phase shift, min 72^o/GHz Insertion phase at min phase setting 170^o/GHz VSWR max 1.6 Insertion loss, max 0.7 dB Time delay nominal at min phase setting 0.45 nsec

1. Non-ideal Power Splitter

With reference to the specifications given in Table 1, a VSWR of 1.3 is used instead of 1.0 for the ideal case. From [12], the relationship between the reflection coefficient Γ and VSWR is given by

$$\Gamma = \frac{VSWR - 1}{VSWR + 1}. \tag{5}$$

By substituting a VSWR of 1.3 into Equation (5), we find the reflection coefficient Γ to be 0.1304. The reflection coefficient Γ of 0.1304 is used as the reflection coefficient of *Port* 1 and *Port* 2 in the simulation. The insertion loss of 0.30 dB is neglected in this simulation for simplicity.

The settings of the power splitter used in the ADS simulator are shown in Figure 18. The basic LCC simulation model (in Figure 8) with a perfectly matched load is simulated for the frequency range of 2.36 GHz to 2.44 GHz in steps of 1.0 MHz. The loss of the attenuator in the LCC is stepped from 0 dB to 25 dB in increments of 0.01 dB

to tune the cancellation circuit. The effects of the reflections at *Port* 1 and *Port* 2 of the power splitters on the cancellation can be seen in Figure 19.

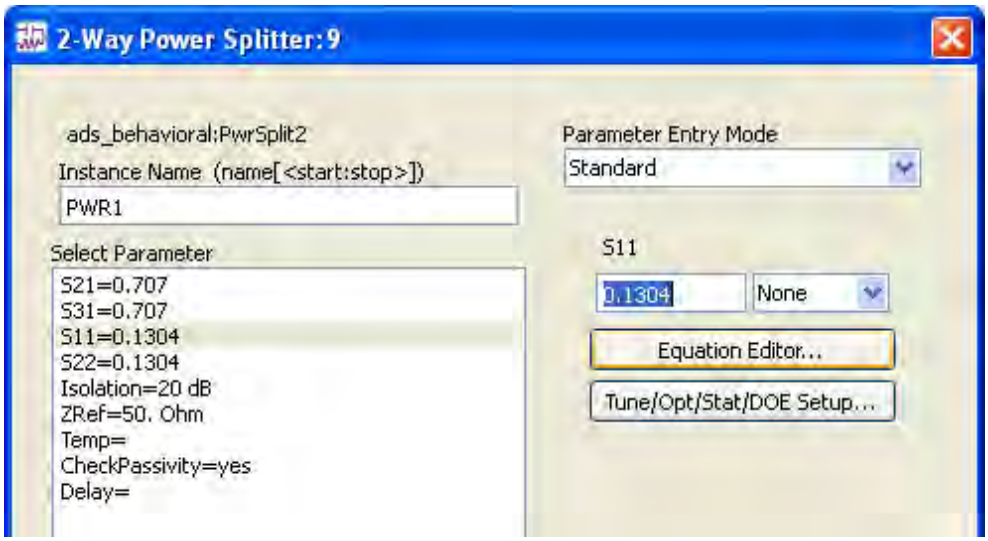

Figure 18. Settings for a realistic power splitter modeling.

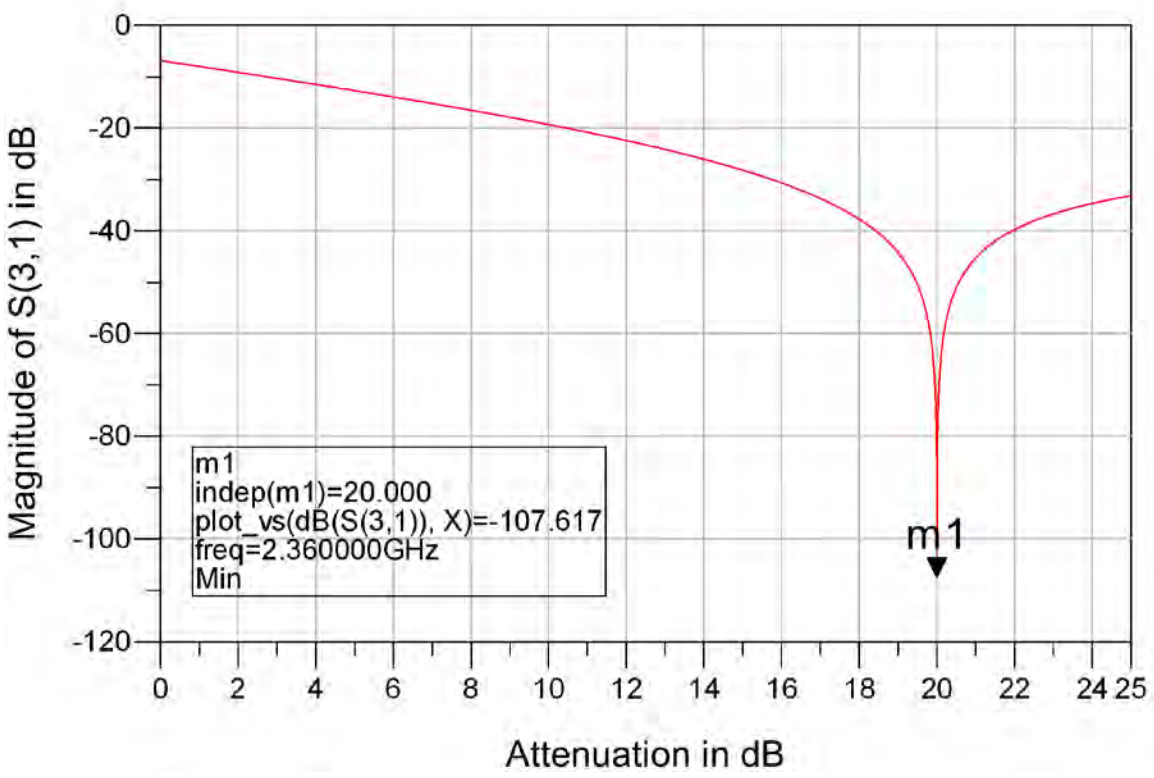

Figure 19. Magnitude of S_{31} under the influence of non-ideal power splitter.

When comparing the results in Figure 9 to those in Figure 19, we observe that there is minimal change in the attenuator loss of the LCC in both cases. There is an improvement in the cancellation performance of the non-ideal case where a deeper notch of −107.617 dB is achieved. It is because part of the residual can be cancelled further by the reflection.

2. Non-ideal Circulator

Using the specification of a non-ideal circulator from Table 1, we set the parameters of the circulator as shown in Figure 20. With this model, there is a 20 dB loss when the circulator is operating below 2.0 GHz or above 4.0 GHz. When operating the circulator between 2.0 and 4.0 GHz, there is an insertion loss of 0.4 dB. The simulation is conducted with the settings listed in Section 1, and in this case, the non-ideal models for both the power splitter and the circulator were used.

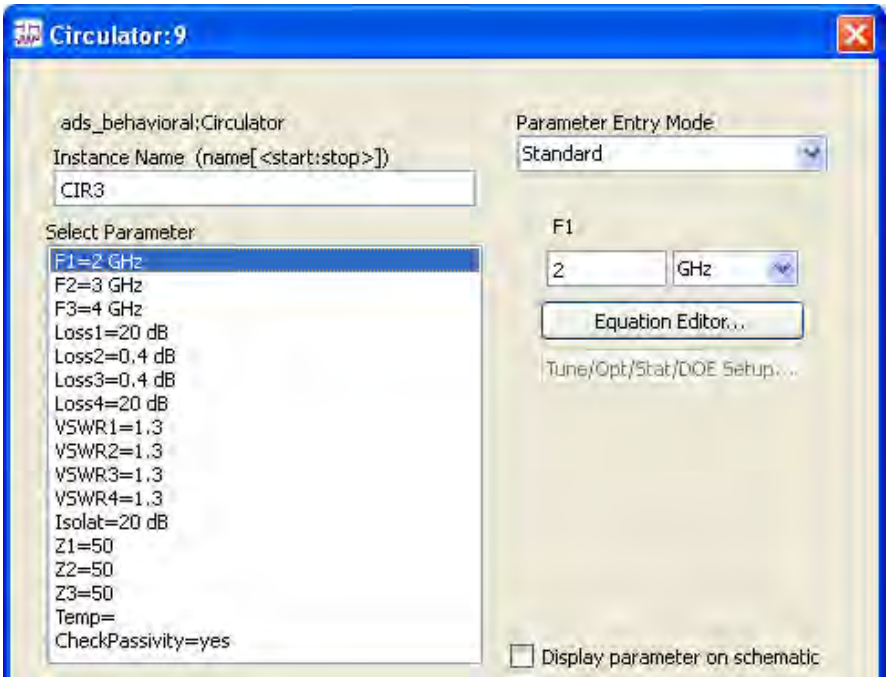

Figure 20. Setting for more realistic circulator modeling.

The combined effect of a non-ideal circulator and power splitter is shown in Figure 21. When comparing the magnitude of S_{31} in Figure 9 and Figure 21, we see that

there is a slight drop in the required loss of the attenuator of the LCC from 19.99 dB to 19.93 dB. We also observe that the cancellation is improved with a deeper notch at −115.276 dB.

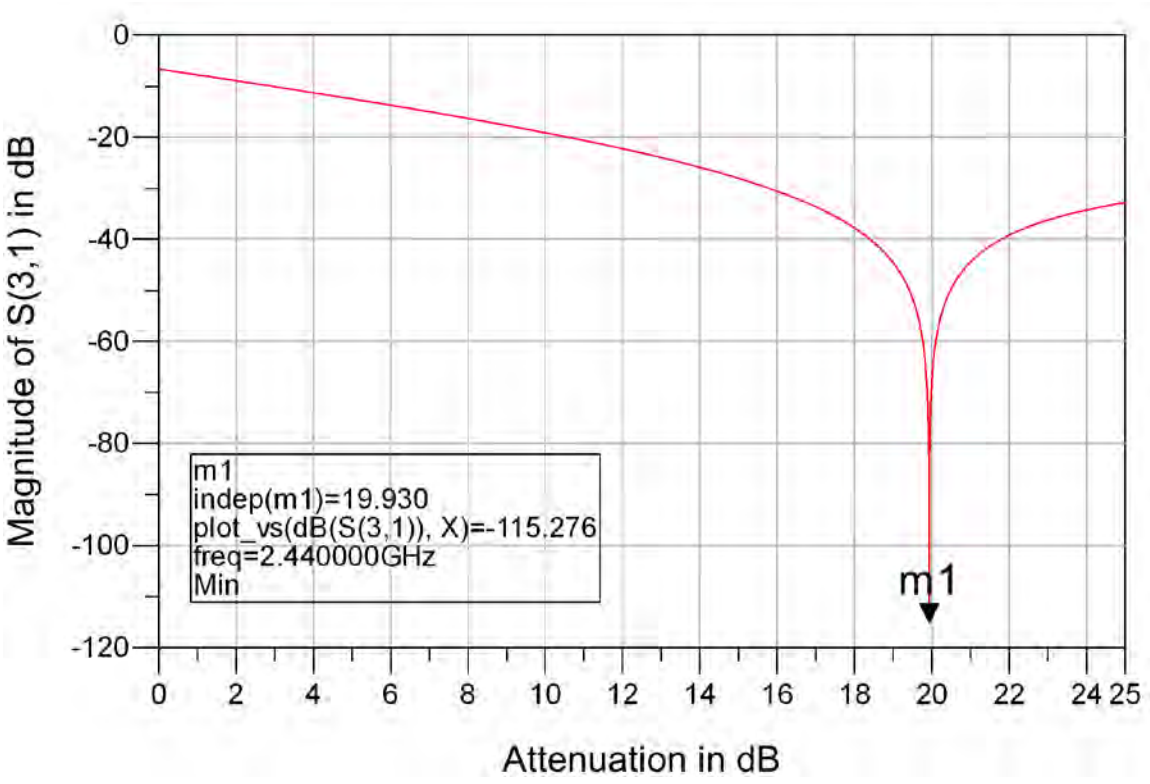

Figure 21. Magnitude of S_{31} under the influence of non-ideal circulator and power splitter.

3. Non-ideal Phase Shifter

In [14], it is stated that a 1.0°/GHz phase shift is equal to 2.78 psec of time delay. Since the phase shifter has a 0.45 psec of nominal time delay, this equates to 161.871°/GHz of phase shift. For our simulation, the LCC operates from 2.36 GHz to 2.44 GHz, and in this range of frequency, the phase shifter is expected to have an error of ±6.475° if the center frequency is set at 2.4 GHz.

In ADS, the phase slope of the phase shifter is modeled by

$$\theta(f) = Phase(f_{start}) + PhaseSlope\left[Log_2\left(\frac{f}{f_{start}}\right)\right] \quad (6)$$

where, $\theta(f)$ is the phase shift at frequency f, $Phase(f_{start})$ is the phase change at the initial frequency f_{start} and $PhaseSlope$ is change of phase with frequency in a frequency octave due to the imperfection of the component.

At 2.36 GHz and 2.44 GHz, the phase shift is 186.475° and 173.525°, respectively. By assigning f_{start} to be 2.36 GHz and substituting the phase shift and frequency into Equation (6), the phase slope is found to be about −270°/frequency octave. The settings for the phase shifter used for the simulation are shown in Figure 22.

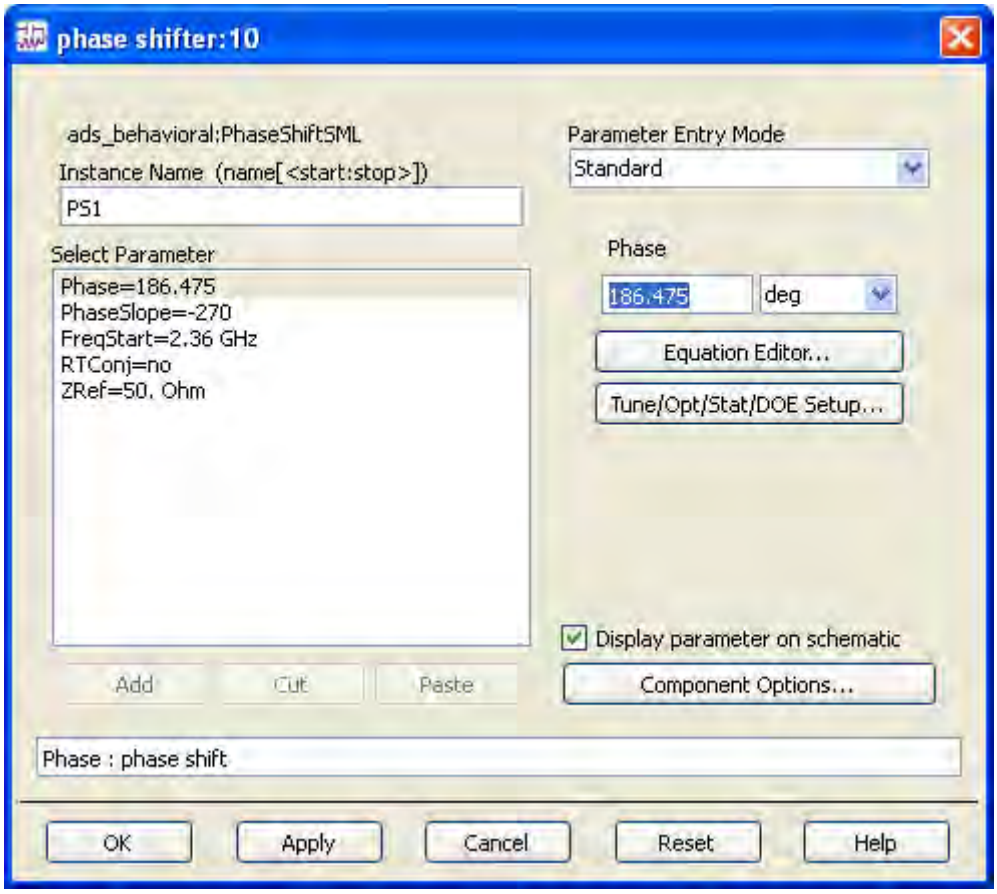

Figure 22. Settings for non-ideal phase shifter.

In order to model the insertion loss of the phase shifter, an additional attenuator (*ATTEN*2) is placed before the phase shifter as shown in Figure 23. The modeling is carried out this way because the basic phase shifter model in ADS does not model loss and VSWR.

The simulation is repeated for source frequency of 2.36 GHz, 2.4 GHz and 2.44 GHz, and the loss of the attenuator of the LCC is varied from 0 to 25 dB in steps of 0.01 dB. The combined effects of the non-ideal circulator, power splitter and phase shifter are shown in Figure 24.

In Figure 24, the magnitudes of S_{31} at 2.36 GHz and 2.44 GHz are plotted in blue, and the parameter at 2.4 GHz is plotted in red. It can be seen in Figure 24 that as the phase of the cancellation signal shifts with the change in operating frequency, the performance of the LCC is degraded and the deep notch disappears. This is because LCC is unable to maintain a phase difference of 180^{o} for perfect cancellation of the leakage signal.

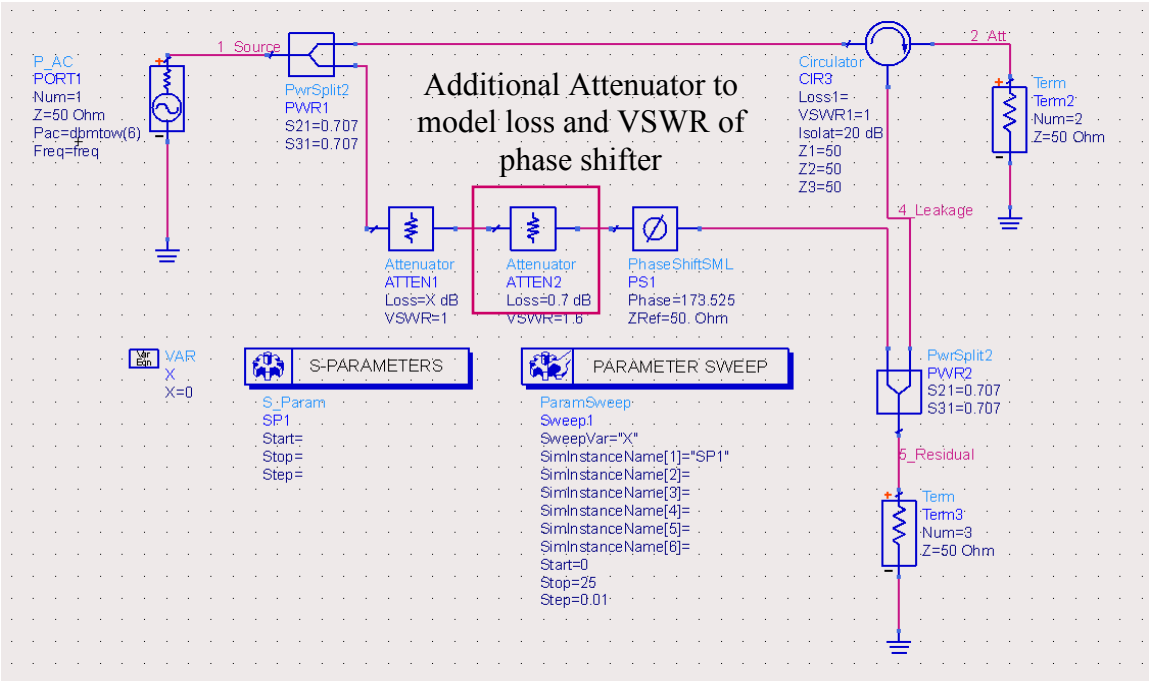

Figure 23. Simulation model for non-ideal components.

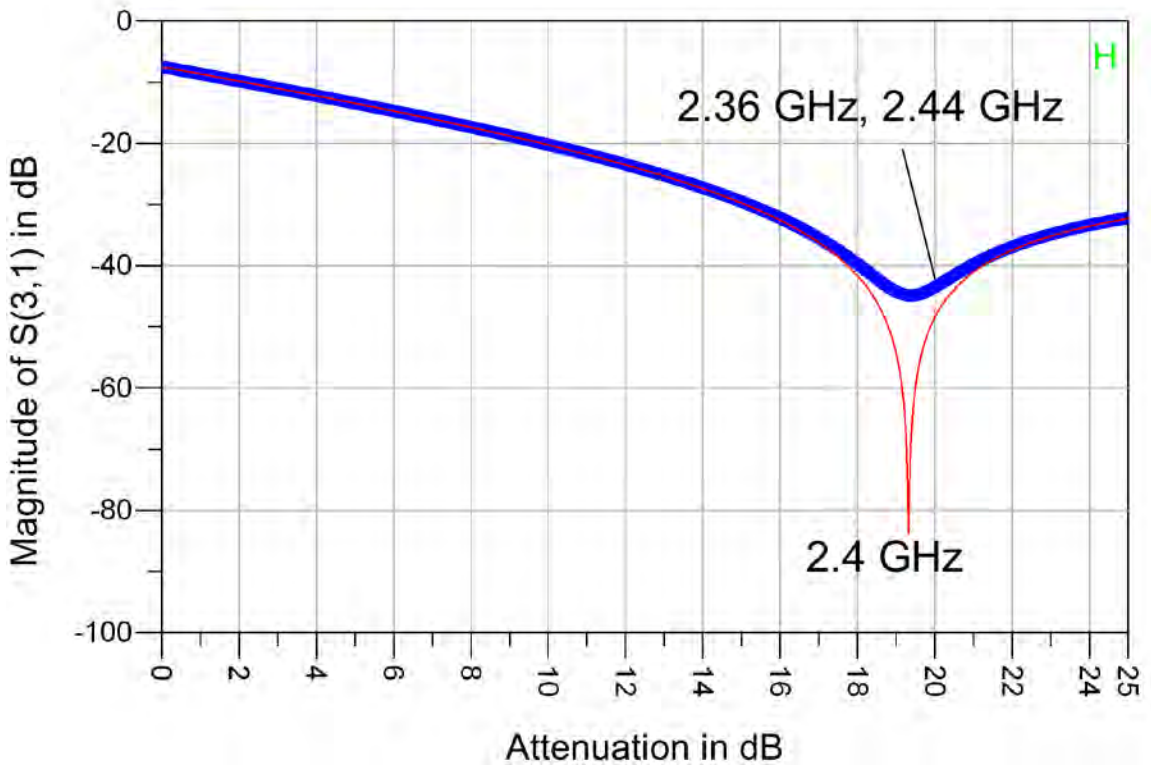

Figure 24. Effects of non-ideal components on magnitude of S_{31}.

By fixing the attenuation of the LCC at 19.320 dB (the location of deep notch in Figure 24, at 2.4 GHz) the simulation is repeated for 2.36 GHz to 2.44 GHz in steps of 1.0 MHz. The magnitude and phase responses of the S_{31} parameter are shown in Figure 25 and Figure 26, respectively.

As shown in Figure 25 and Figure 26, the response of the S31 parameter, which is related to the residual signal, is changed significantly from the ideal case when imperfect components are introduced. The actual phase shifter is unable to maintain a fixed phase change of 180o at all the operating frequencies. As a result, the behavior of the LCC is no longer wideband as can be seen in Figure 25. The notch disappears when the operating frequency is shifted from 2.4 GHz.

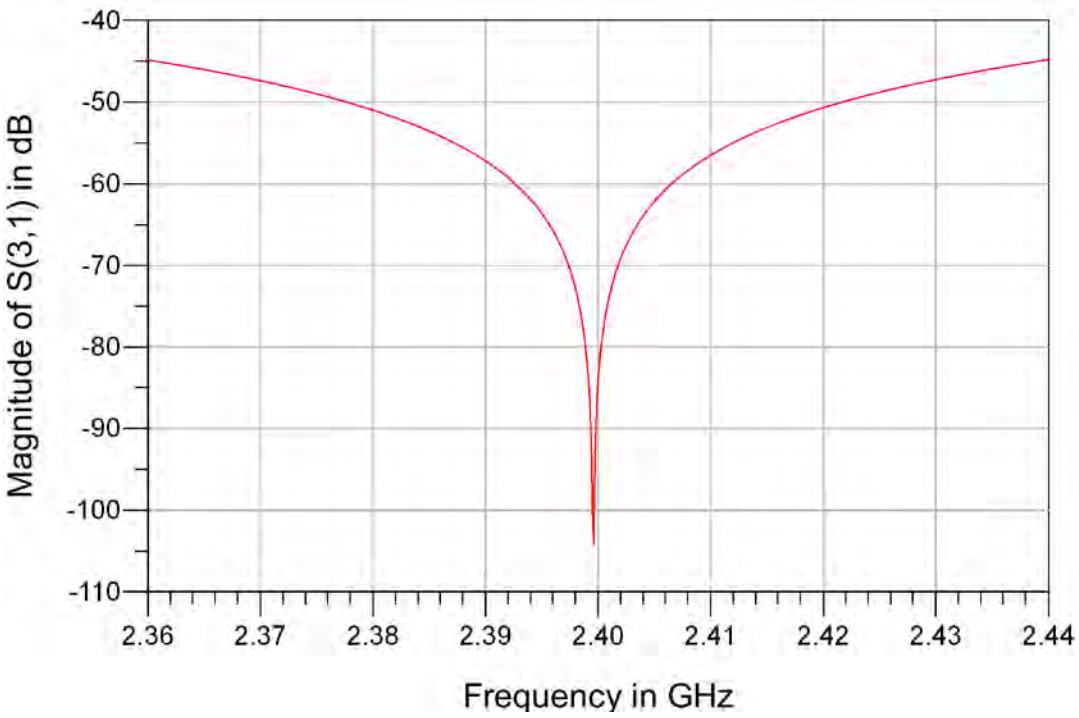

Figure 25. Magnitude of S_{31} parameter versus frequency with non-ideal components.

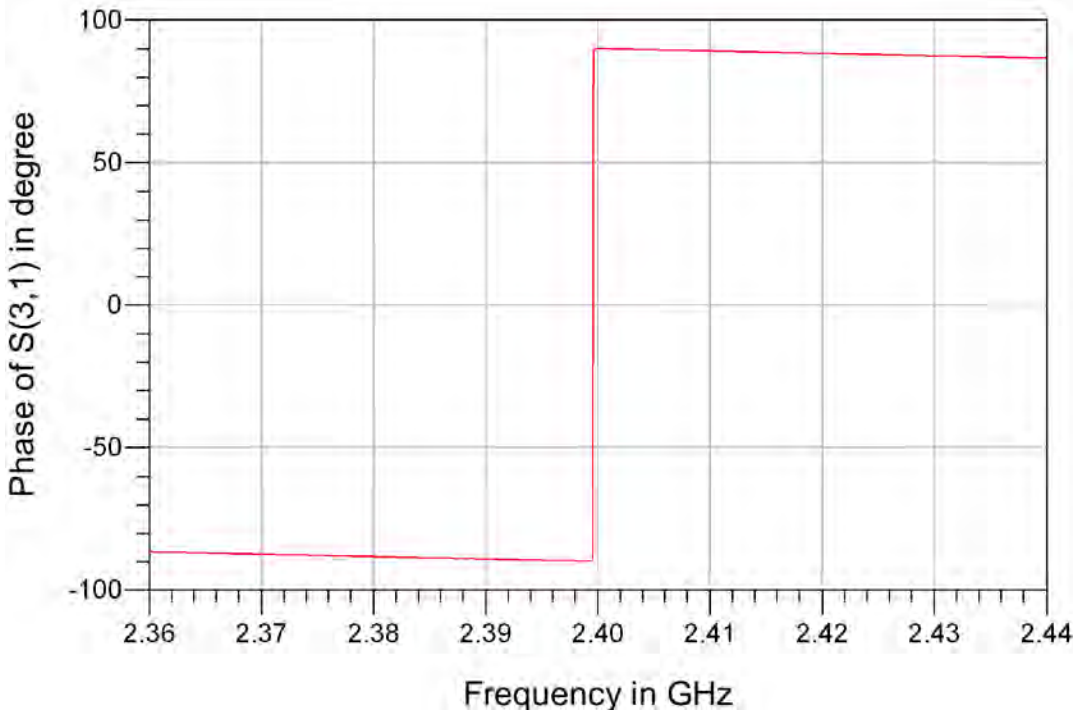

Figure 26. Phase of S_{31} versus frequency with non-ideal components.

F. SUMMARY

In this chapter, analysis of the ideal LCC was presented, and it was shown that the ideal LCC exhibits the characteristics of a wideband cancellation circuit with ideal components. Effects of a mismatched load antenna were presented, and from the analysis, it was shown that by retuning the LCC, the residual signal power level can be lowered.

The cancellation performance of the LCC is limited by the precision of the components used in the simulation. In actual LCC hardware implementation, the performance may be further degraded due to limitation of hardware components.

The imperfection of the components introduces reflection and phase distortion that degrade the bandwidth of the LCC. With a phase slope introduced in the phase shifter of the LCC, the LCC can no longer maintain a constant cancellation magnitude throughout the operating range of frequencies.

In the next chapter, analysis of a FDMC model for WLCC is presented. Investigation into the phase slope and its effect on performance of the WLCC is reviewed.

THIS PAGE INTENTIONALLY LEFT BLANK

III. WIDEBAND LCC

In Chapter II, it was shown that the cancellation power of the LCC was reduced by the imperfections in the hardware components such as mismatched load impedance and losses in phase shifters. The frequency dependent phase characteristics of phase shifters further degrade the performance of the LCC by narrowing its cancellation bandwidth. In this chapter, a WLCC design based on the FDMC is presented. An analysis on the magnitude and phase response of the WLCC is carried out. Phase alignment techniques that can be used for compensating for phase errors in the WLCC and phase shifter are investigated.

A. INTRODUCTION

The concept of the FDMC is to divide the entire operating frequency band into multiple frequency sub-bands, and on each sub-band, a narrow band LCC is applied. The signals in each sub-band are then multiplexed to give a wideband cancellation signal that subtracts the leakage signal. In [11], a FDMC based WLCC using elliptic band-pass filters and power splitters was proposed. The ADS model is shown in Figure 27. In this ADS model, an AC simulator is used so that signal characteristics can be observed at any point in the circuit, unlike the S-parameters simulator that only allows observations to be made at the terminations. The source power is set at 6.0 dBm for the simulation shown in Figure 27.

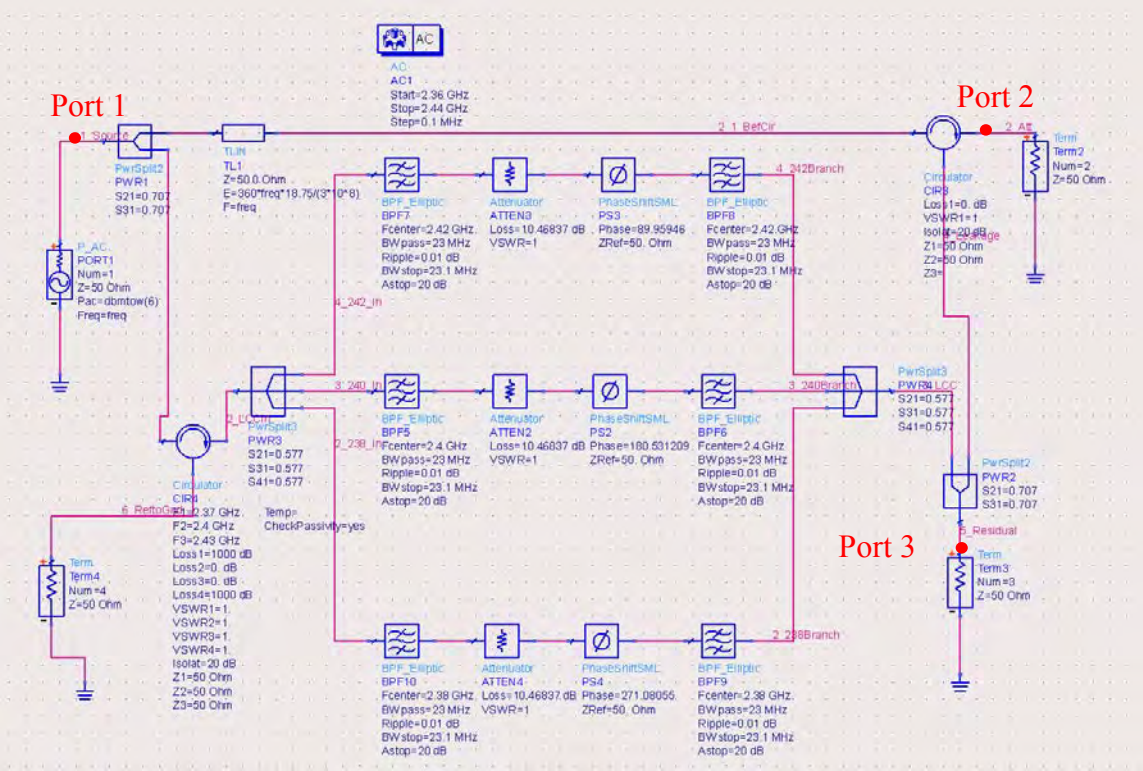

Figure 27. ADS model of WLCC with FDMC using power splitters (After [11]).

As shown in Figure 27, the WLCC is divided into three frequency branches. Each branch is designed with a pass-band of 20 MHz and center frequencies of 2.38 GHz, 2.40 GHz and 2.42 GHz. In each sub-band, elliptic filters are selected to separate the desired frequency because of the steeper roll off in the magnitude response in the stop-band. An arrangement employing power splitters vice circulators in the WLCC design was recommended in [11] because the phase response was more linear compared to the case of using circulators. The model of WLCC with circulators is shown Figure 28.

It should be noted that the design of the elliptic filters and narrowband LCC in both Figure 27 and Figure 28 are the same. The only difference between the two designs is in the components used for multiplexing and demultiplexing sub-band signals.

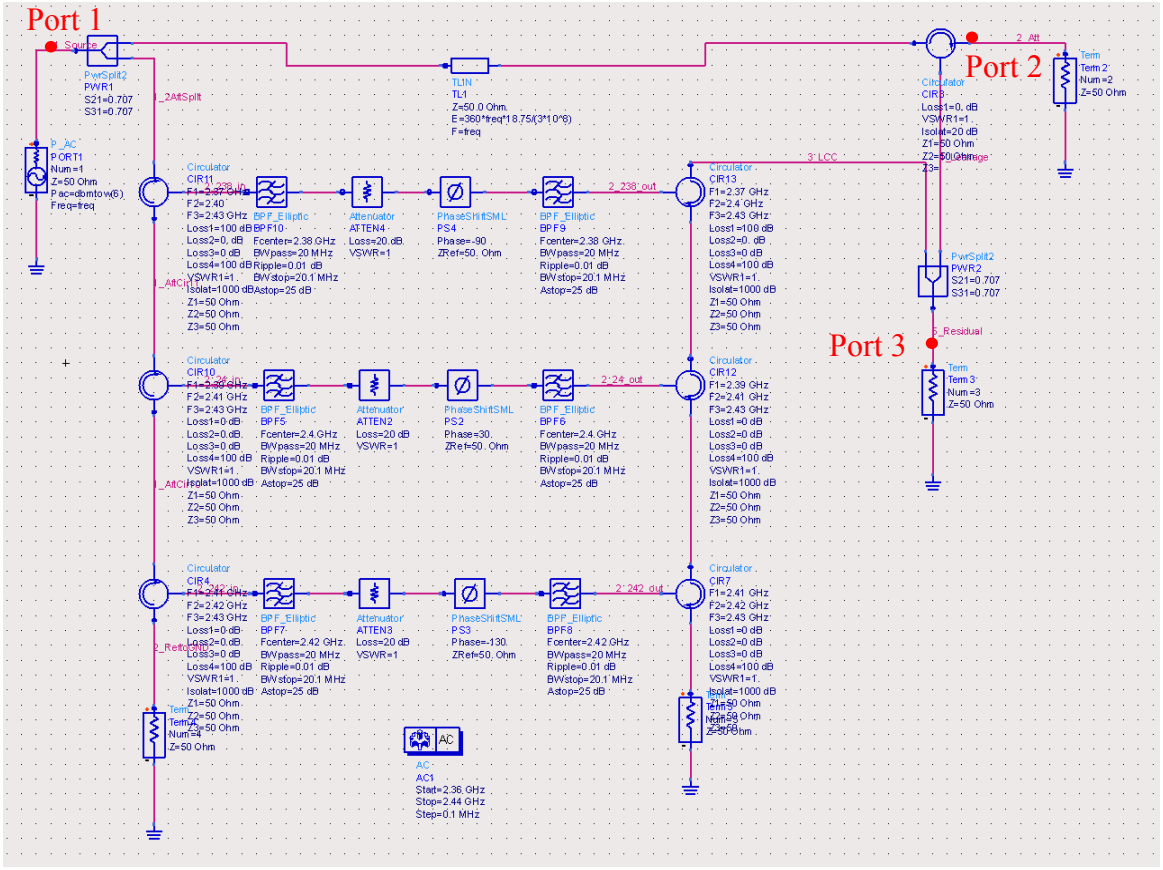

Figure 28. ADS model of WLCC with FDMC using circulators (After [11]).

B. RESPONSE OF WLCC

In this section, analysis on the magnitude and phase response of the WLCC is presented. Analysis of the magnitude and phase response of the WLCC helps to determine if the leakage signal can be subtracted coherently by the cancellation signal.

1. Magnitude Response of the Residual Signal

The ADS models that are shown in Figure 27 and Figure 28 are simulated with a source signal power of 6.0 dBm in the frequency range from 2.36 GHz to 2.44 GHz in steps of 1.0 MHz. The amplitude of the residual signal (*Port* 3 shown in Figure 27 and Figure 28) are shown in Figure 29 and Figure 30.

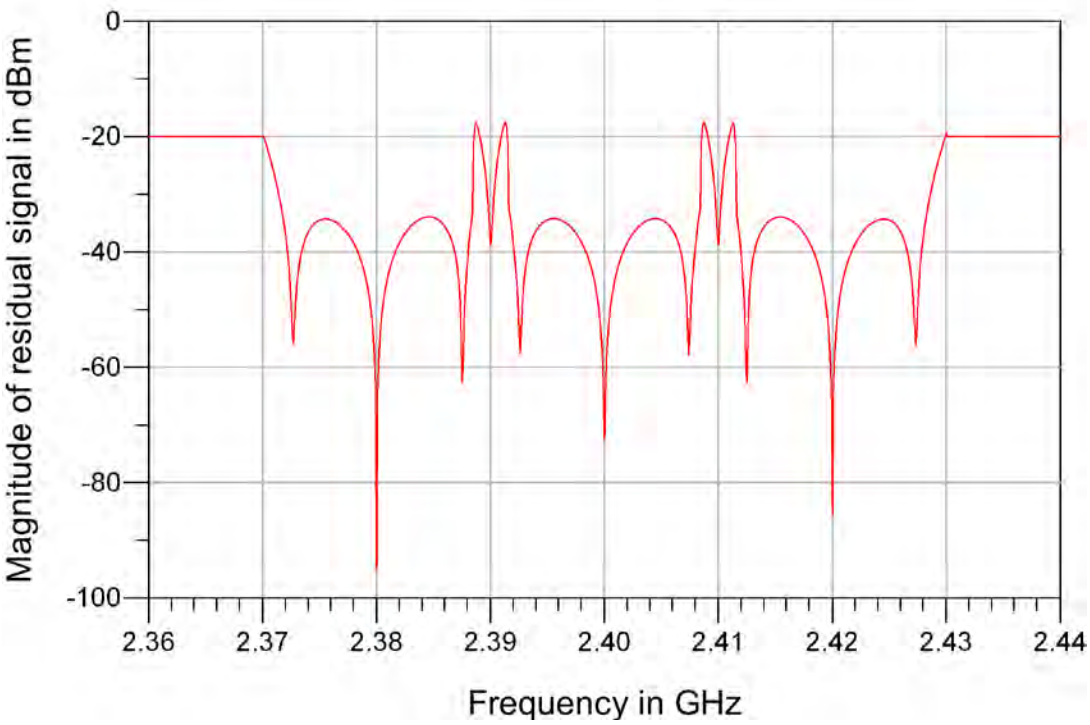

Figure 29. Amplitude of residual using FDMC with power splitters (After [11]).

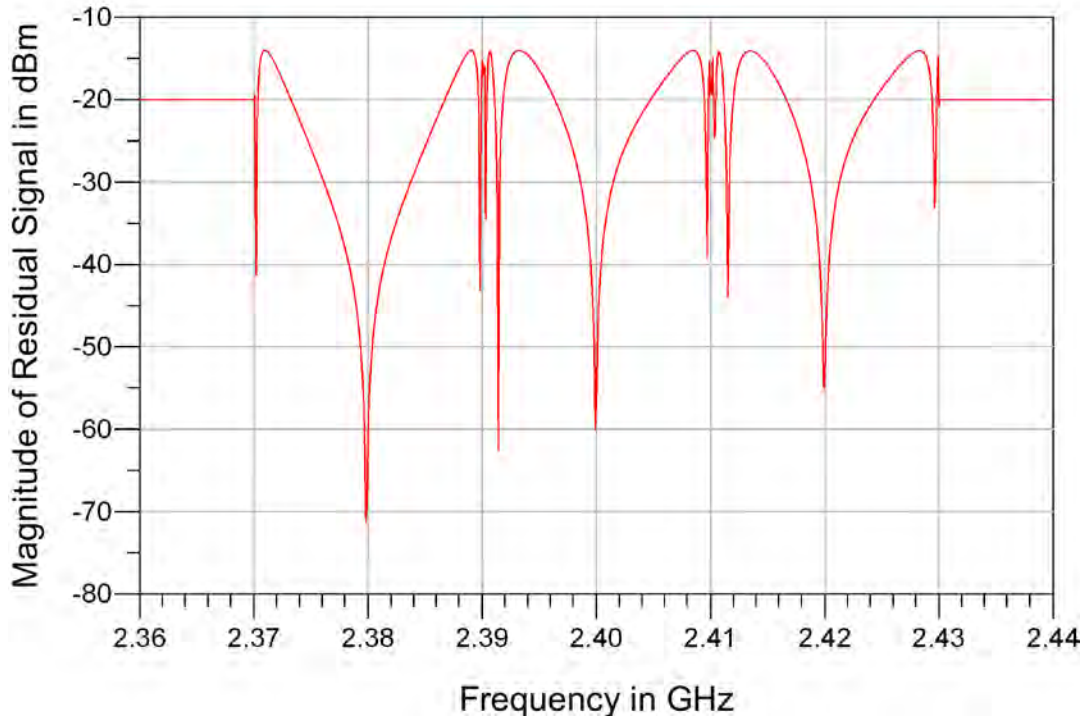

Figure 30. Amplitude of residual signal using FDMC with circulators (After [11]).

The amplitude of the residual signal shown in Figure 29 and Figure 30 is processed using Matlab to determine the average power level over the frequency band of interest. The mean amplitude of the residual signal for the case where power splitter is used is found to be −33.142 dBm on average. For the case where circulator is used, the residual signal is found to be −23.155 dBm on average. This is consistent with the results presented in [11]. It was recommended that the design with power splitters be adopted because of the higher cancellation power. From Figure 29 and Figure 30, we observe that the residual power level is significantly higher than what is expected from coherent cancellation presented in Section B of Chapter II. Therefore, it is deduced that the output of the WLCC cannot coherently cancel the leakage signal.

In order to identify the possible source of amplitude imbalance in the WLCC design, the magnitude response of each model is plotted and analyzed. The amplitude of the LCC output for the case where power splitter is used is shown in Figure 31.

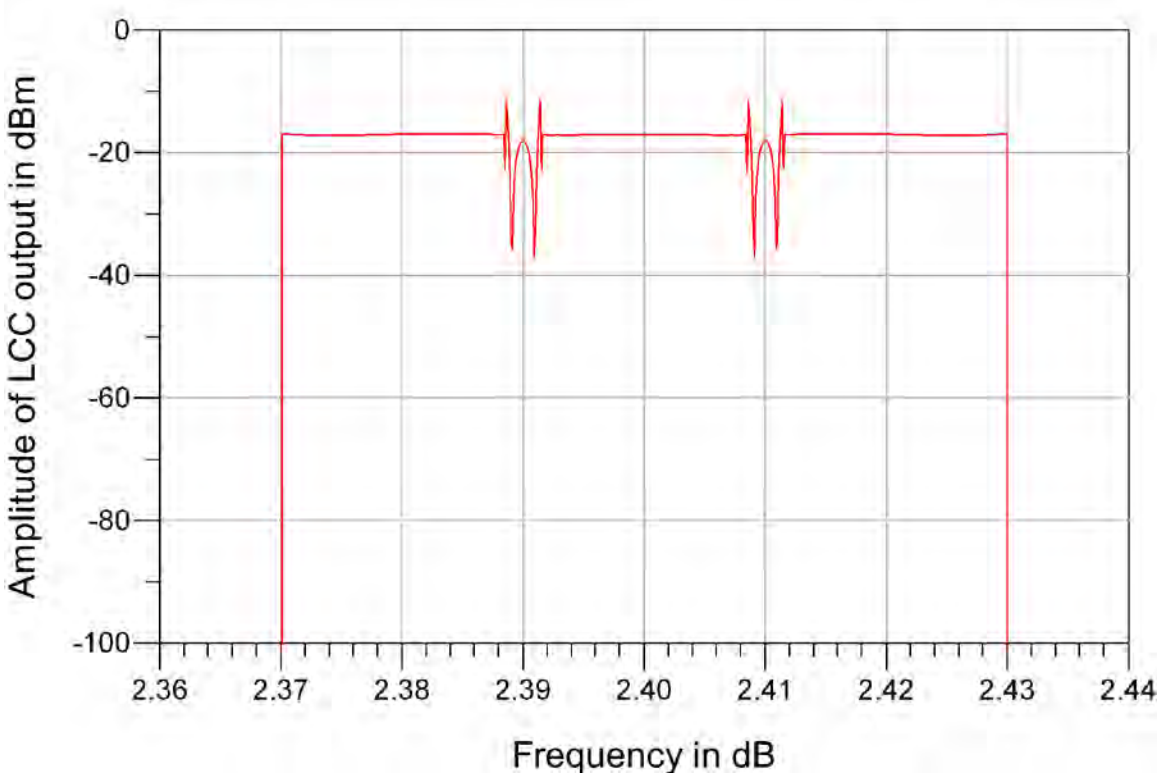

Figure 31. Cancellation signal using FDMC with power splitters (After [11]).

It is observed from Figure 31 that there are some ripples occurring at the boundaries of the frequency sub-bands. The variations in the magnitude response with frequency introduces amplitude imbalance in the WLCC design as the cancellation loss is no longer uniform throughout the frequency band of interest. It is also noticed that the LCC output has a sharp cut-off at frequencies lower than 2.37 GHz and higher than 2.43 GHz. It is because the WLCC is designed specifically for the frequency band from 2.37 GHz to 2.43 GHz

The amplitude of the WLCC output in the case where circulators are used is shown in Figure 32. In this case, it can be observed from Figure 32 that the magnitude response of the WLCC is almost uniform throughout the band of interest. Such frequency independent magnitude response (within the pass-band) is desired as it minimizes the occurrence of amplitude imbalance. In Figure 32, again it is noticed that there is a sharp cut-off at frequencies lower than 2.37 GHz and higher than 2.43 GHz. This is because the WLCC is designed specifically for the frequency band of interest.

Figure 32. Cancellation signal using FDMC with circulators (After [11]).

2. Effects of Phase Imbalance

As discussed in Chapter II, it is important for the LCC output to maintain 180^{o} phase shift with respect to the leakage signal through the entire frequency band of interest to achieve coherent cancellation. Frequency dependency of the phase response in the LCC leads to narrowband leakage cancellation if it is not corrected as discussed in Section D of Chapter II. In this section, the phase response of the WLCC for both FDMC designs is investigated. In Figure 33, the phase response of the LCC output where power splitters are used is shown.

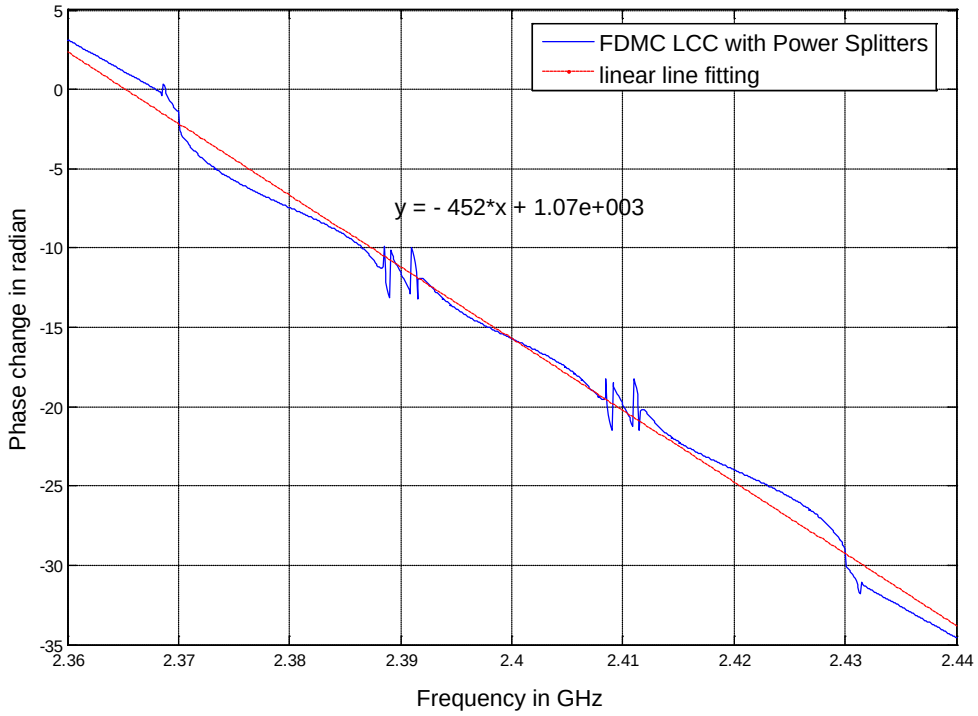

Figure 33. Phase change of signal through WLCC using FDMC with power splitter versus frequency.

The phase change between the input and output signal through the WLCC is shown in Figure 33. The phase response of the WLCC is dependent on the frequency and follows a negative phase slope in general. By fitting the phase response of the WLCC to

a straight line using the linear regression technique in Matlab, the phase slope is found to be −452 radians/GHz.

In the case where circulators are used in the LCC, the insertion phase of the LCC is as shown in Figure 34. It is observed in Figure 34 that the phase change in the cancellation signal is more oscillatory when compared to the case where power splitters are used. It is also found that the phase slope is about −1650 radians/GHz in the case where circulators are used.

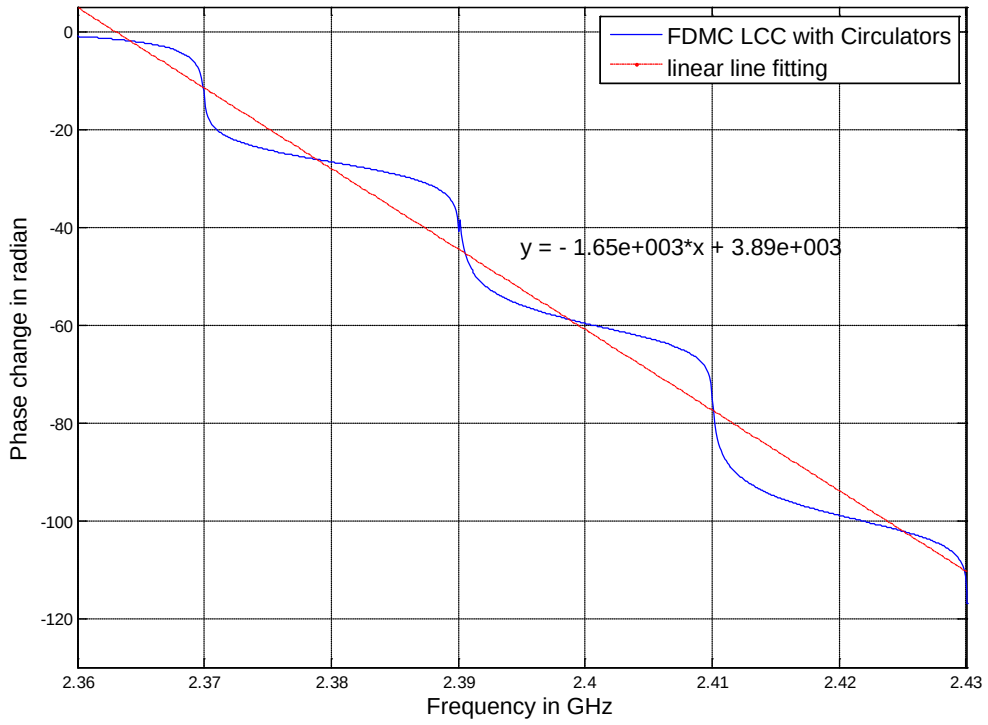

Figure 34. Phase change of signal through WLCC using FDMC with circulator versus frequency.

From Figures 33 and 34, it can be observed that the phase change in FDMC LCC is frequency dependent in general. Even though the phase slopes are not exactly linear, the phase slope of the LCC must match the phase slope of the leakage signal. As discussed in Section D3 of Chapter II, phase change that is frequency dependent must be compensated or it reduces cancellation. There is a need to align the phase slope of the

LCC with the leakage signal for coherent cancellation. In the next section, a technique of phase alignment using shunt and series stubs is presented.

C. PHASE SLOPE ALIGNMENT

1. Concept of Phase Slope Alignment

The concept of the phase slope alignment in LCC is shown in Figure 35. The LCC is represented using an attenuator and a non-ideal phase shifter (PS1) as discussed in Section D of Chapter 2 and shown in Figure 35. An additional phase shifter (PS2) is placed along the leakage path. The phase slope of PS2 is adjusted to match the phase slope of the phase shifter in the LCC model so that the leakage signal is coherently subtracted by the cancellation circuit. A simulation using a source frequency from 2.36 GHz to 2.44 GHz in 1.0 MHz steps and with LCC attenuation sweeping from 0 dB to 24 dB in steps of 0.01 dB was conducted. The plot of residual power with LCC attenuation is shown in Figure 36.

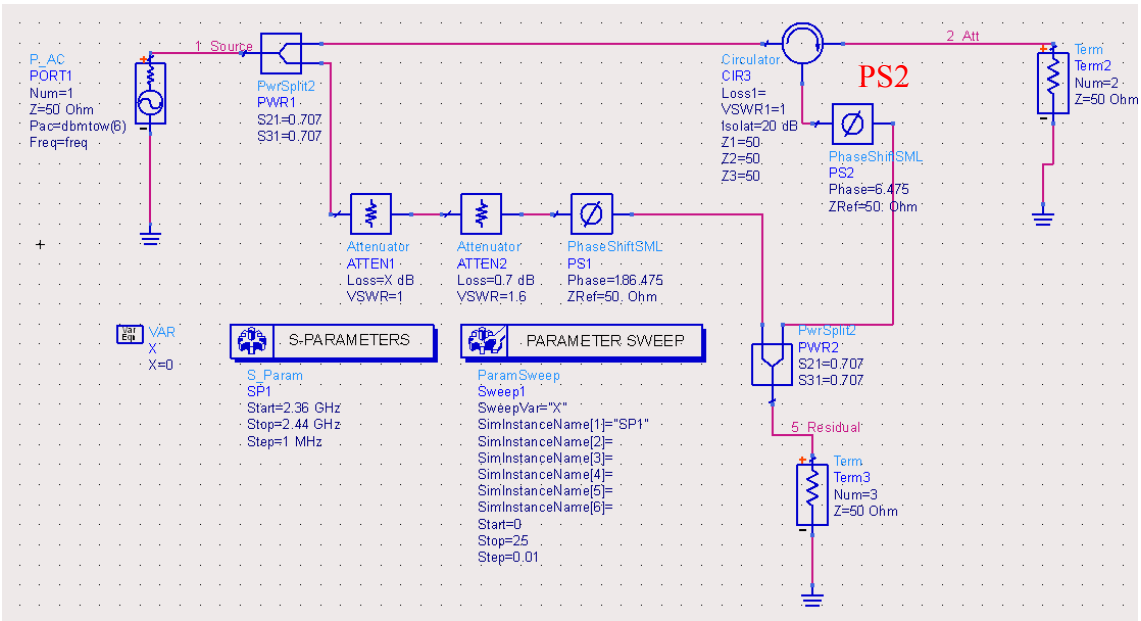

Figure 35. Model of LCC with phase slope alignment.

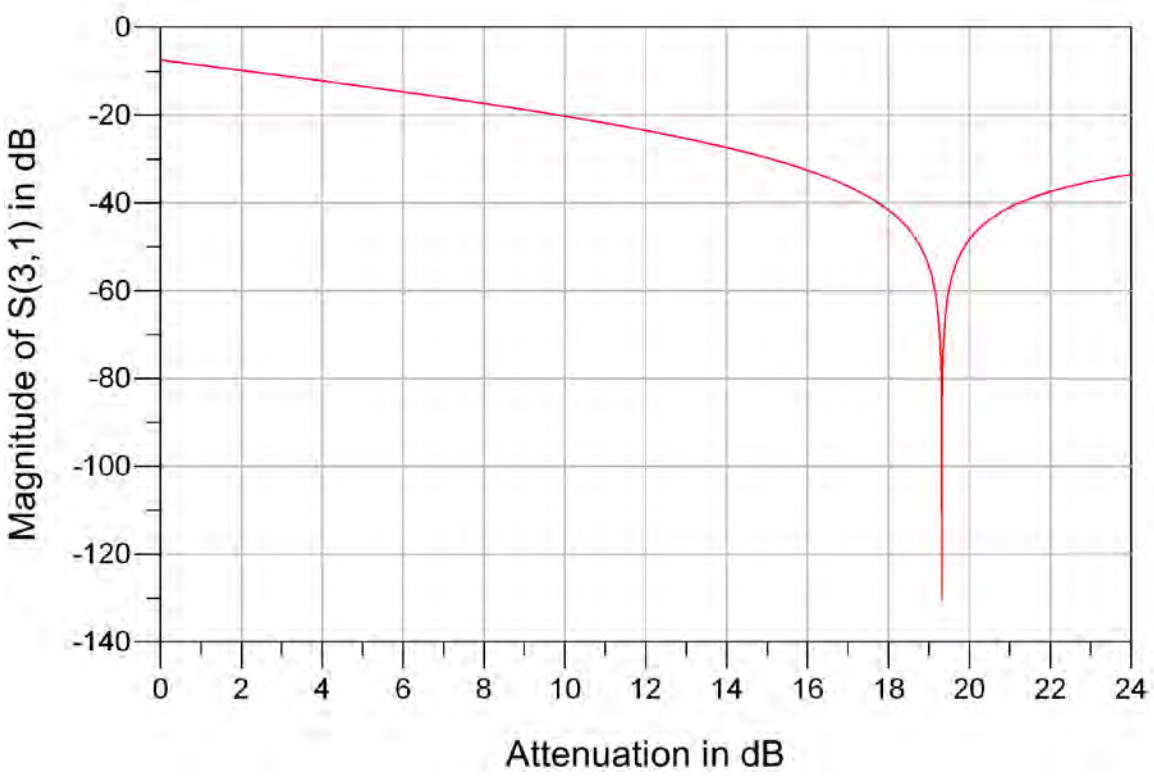

Figure 36. Magnitude of residual power versus attenuation in LCC over frequency of 2.36 GHz and 2.44 GHz.

By tuning the attenuator in the LCC, the deep notch in cancellation is achieved as shown in Figure 36. It is also shown that by aligning the phase slope of the leakage signal and cancellation signal, it is possible to reduce the residual power to a minimal level, below −130 dB in this case, at all frequencies (the frequency curves overlay each other in Figure 36). However, manufacturing processes can limit consistency in hardware performance, and it will be challenging to find two phase shifters with identical phase slopes for this application. Also, the phase slope of the circulator and antenna mismatch must also be compensated for in some manner.

2. Shunt Stub Circuit for Phase Slope Alignment

A phase slope alignment circuit can consist of stubs of transmission line connected in series and parallel as shown in Figure 37. Using stubs for phase shift and

phase slope alignment is commonly used in the design of phase shifters [15]–[17]. For the purpose of analysis, stub lengths of a quarter wavelength are considered.

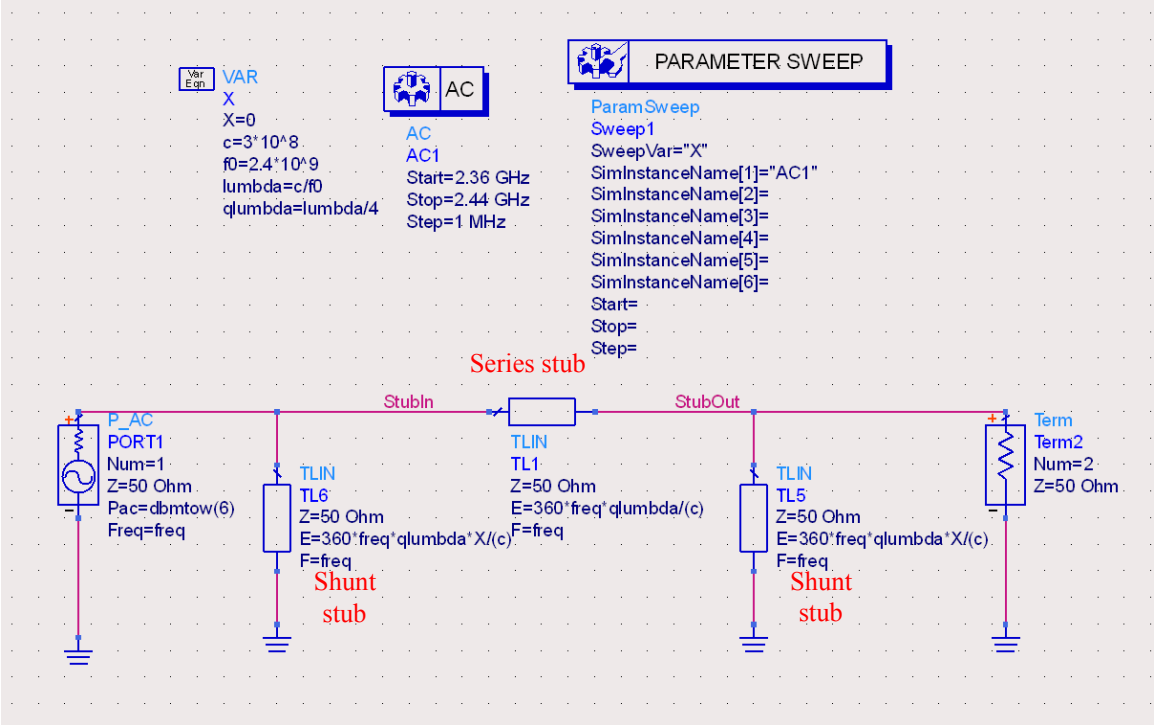

Figure 37. Phase slope alignment circuits consisting of quarter wave length stubs connected in series and parallel.

In Figure 37, the phase slope alignment circuit consists of two sets of shunt stubs a quarter wavelength long that are grounded. An additional quarter wavelength series stub is connected between the two grounded stubs. Using ADS, we simulated the phase slope alignment circuit with a source signal of frequency ranging from 2.36 GHz to 2.44 GHz in steps of 1.0 MHz. Therefore, the center frequency for the simulation is 2.40 GHz, and the wavelength at 2.40 GHz is 0.125 m. The phase response of the phase slope alignment circuit is shown in Figure 38.

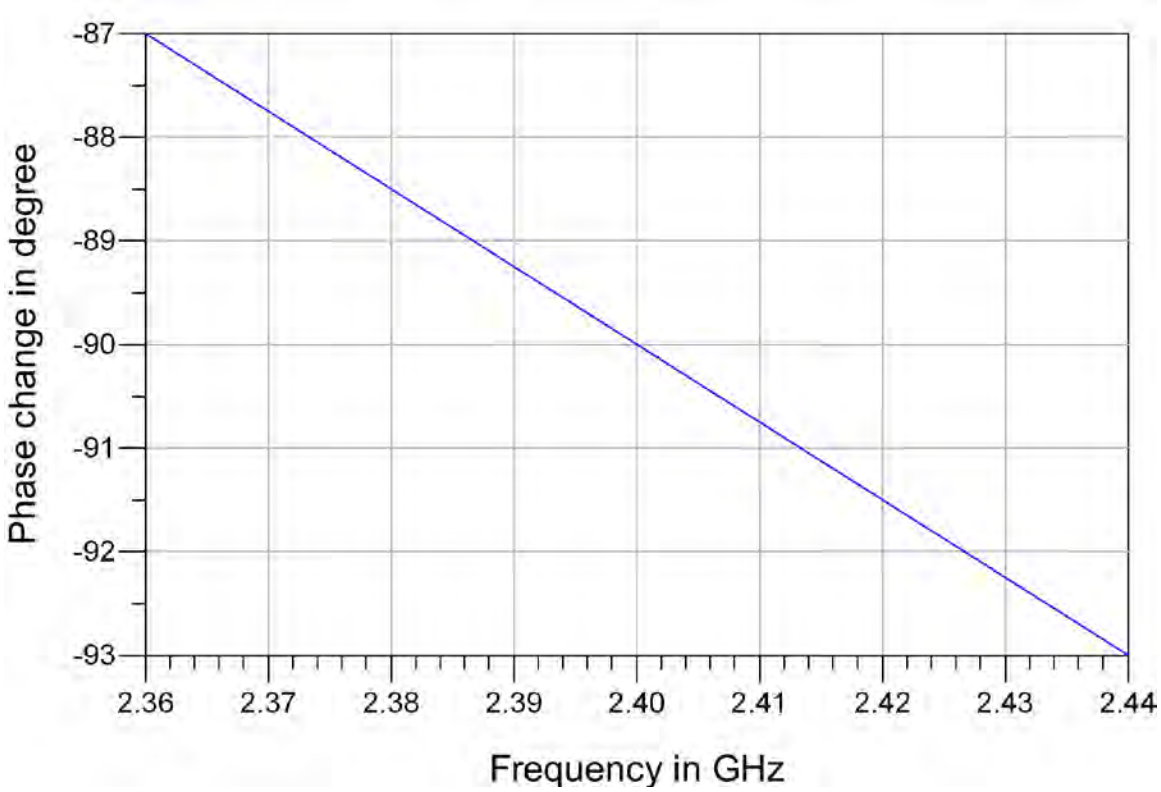

Figure 38. Phase response of the quarter wavelength stub phase slope alignment circuit.

In general, the phase slope of the alignment circuit is observed to be negative with the increasing frequency as seen in Figure 38. Various lengths of grounded shunt stubs and series stub are simulated in ADS to determine the required length of stubs to compensate the phase slope in the WLCC. The variation of phase slope with stub length is shown in Table 2. Two basic configurations were simulated. In the first configuration, the length of the series stub is fixed at quarter wavelength, and the shunt stubs are increased in multiples of a quarter wavelength. In the second configuration, the length of the shunt stubs are fixed at a quarter wavelength, and the length of the series stub is increased in multiples of a quarter wavelength.

Table 2. Variations of phase slope with stub length.

Shunt Stub length (λ)	Series Stub length (λ)	Phase slope (degree/GHz)	Phase shift at 2.40 GHz (degree)
0.25	0.25	−75	−90
0.75	0.25	−150	−90
1.25	0.25	−225	−90
1.75	0.25	−300	−90
2.25	0.25	−375	-90
2.75	0.25	−450	−90
0.25	0.25	−75	−90
0.25	0.5	−75	−180
0.25	0.75	−150	−270
0.25	1	−150	0
0.25	1.25	−225	−90
0.25	1.5	−225	−180
0.25	1.75	−300	−270
0.25	2	−300	0
0.25	2.25	−375	−90
0.25	2.5	−375	−180
0.25	2.75	−450	−270
0.25	3	−450	0

In the first configuration, when the grounded shunt stubs are varied in steps of an integer number of half wavelength (for example, half a wavelength, 1.0 wavelength and 1.5 wavelength), it is observed from the simulation that the alignment circuit acts like an short circuit at the center frequency of 2.4 GHz. Therefore, the cases where the shunt stubs are an even number of a quarter wavelength are not considered for this application. It is observed that when the length of the series stub is fixed at a quarter wavelength, there is always -90^{o} phase change in the input signal. As the length of the shunt stubs increases by an interval of a quarter wavelength, the phase slope of the phase response decreases at a rate of -75^{o}/GHz.

For a second configuration, where the length of the shunt stubs are fixed at a quarter wavelength, the phase response of the circuit decreases by multiples of -90^{o} whenever there is an increase in the length of the series stub by a quarter wavelength. It is also observed that the phase slope of the phase alignment circuit reduces at a rate of -75^{o}/GHz as the length of the series stub increases in intervals of a half a wavelength.

Based on previous simulations in Chapter II and Section B2 of this chapter, the phase slope introduced by the non-ideal phase shifter and FDMC-based WLCC are shown in Table 3.

Table 3. Phase slope introduced by various WLCC configurations.

Case	LCC Design	Phase slope
1	LCC with attenuator and non-ideal phase shifters	-161.861^{o}/GHz, or -270^{o}/frequency octave
2	FDMC with power splitters	−452 radians/GHz, or -25897.692^{o}/GHz
3	FDMC with circulators	−1650 radians/GHz, or -94538.036^{o}/GHz

In order to achieve zero phase shifts along the leakage path, the second configuration is used, where the length of the shunt stubs is set to a quarter wavelength. The length of the series stub is determined by using the case where the phase slope is the closest to that of the LCC branch. For case one in Table 3 (non-ideal phase shifter), the phase slope of the cancellation path is -161.861^{o}/GHz; therefore, to achieve no phase change in the leakage path with the matching path slope, the configuration with quarter wavelength shunt stubs and 1.0 wavelength series stubs is used (in Table 2). For the case where a FDMC with power splitters is used, the phase slope of the cancellation path is -25897.692^{o}/GHz, but it is also observed that the phase change at 2.4 GHz is -905.746^{o}. This makes it difficult to design a phase slope alignment circuit that has a phase change of -905.746^{o} at center frequency of 2.4 GHz. Similarly, for the case of FDMC where circulators are used, there is a phase shift of -3427.794^{o} at 2.4 GHz. The irregularities in the phase slope curves of the FDMC designs can potentially reduce the effectiveness of

the phase slope alignment circuit. Therefore, in order to reduce the complexity and maximize the effectiveness of the LCC design, the two FDMC designs are not considered for further analysis. A summary of the length of the series stub required for the LCC configuration is shown in Table 4. The corresponding phase slope of the phase alignment circuit is also shown in Table 4.

Table 4. Length of shunt stubs for LCC design.

Wideband leakage cancellation circuit configuration	Length of series stub (wavelength)	Corresponding phase slope of phase alignment circuit (degree/GHz)
LCC with attenuator and non-ideal phase shifter	0.5	−150

When comparing data in Table 3 with that in Table 4, we find the errors in the phase slopes between the cancellation and leakage paths to be 11.861^{o}/GHz. The phase slope alignment circuit is designed and applied on the leakage path in ADS. The results and analysis are shown in the next section.

3. Application of Shunt Stub Circuit to the Leakage Path

As discussed in Section B3, the required length of the series stub is half a wavelength, and the phase slope alignment circuit is applied on the leakage path as shown in Figure 39. The simulation is carried out with source signal of frequency ranging from 2.36 GHz to 2.44 GHz in steps of 1.0 MHz. The loss of the attenuator in the LCC is swept from 0 to 25 dB in steps of 0.01 dB. The source power is set at 6.0 dBm, and an AC simulator with parameter sweep is used for this simulation.

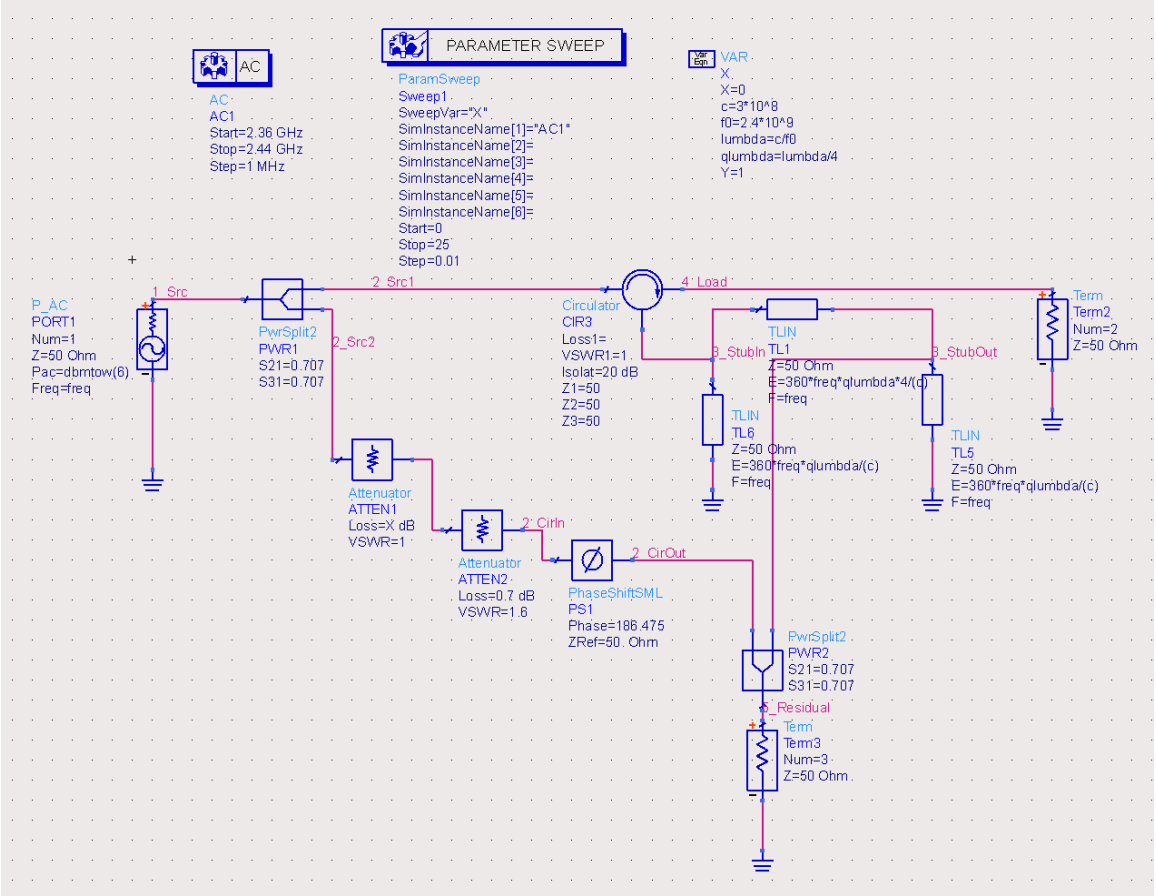

Figure 39. Application of phase slope alignment circuit on LCC with non-ideal circulator.

The amplitude of the residual signal versus the attenuation in the cancellation path is shown in Figure 40. It can be seen that the optimal LCC attenuation is about 19.32 dB. It is also observed that the power of the residual signal ranges from −110.663 dB to −64.748 dB for frequency band of interest. When compared to the results in Figure 24, there is an improvement of about 10 to 15 dB in cancellation power at 2.4 GHz when the phase slope alignment is applied to the leakage path. However, alignment error of 11.861^{o}/GHz results in losses in the cancellation power at the boundary of the frequency band of interest, 2.36 GHz and 2.44 GHz (*Marker M*1).

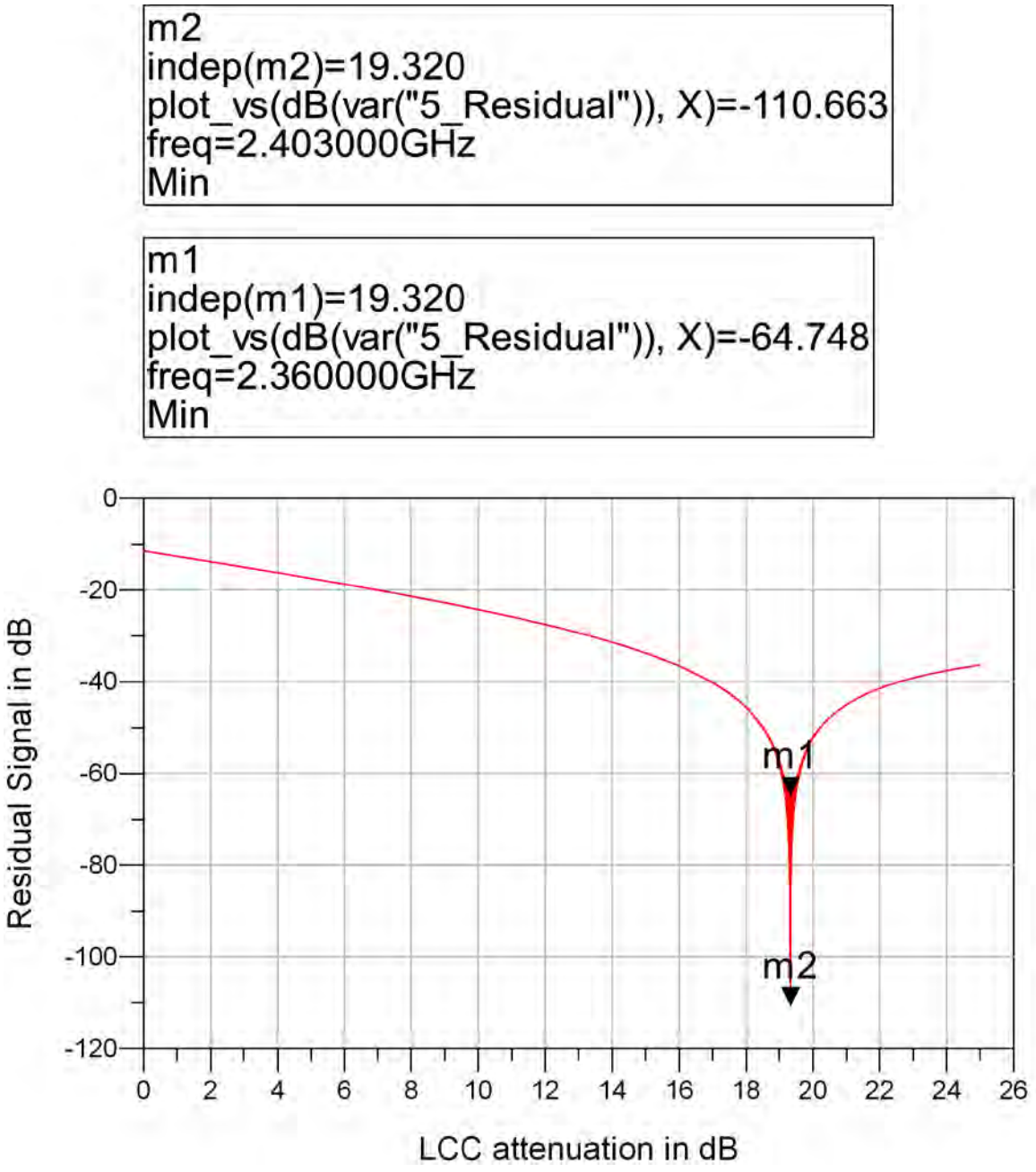

Figure 40. Plot of residual power versus LCC attenuation.

In order to further improve the performance of the cancellation circuit, a shunt stub circuit is used in the cancellation circuit to replace the phase shifter as described in the next section.

4. Application of Shunt Stub Circuit to the Cancellation and Leakage Paths

As discussed in Section C3, slight misalignment in the phase slope of the LCC and leakage signal resulted in cancellation losses. In order to achieve coherent cancellation of the leakage signal, the cancellation signal has to be of the same magnitude and 180° out of phase when compared to the leakage signal. A shunt stub circuit can be used to phase shift a signal and alter the change of phase over a range of frequencies, as shown in Table 2. Therefore, in order to maintain 180° phase difference and common phase slope between the cancellation signal and leakage signal, it is possible to select two different sets of shunt stub circuits. The design of the LCC using stubs of transmission lines in both paths is shown in Figure 41. The simulation is carried out with source signal frequencies ranging from 2.36 GHz to 2.44 GHz in steps of 1.0 MHz. The loss of the attenuator in the LCC is swept from 0 to 25 dB in steps of 0.01 dB. The source power is set at 6.0 dBm, and an AC simulator with parameter sweep is used for this simulation.

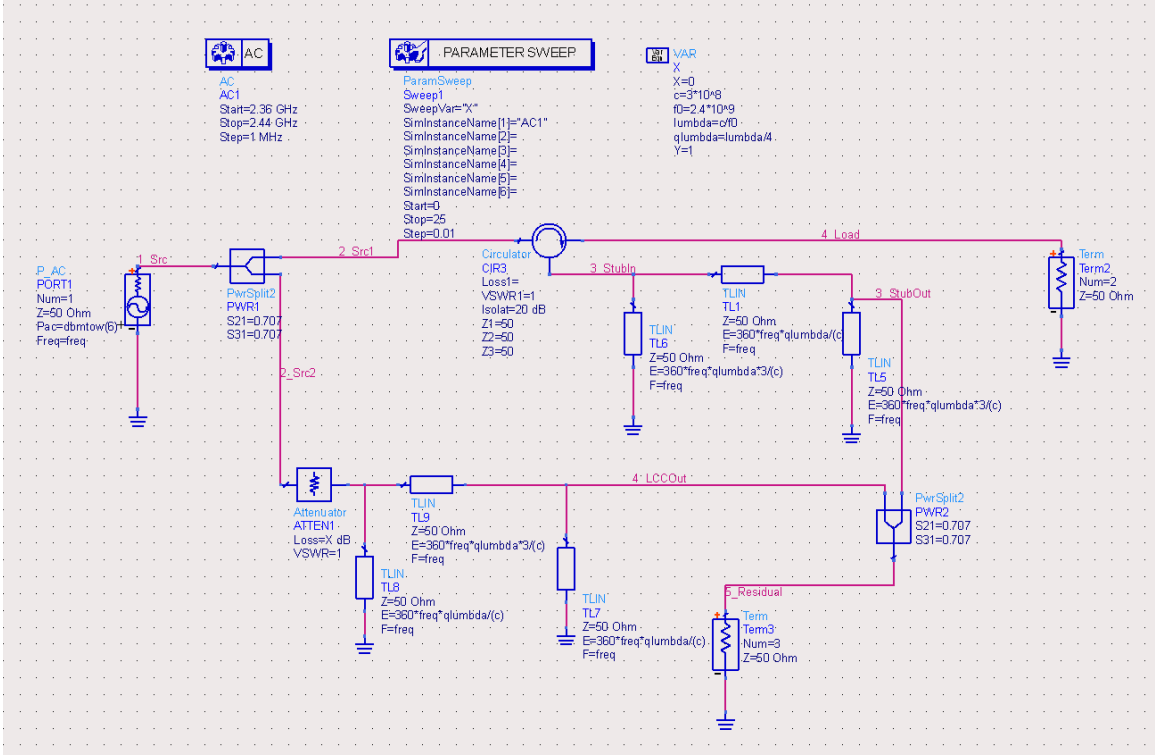

Figure 41. Application of shunt stub circuits on both cancellation and leakage paths.

The shunt stubs with length of three quarter wavelength and series stub with length of one quarter wavelength is applied on the cancellation path as part of the LCC circuit (in Figure 41) and results in a -270^{o} phase change at 2.4 GHz with a phase slope of -150^{o}/GHz. At the same time, the shunt stubs with length of one quarter wavelength and a series stub with a length of three quarter wavelength are applied on the leakage path as shown in Figure 41. The introduction of the stubs in the leakage path causes the leakage signal to be phase shifted by -90^{o} at 2.4 GHz with a phase slope of -150^{o}/GHz. The simulation is conducted with source frequency from 2.36 GHz to 2.44 GHz in steps of 1.0 MHz. The LCC is tuned by sweeping the attenuator in the cancellation path from 0 dB to 25 dB in intervals of 0.01 dB. The variation of the residual signal with respect to the LCC attenuation is shown in Figure 42.

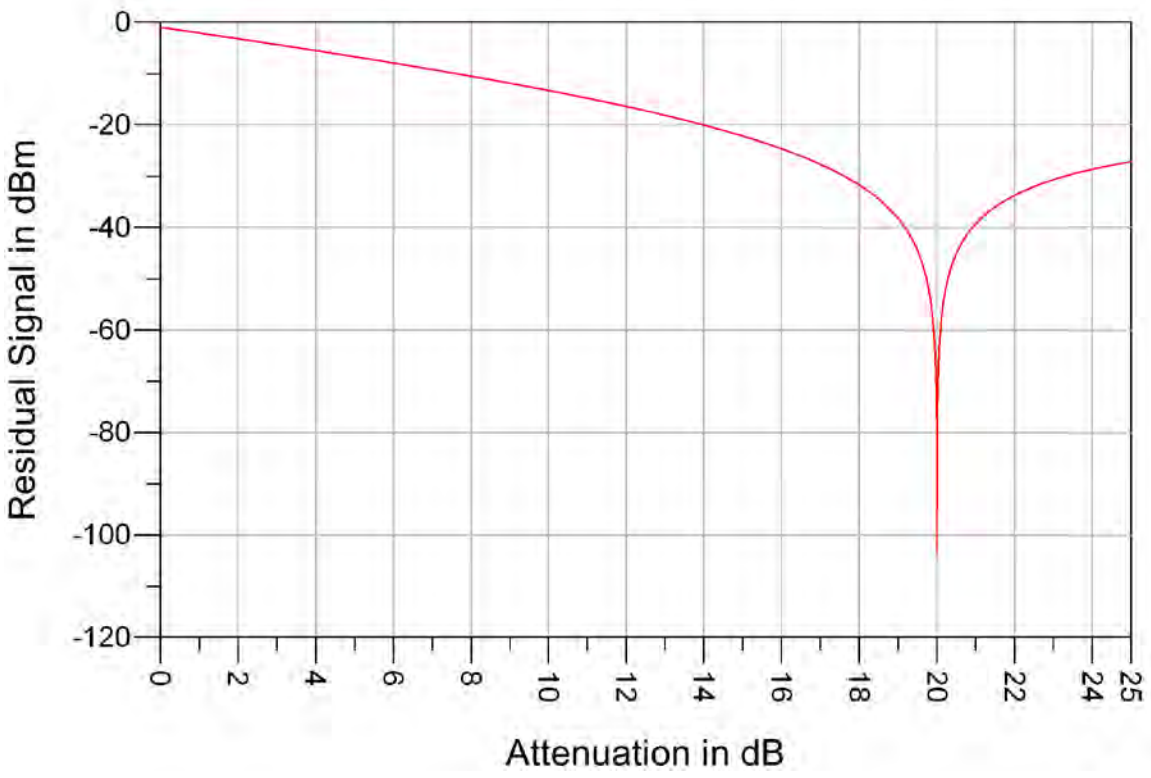

Figure 42. Plot of residual power versus LCC attenuation with 2 sets of shunt stubs circuits.

As it is observed from Figure 42 that with better alignment of the phase slope between the cancellation and leakage paths, the residual signal can be reduced by about

−110 dB. It is also observed that the deep notch of cancellation occurs when the attenuation of the LCC is set to 20 dB. By setting the attenuation of the LCC at 20 dB, the simulation is repeated for the purpose of amplitude and phase analysis. The phase of the leakage and cancellation paths is shown in Figure 43.

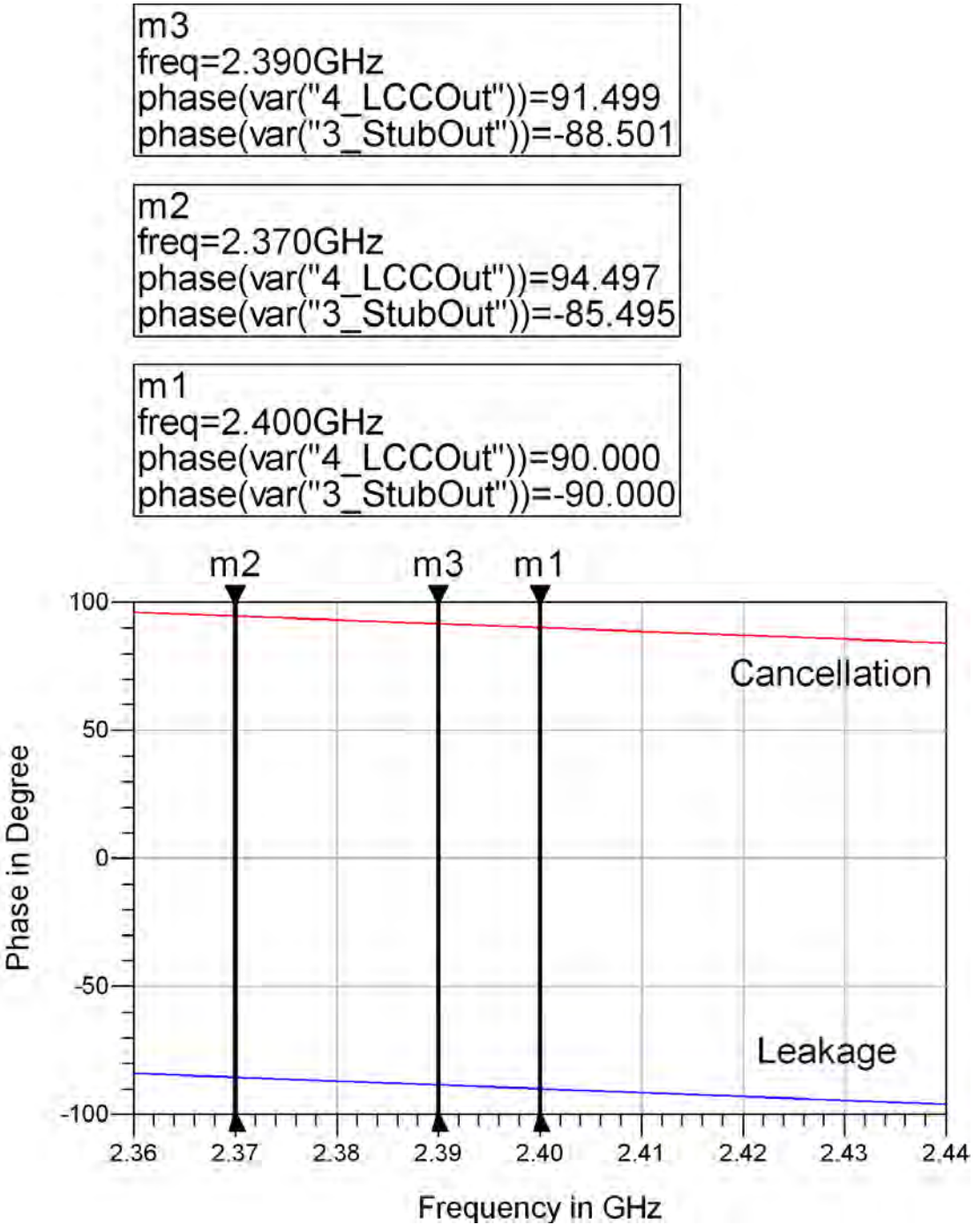

Figure 43. Phase angles of the leakage and cancellation paths versus frequency.

As in Figure 43, the phase difference between the leakage and cancellation is maintained at 180^{o} in general (*Markers M*1 and *M*3). However, there are slight errors in the phase difference between the two signals as can be observed in *Marker M*2 shown in Figure 43.

The slight imbalance between the leakage and cancellation results in a non-uniform magnitude response of the cancellation. The magnitude of the residual signal is shown in Figure 44.

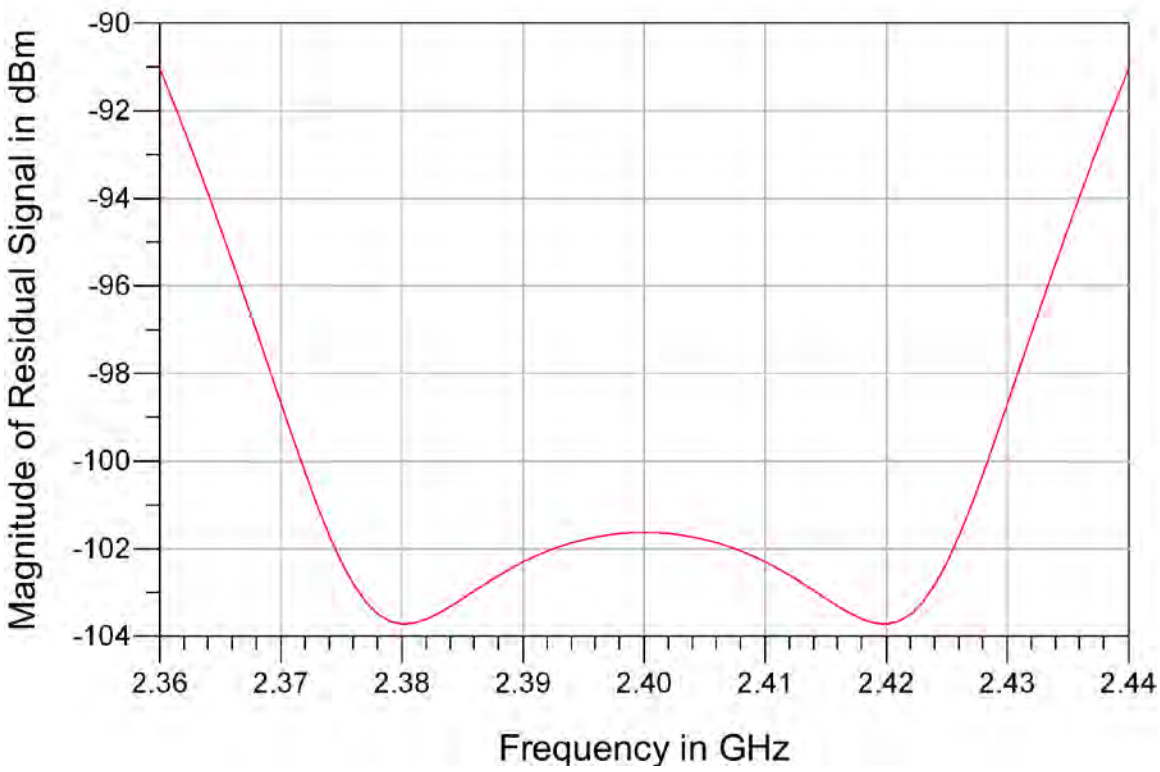

Figure 44. Magnitude of residual signal versus frequency.

It is observed from Figure 43 that the slight variations between the two paths result in a difference of about 13 dB across the frequency band of interest. However, in this case, the variation is more controlled when compared to the case shown in Figure 40 where the variation is approximately 55 dB.

The magnitude responses of the two shunt stub circuits are shown in Figure 45 and Figure 46 for amplitude imbalance analysis. As can be seen in Figure 45 and Figure

46, the difference between the magnitude response at 2.36 GHz and 2.44 GHz is 0.022 dB; this slight amplitude imbalance contributes to the variations of the residual signal with frequency as shown in Figure 44. Such a small difference in the magnitude response cannot be measured reliably.

With the amplitude and phase imbalance introduced by the pair of stubs circuits, the cancellation power of the LCC is shown in Figure 47. It is observed in Figure 47 that the peak cancellation occurs at about 2.38 GHz and 2.42 GHz with cancellation power of about 87 dB. The 3.0 dB bandwidth of the cancellation circuit is about 56 MHz.

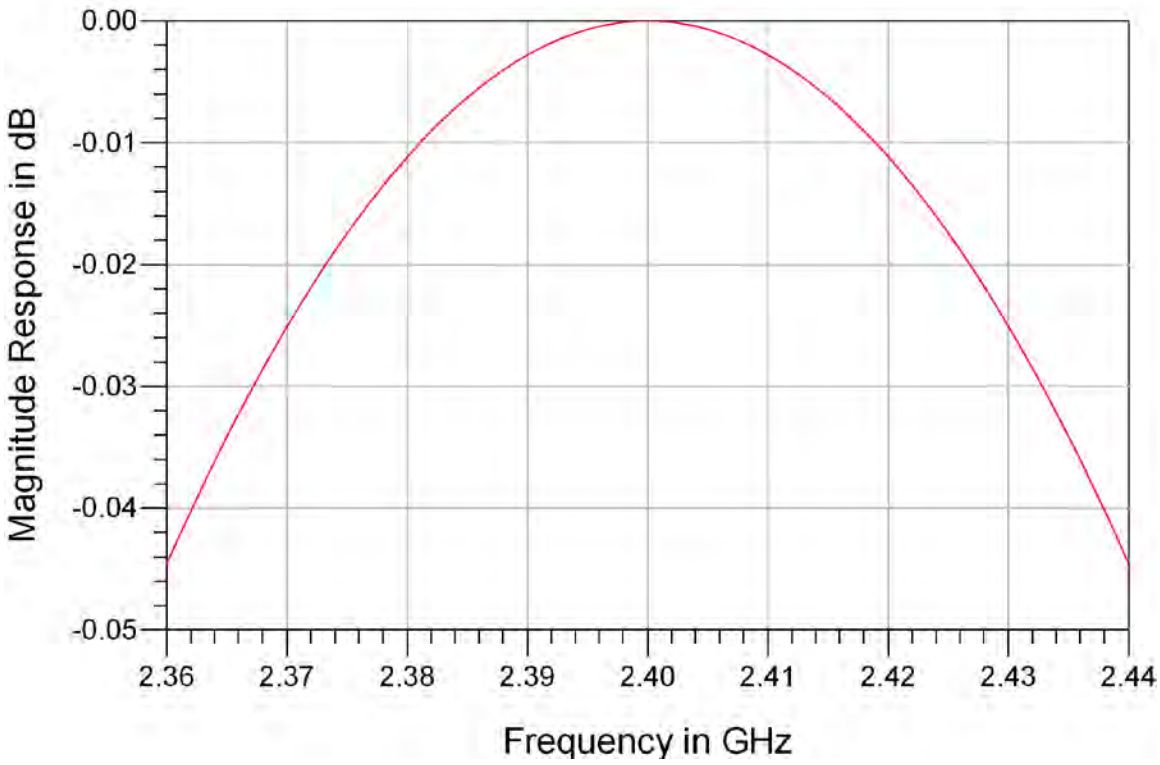

Figure 45. Magnitude responses of phase slope alignment circuits with three quarter wavelength shunt stubs and quarter wavelength series stubs applied to leakage path.

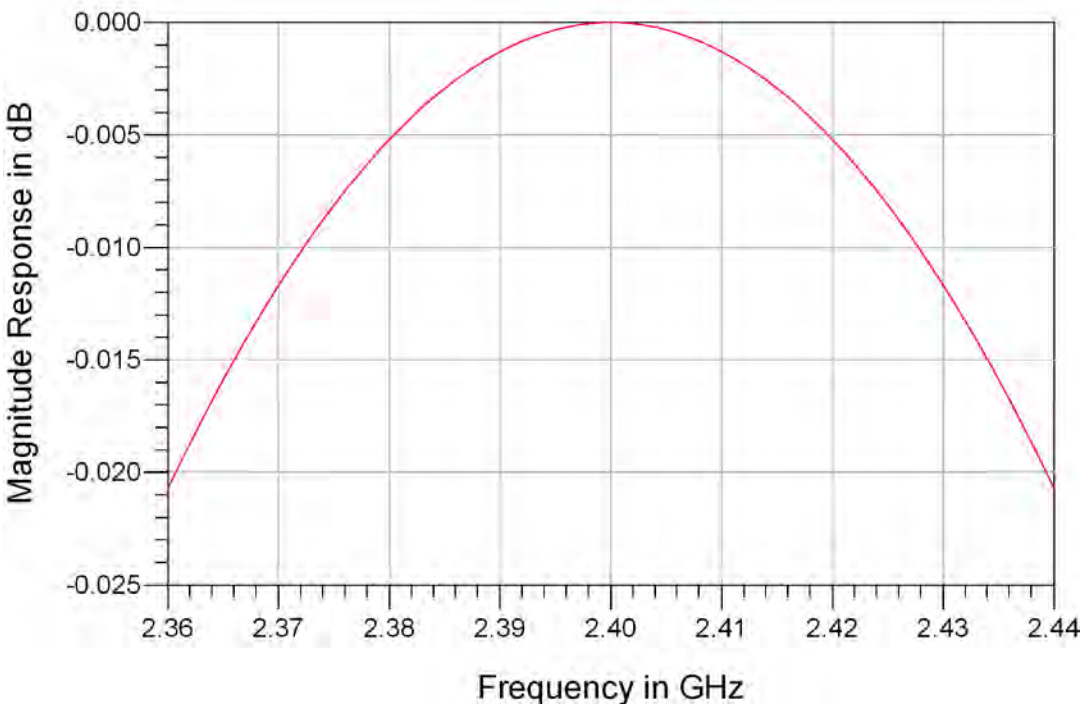

Figure 46. Magnitude responses of WLCC with phase slope alignment circuits with quarter wavelength shunt stubs and three quarter wavelength series stub.

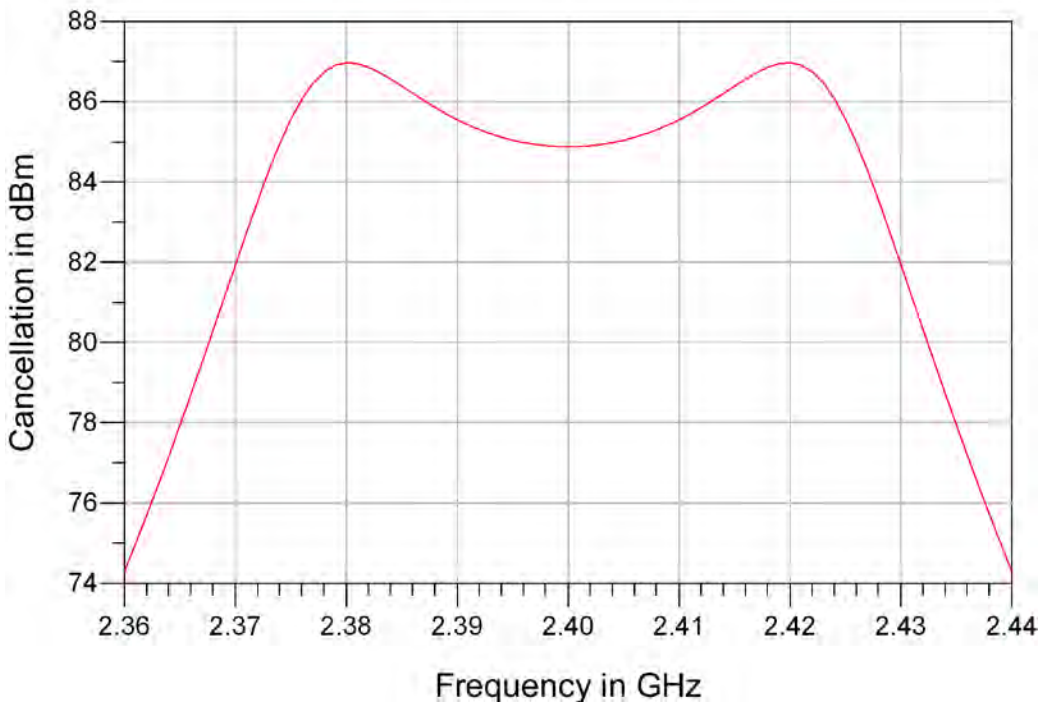

Figure 47. Cancellation *C* versus frequency.

5. Mismatch Effects of a Dipole Antenna

The analysis of WLCC performance so far has been carried out using a constant real impedance. Such a termination circuit cannot truly represent the behavior of an antenna, as the input impedance of the antenna such as a dipole has a reactive part that is frequency dependent. Other characteristics of the antenna affect its VSWR and make it frequency dependent, as it can be observed in Figure 48.

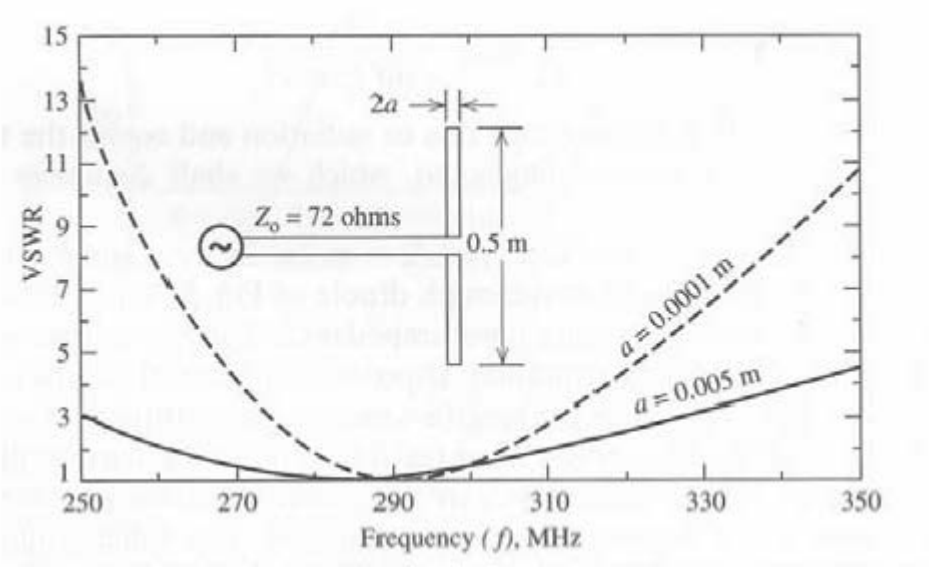

Figure 48. Calculated VSWR as a function of frequency for dipoles of different wire diameter (From [18]).

The bandwidth of a dipole antenna is usually narrow because of its resonant-type structure [18]. Reflections from the dipole terminals are more serious when operating in a wideband scenario. For the case of a thin dipole antenna, the length-to-diameter ratio is about 50, and the input resistance is given by

$$R_{ri} = 24.7\left(\pi \frac{L}{\lambda}\right)^{2.4} \tag{7}$$

where R_{ri} is the input resistance, L is that length of dipole antenna and λ is the wavelength at center frequency.

For the case where the center frequency is 2.40 GHz, the wavelength is found to be 0.125 m. The length of the dipole is taken to be 0.475λ so that the antenna can be

made to resonate [18]. The input resistance of the dipole antenna is found to be 64.554 Ω. In order to match the impedance of the dipole antenna to that of the rest of the circuit, a quarter-wave transformer is used [12].

The desired input impedance of the quarter-wavelength transformer is given by

$$Z_1 = \sqrt{Z_0 R_{ri}} \tag{8}$$

where, Z_1 is the impedance of the quarter-wavelength transformer and Z_0 is the characteristic impedance of the feedline which is 50 Ω. The impedance of the quarter-wavelength transformer is found to be 56.813 Ω.

The ADS model of the LCC with a dipole antenna is shown in Figure 49. The attenuation of the LCC is set to 20 dB, and the simulation is carried out with source frequency ranging from 2.36 GHz to 2.44 GHz in steps of 1.0 MHz. In the simulation, the source power is set at 6.0 dBm. The result of the simulation is shown in Figure 50, where the WLCC is set for a 50 Ω antenna impedance. In Figure 50, it is found that with the introduction of a dipole antenna, the cancellation power is reduced by 55 to 75 dB.

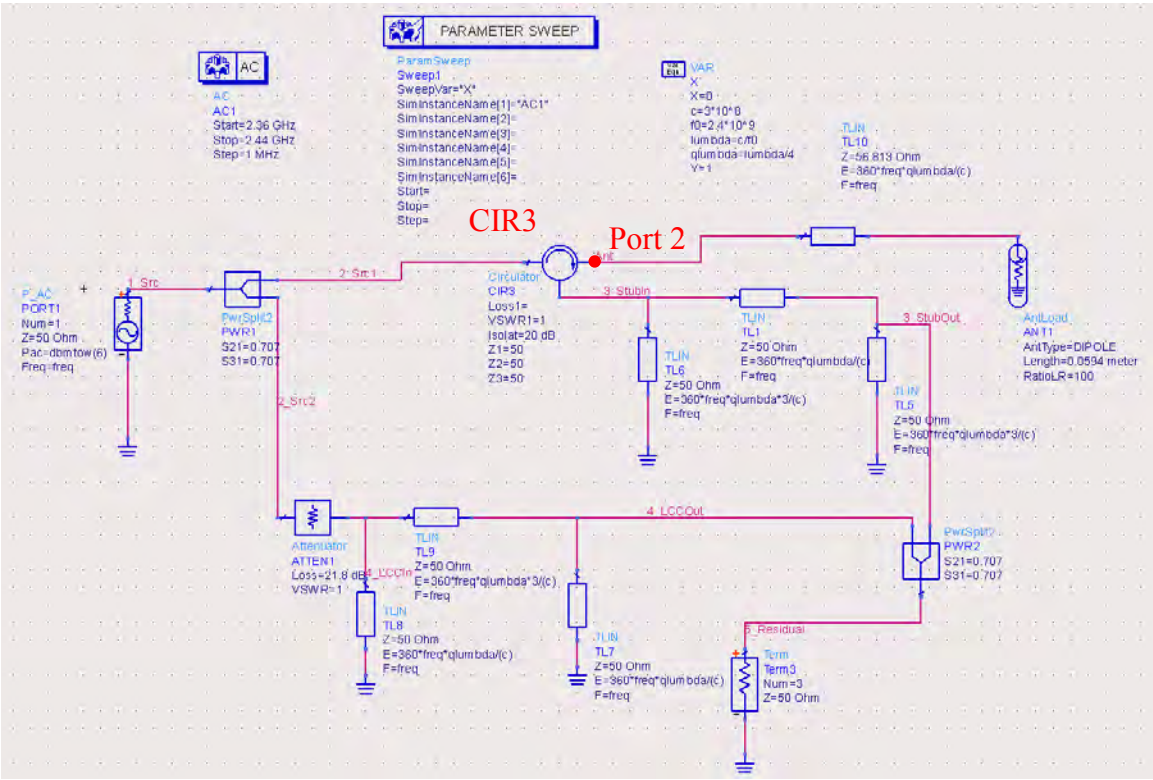

Figure 49. ADS model of LCC with a dipole antenna.

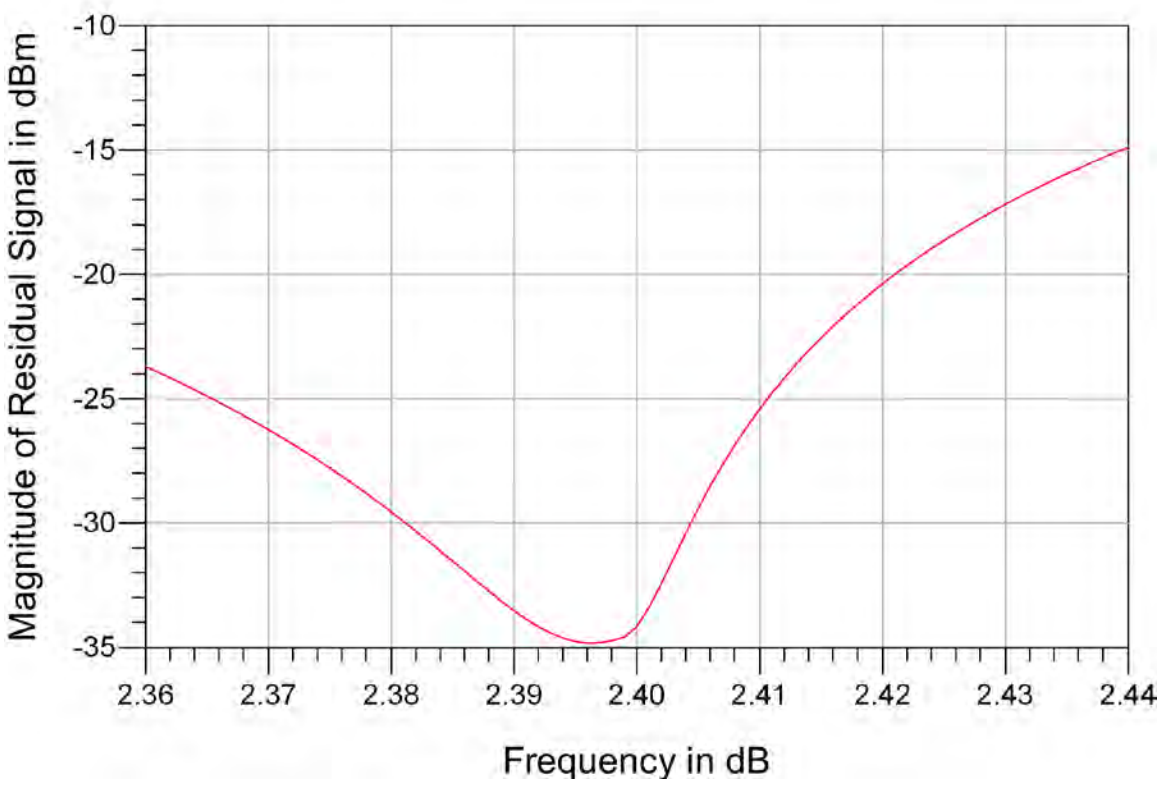

Figure 50. Residual signal level with dipole antenna, LCC attenuation of 20 dB.

The attenuator in the LCC is tuned to obtain a minimum in the residual signal. It was found through simulation that the residual signal is minimal when the attenuation is set to 21.8 dB. The residual signal of the retuned circuit is shown in Figure 51.

It is observed that by retuning the LCC, the cancellation power is slightly improved by about 25 dB at around the center frequency. In order to understand the source of loss of cancellation power, the signal at *Port* 2 of the circulator *CIR*3 in Figure 49 is analyzed and shown in Figure 52.

It is observed in Figure 52 that the power of the signal along the antenna path is dependent on operating frequency. This is because the dipole mismatch is frequency dependent. This can give rise to both amplitude and phase imbalance between the leakage and cancellation paths. This is because the reflected dipole signal is circulated into the leakage path. The magnitude and phase of the leakage and cancellation path is shown in Figure 53 and Figure 54, respectively.

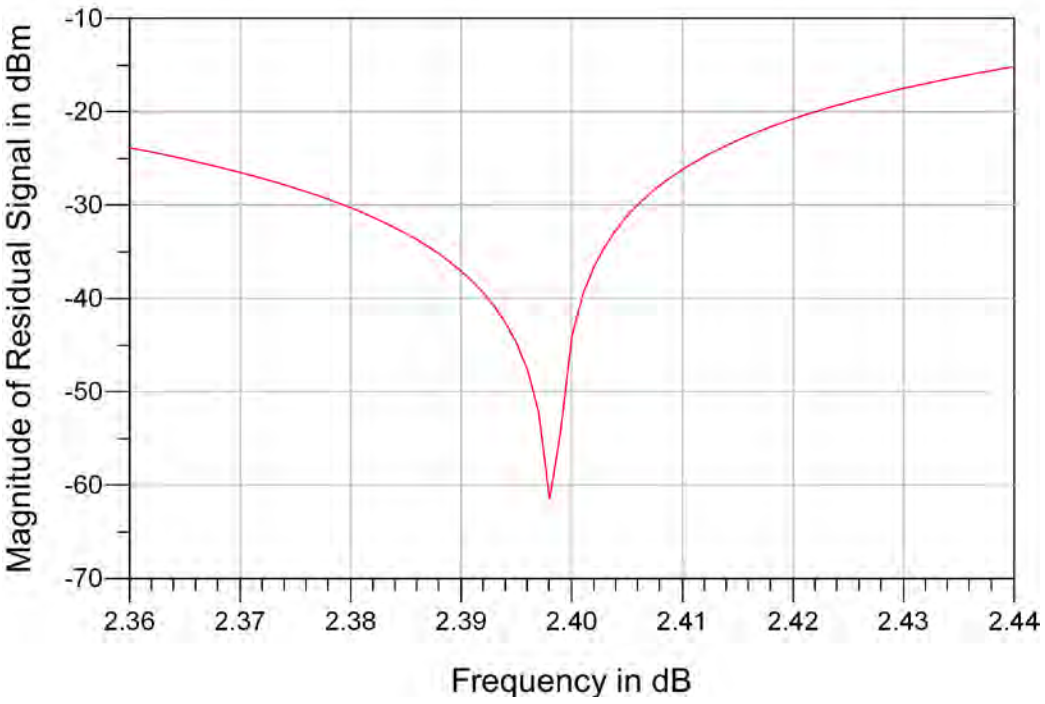

Figure 51. Residual signal level with dipole antenna, LCC attenuation of 21.8 dB.

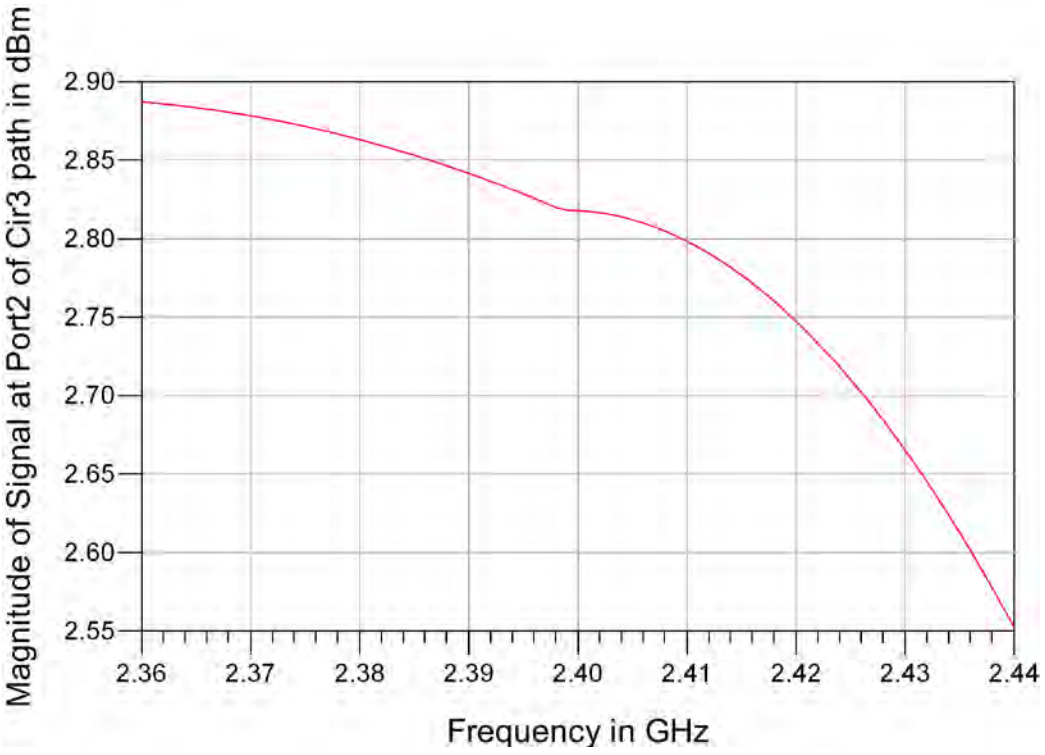

Figure 52. Signal level at the *Port* 2 of circulator along the antenna path.

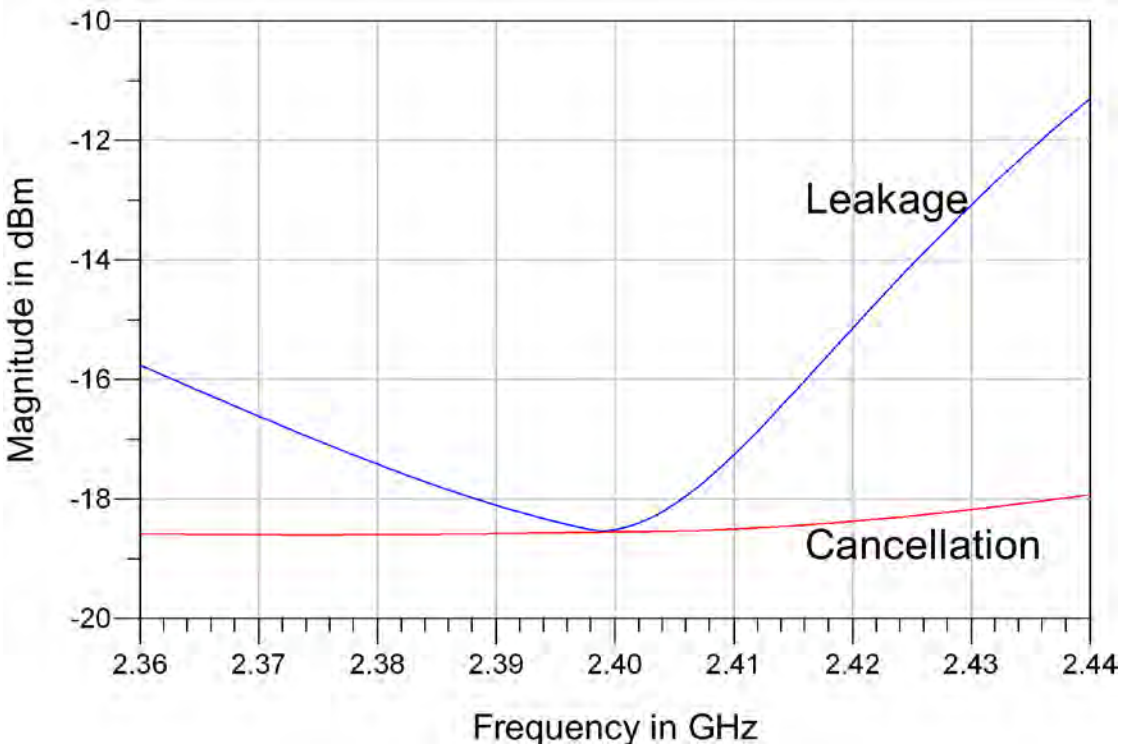

Figure 53. Magnitude of the leakage and cancellation signals with source of 6.0 dBm.

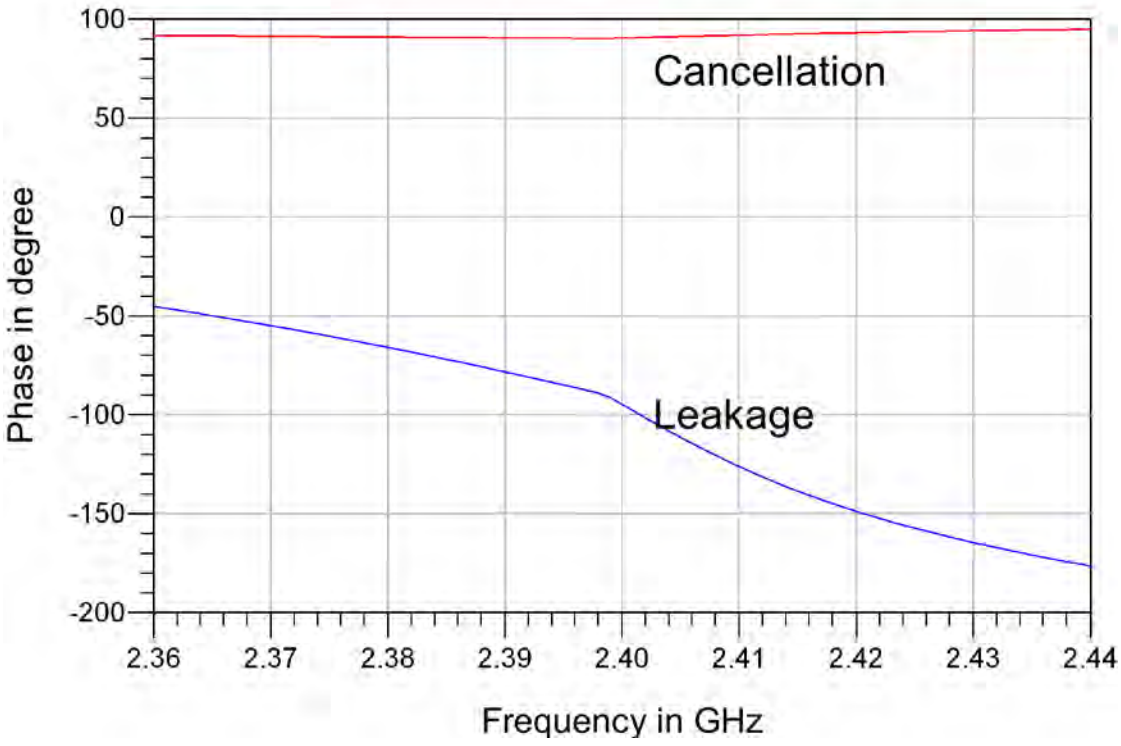

Figure 54. Phase of the leakage and cancellation signals.

It is shown in Figure 53 that the magnitude of the leakage signal is different from the cancellation signal for frequencies other than the center frequency of 2.40 GHz. Therefore, with the amplitude imbalance between the leakage and cancellation signals, the leakage signal is not cancelled completely.

In coherent cancellation, when the amplitude is balanced, the phase angle between the leakage and cancellation signals is maintained at 180^{o}. However, as shown in Figure 54, the phase difference between the two signals is not maintained at 180^{o}. With the magnitude and phase imbalance between the leakage and cancellation paths, the LCC is not effective in handling frequency dependent reflection from a load antenna.

It should be pointed out that since the dipole is a narrowband device, there is no need for a wideband LCC. A narrowband LCC will suffice. Techniques to increase the antenna bandwidth are discussed in [19]. Broadbanding involves synthesizing a circuit to match one impedance to another impedance over a specific frequency range to within a specific tolerance. The impedance to be matched is a function of frequency that is usually complex. It is recommended in [19] to adopt an iterative approach for broadbanding. Discussion and analysis of broadbanding techniques are beyond the scope of this thesis.

6. Application of Spiral Antenna

As was discussed in Section 5, the frequency response of a dipole antenna is narrowband in general, and this affects the overall performance of the WLCC. In this section, the performance of the WLCC when operating with a broadband spiral antenna is investigated. For the purpose of this study, the reflectivity or S_{11} parameter of a spiral antenna (in Table 5) is considered.

The magnitude and phase responses of the S_{11} parameter of the spiral antenna are shown in Figure 55 and Figure 56, respectively. It can be observed in Figure 55 and Figure 56 that the variations in the amplitude and phase of the S_{11} parameter of the spiral antenna are frequency dependent.

Table 5. S_{11} parameters of spiral antenna used for simulation.

Frequency in GHz	Magnitude of S_{11}	Phase of S_{11} in degree
2.36	0.027134791	-1459.6083
2.3639996	0.013727983	-1396.1334
2.3759999	0.03184228	-1354.0186
2.388	0.055112332	-1353.222
2.3999996	0.077660158	-1359.1818
2.4119999	0.098555103	-1367.325
2.424	0.011720579	-1376.578
2.4359996	0.13300213	-1386.578
2.44	0.14528446	-1397.1576

The ADS model of the WLCC with the spiral antenna is shown in Figure 57. The spiral antenna is modeled by a *S1P* (1-Port S-parameter File) in ADS using the S_{11} parameter as shown in Table 5. An AC simulator is used for the simulation in this section. The simulation is carried at source power of 6.0 dBm and frequency from 2.36 GHz to 2.44 GHz in steps of 1.0 MHz. It should be noted that the attenuation of the WLCC is set to 20 dB as it has been tuned for wideband application.

Figure 55. Magnitude of S_{11} parameter of spiral antenna with frequency.

Figure 56. Phase responses of the S_{11} parameter of spiral antenna with frequency.

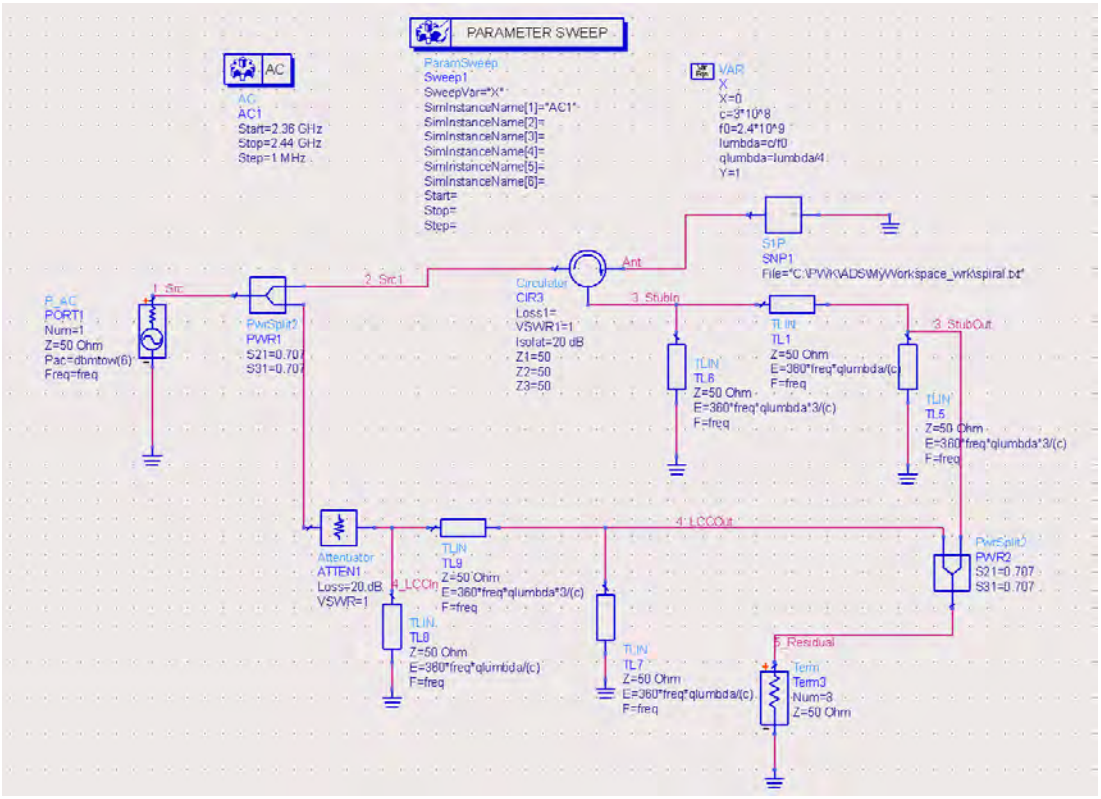

Figure 57. ADS model of WLCC with spiral antenna.

The simulation settings for the spiral antenna model are shown in Figure 58. In order to use ADS, the S_{11} parameter of the spiral antenna has to be formatted and stored in a text file. The syntax of the S_{11} parameter text file is shown in Figure 59.

The magnitude of the residual signal is shown in Figure 60. It is observed that the magnitude of the residual signal is very similar to the magnitude response of the S_{11} parameter of the spiral antenna (in Figure 55). This is because the leakage signal is dominated by the reflection of the spiral antenna in this case.

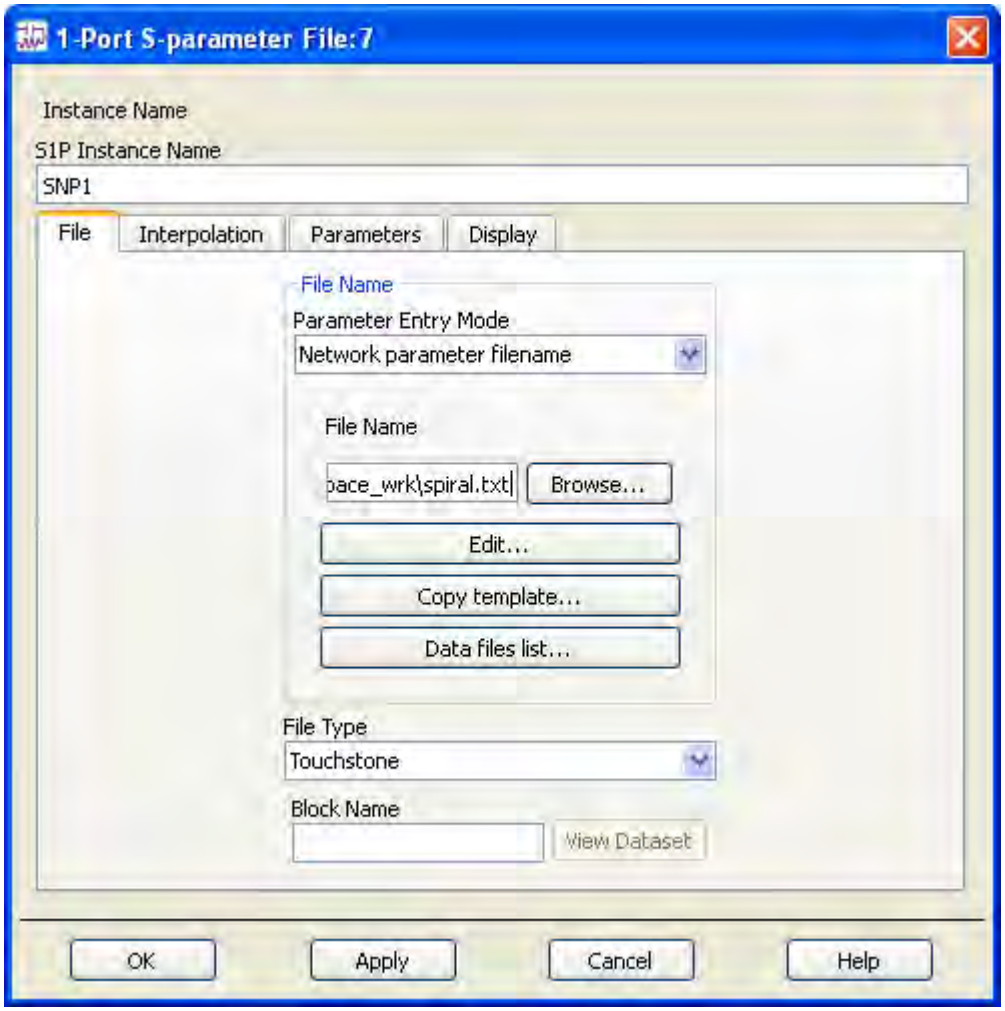

Figure 58. ADS simulation setting for the spiral antenna model.

```
!       Frequency / GHz       S1,1/abs,linear        S1,1/arg,degrees
!-------------------------------------------------------------------
#       GHZ    S      MA     R      50
!       freq          magS11         angS11         (commented header line)
        2.36          0.027134791    -1459.6083
        2.3639996     0.013727983    -1396.1334
        2.3759999     0.03184228     -1354.0186
        2.388         0.055112332    -1353.222
        2.3999996     0.077660158    -1359.1818
        2.4119999     0.098555103    -1367.325
        2.424         0.11720579     -1376.578
        2.4359996     0.13300213     -1386.578
        2.44          0.14528446     -1397.1576
```

Figure 59. Syntax of spiral antenna S_{11} parameter file.

Figure 60. Magnitude of residual signal in dBm with frequency at source power of 6.0 dBm.

The magnitude and phase of the WLCC output and the leakage signal are shown in Figure 61 and Figure 62, respectively. It is observed that there are both amplitude and phase imbalances between the cancellation and leakage signals. As a result, there is always some substantial leakage power as shown in Figure 60. It is also observed that the amplitude and phase differences between the cancellation and leakage signals vary with frequency.

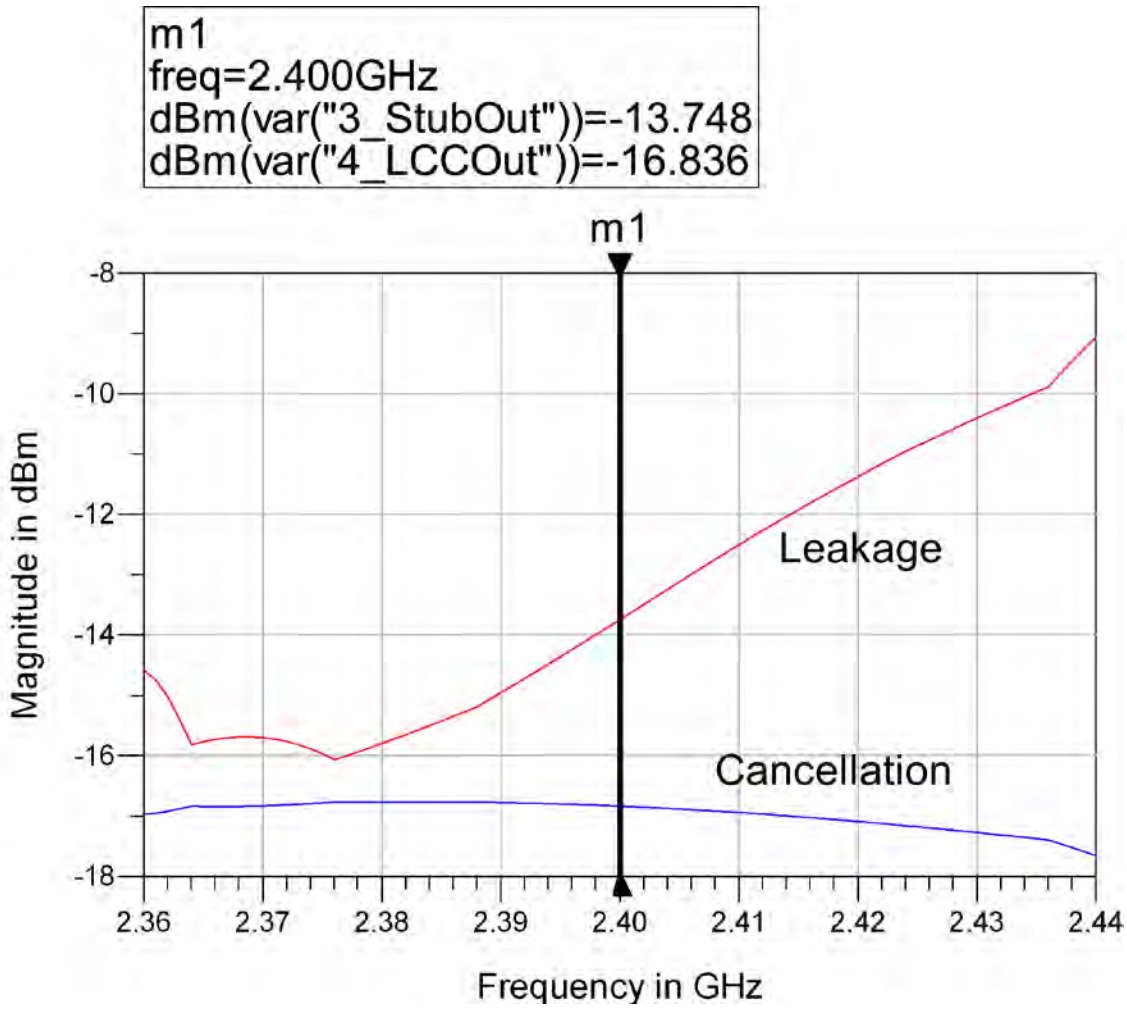

Figure 61. Magnitude of the cancellation and leakage signals.

From Figure 61 and Figure 62, it is observed that at the center frequency of 2.4 GHz there are amplitude and phase difference of 3.088 dBm and 139.222°. In order to fine tune the difference between the cancellation and leakage signal, the amplitude and

phase of the cancellation signal are adjusted. An additional phase shifter is added along the cancellation path to introduce the phase lag in the cancellation signal (in Figure 63). The simulation is conducted with a 6.0 dBm source and source frequency from 2.36 GHz to 2.44 GHz with steps of 1.0 MHz.

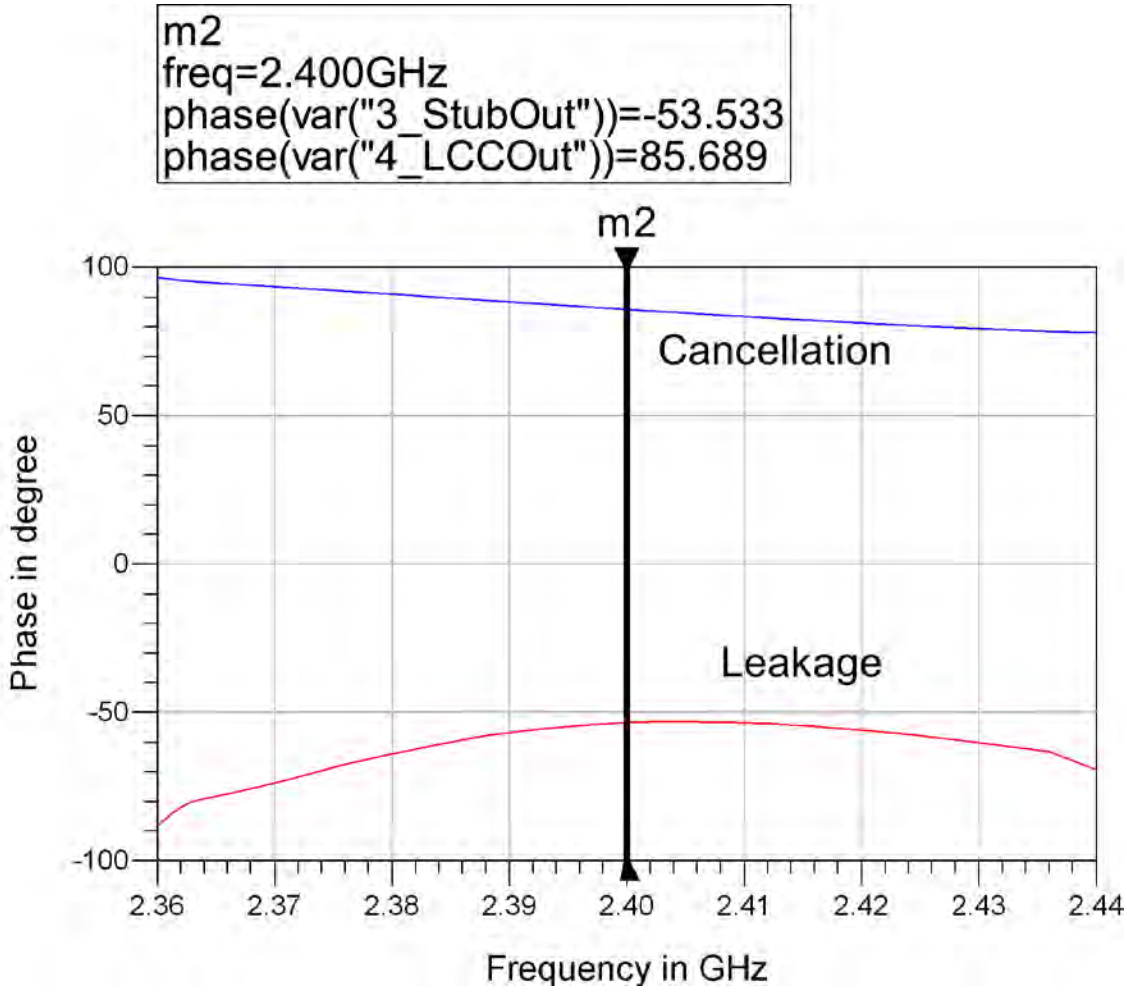

Figure 62. Phase of cancellation and leakage signals.

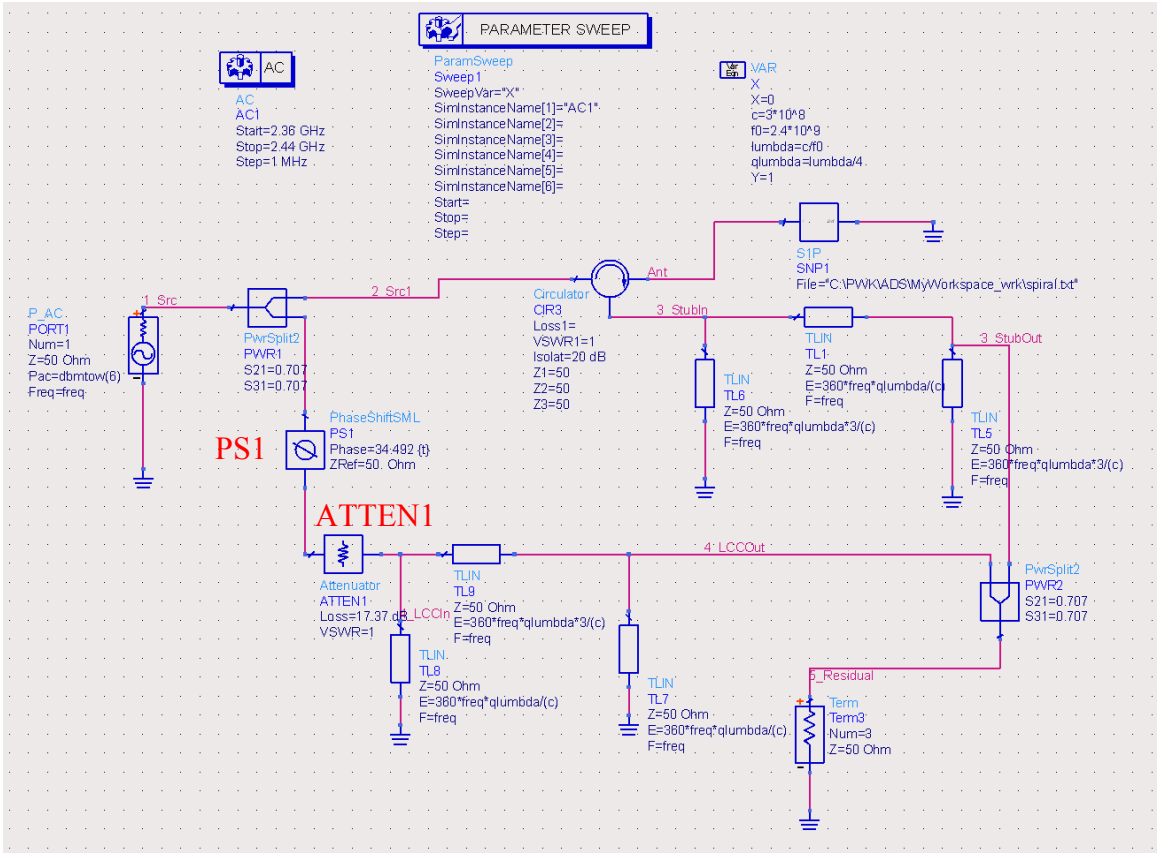

Figure 63. ADS model of modified WLCC with spiral antenna.

The phase shifter (*PS*1) and the attenuator (*ATTEN*1) are tuned such that the cancellation and leakage signals are of same amplitude and 180^{o} out of phase as shown in Figure 64 and Figure 65. It is observed from Figure 64 and Figure 65 that coherent cancellation occurs only at the center frequency, and beyond that there are losses in the cancellation power.

In Figure 66, the amplitude of the residual power is shown. It is observed from Figure 66 that the cancellation is narrowband with a notch at about −61 dBm. The WLCC design with grounded shunt stubs is ineffective in reducing the leakage signal over the entire frequency band in this case.

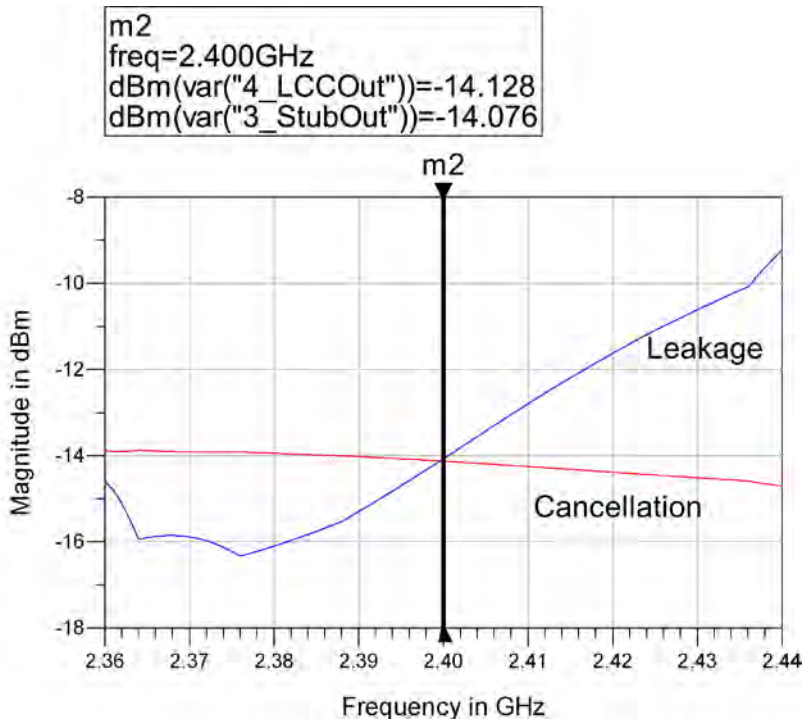

Figure 64. Magnitude of cancellation and leakage signal with frequency at source power of 6.0 dBm.

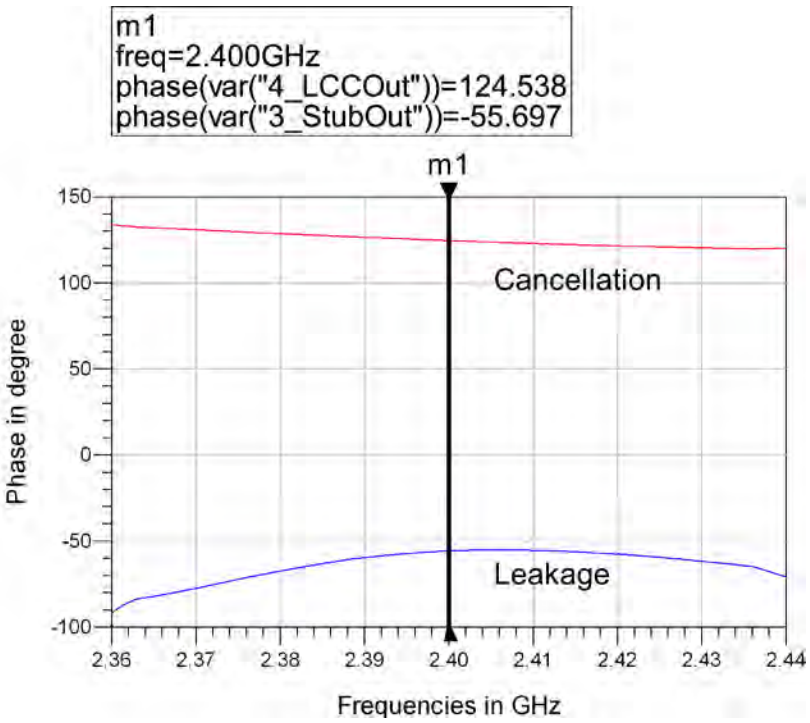

Figure 65. Phase of the cancellation and leakage signals with frequency.

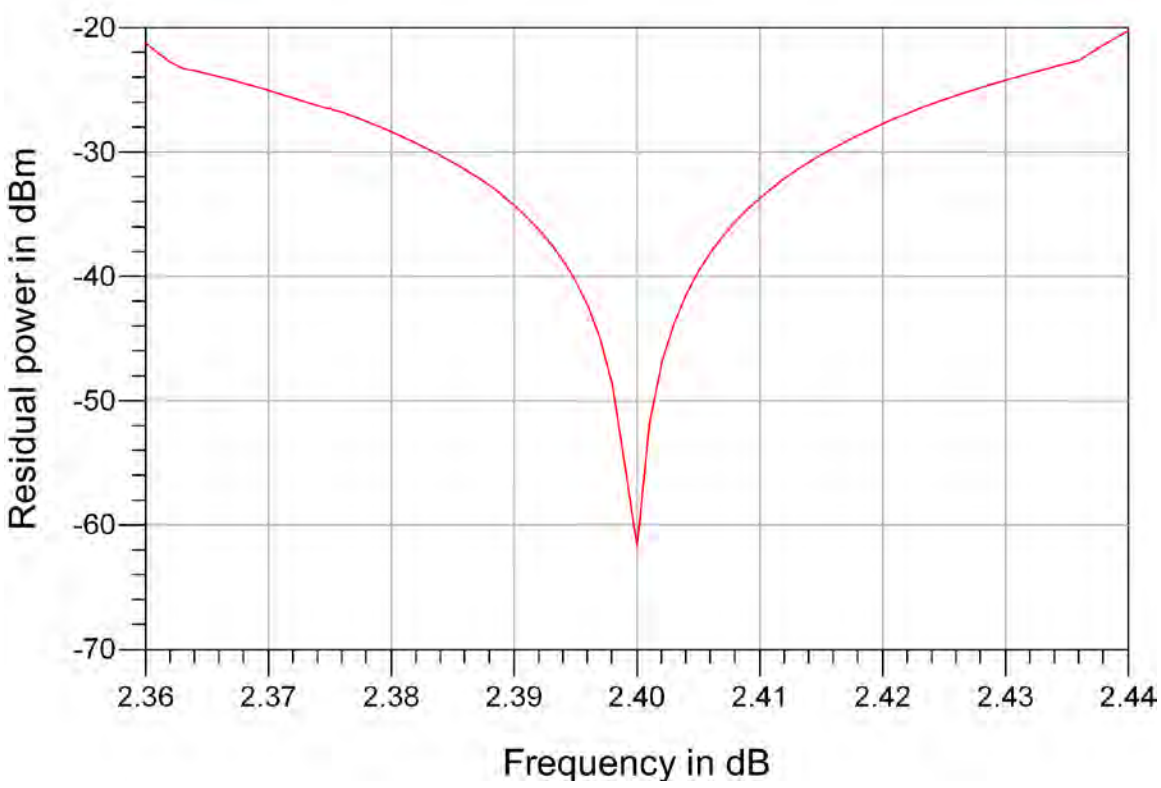

Figure 66. Magnitude of residual signal with frequency.

The reflections from the spiral antenna vary with frequency in a non-linear manner. However, the WLCC is designed to cancel leakage signal that has a similar characteristics of the source signal. The WLCC is able to cancel the linear phase slope in the leakage signal but not non-linear phase slopes. For this reasons, there is a reduction in cancellation when operating over a wideband.

D. SUMMARY

In this chapter, it was shown that the cancellation of the FDMC WLCC is not optimal as the design introduced both amplitude and phase imbalance. It was shown there is a negative phase slope that is associated with the phase response of the FDMC LCC.

A phase slope alignment circuit that consists of both shunt and series stubs is used to compensate the frequency dependent phase shift characteristics of the WLCC. In order

to keep the design of the LCC simple, the FDMC with phase slope alignment circuit was not considered. In general, the phase characteristics of the phase slope alignment circuit are discrete; for example, phase slope decreases in steps of 75^{o}/GHz with an increase in the length of the shunt stub by a quarter wavelength. This characteristic limits the tuning of stub circuit to perfectly match the phase slope of a phase shifter in a LCC design. The phase mismatch results in losses in the cancellation power. In order to achieve coherent cancellation of the leakage signal, stub circuits were applied in both cancellation and leakage paths.

Dipole antennas are narrowband and introduce both amplitude and phase imbalance when operating beyond the center frequency. This results in loss in the cancellation power. Techniques that match the antenna impedance to the characteristic impedance of the feedline over a wideband should be investigated.

In general, the magnitude response of the WLCC is frequency independent and phase response varies linearly with frequency. The performance of the WLCC degrades for situation where the reflection from a load antenna varies with frequency non-linearly.

THIS PAGE INTENTIONALLY LEFT BLANK

IV. SUMMARY, CONCLUSIONS, AND RECOMMENDATIONS

A. SUMMARY

The aim of this research was to improve the cancellation performance of a WLCC. The approach of the research was to investigate LCC techniques in the analog domain. ADS was used to model and simulate characteristic of various LCC configurations for analysis purposes.

One of the ways to isolate transmit and receive signals in a simultaneous transmit and receive radar is with a circulator. Typical isolation of a circulator is about 20 to 30 dB between the three ports of the device. As a result of this imperfect isolation, leakage of the transmit signal into the receive path occurs. The problem with transmit signal leakage into the receive path is that the strong leakage tends to overwhelm the power detector in the receive path and degrade the receiver's sensitivity.

The idea of a leakage cancellation circuit is to coherently subtract the leakage signal using transmit signal itself. The transmit signal was attenuated and phase shifted so that an equal but 180^{o} out-of-phase cancellation signal was produced to cancel the leakage signal. However, hardware components do not behave ideally, and this results in losses in the cancellation. When non-ideal devices are used, it was found that the residual signal can be minimized by retuning the attenuator in the cancellation path. Non-ideal frequency dependent phase response of the phase shifter narrows the bandwidth of the cancellation circuit. This restricted the application of the LCC in wideband cancellation.

The concept of the FDMC based WLCC was to divide the signals into multiple frequency sub-bands, and subsequently, a narrowband LCC was applied on each frequency sub-band. Elliptic band-pass filters were applied in the design of the FDMC WLCC. As both the magnitude and phase responses of the FDMC WLCC were frequency dependent, coherent cancellation could not be achieved. This was because of the amplitude and phase imbalance between the cancellation and leakage signals.

The use of shunt and series stubs of transmission lines could be used to design phase alignment circuit. By applying the phase slope alignment circuit on a non-ideal phase shifter, higher cancellation can be achieved if the rate of phase change with frequency of phase slope alignment circuit matches that of the phase shifter. The phase alignment circuit changed in steps of -90^{o} and -75^{o}/GHz. As a result, it was impossible to tune the phase alignment circuit such that its phase slope matched exactly that of the phase shifter.

The idea of using a pair of phase slope alignment circuits was studied in this thesis. Phase slope cancellation circuits were employed on both cancellation and leakage paths to maintain amplitude and phase balance between the two signals. It was found that this configuration could greatly improve the performance of the LCC by reducing the residual signal below −110 dB.

The WLCC has its limitation in cancelling leakage signals that vary with frequency non-linearly. Techniques that control the reflections from the antenna load should be further studied.

B. CONCLUSIONS

In conclusion, the LCC can be applied to provide isolation between the transmit and receive paths of simultaneous transmit and receive systems. Detailed design is required in the building of the LCC to ensure amplitude and phase balance between the cancellation and leakage signals.

Accurate modeling of LCC components such as the phase shifter provides better understanding of bandwidth and cancellation limitation of the LCC. This has helped to fine tune LCC design concepts developed in earlier research. The main contributions of this thesis are the analysis of the LCC designs presented in earlier thesis research, analysis of grounded shunt stub circuits and the use of shunt stub based phase slope alignment circuits to improve LCC cancellation performance. The maximum cancellation of a stub circuit based LCC is about 87 dB. The three dB bandwidth of the cancellation is about 56 MHz.

C. RECOMMENDATIONS

1. Broadbanding Techniques for Antenna Impedance Matching

The impedance of the antenna can be frequency dependent as presented in Chapter III, and this resulted in loss in cancellation. Broadbanding can be a possible technique used to match the antenna impedance over a wider frequency range of interest. This helps to reduce the reflection from the antenna and, hence, reduce leakage from the transmit path. An ADS model of a matching circuit can be created for the study of broadbanding.

2. Modeling of Transmit and Receive Module

As was seen in this thesis, coherent cancellation of a leakage signal is sensitive to amplitude and phase imbalance. Transmit and receive modules (TRMs) used in a WNDDPA may introduce reflections that can affect the LCC by introducing amplitude and phase imbalance between cancellation and leakage paths. An ADS model can be built to investigate the effects of the TRM on the LCC.

3. Modeling with ADS Transient Simulator

The modeling of the WLCC was carried out using ADS AC Simulator and the steady state results were presented. The simulation model can be extended to study the transient performance of the WLCC using the ADS transient simulator. This can help to understand the impact of a fast changing source signal and various waveform modulations.

4. Hardware Prototype

With the understanding of the reflections from the antenna and TRM and the ways to minimize their impacts on the LCC, a hardware prototype can be fabricated for the transmit signal and receive signal isolation in WNDDPA. The hardware prototype of the WLCC can be used for further study of the related field for future field implementation of a WNDDPA.

THIS PAGE INTENTIONALLY LEFT BLANK

LIST OF REFERENCES

[1] Jane's Information Group, Airborne radar systems, http://search.janes.com.libproxy.nps.edu/Search/documentView.do?docId=/content1/janesdata/yb/jav/jav_9788.htm@current&pageSelected=allJanes&keyword=FMCW%20radar&backPath=http://search.janes.com/Search&Prod_Name=JAV&, accessed on 22 Oct 2011.

[2] K. L. Fuller, "To see and not to be seen," Radar and Signal Processing, *IEEE Proceedings F*, vol. 137, pp 1–10, Issue 1, 1990.

[3] M. I. Skolnik, *Introduction to Radar Systems*, 2nd Edition, McGraw-Hill, 1980.

[4] A. Moussa, Y. Khalaf and A. Khalil, "Design of a novel circulator for wireless transceivers," *International Conference on Microelectronics*, pp267–270, December 2007.

[5] S. D. Andrenko, I. A. Vyazmitinov and Y. B. Sidorenko, "An antenna system of a continuous wave radar," *4th International Conference on Antenna Theory and Techniques*, pp 300–303, September 2003.

[6] Qi Jiming, Qu Xinjian and Ren Zhijiu, "Development of A 3cm Band Reflected Power Canceller," in *Proceedings of International Conference on Radar*, pp1098–1102, October 2001.

[7] Jun Zhang and Xu Zhou, "Investigation on adaptive leakage nulling for Pseudo-random code CW radar," *IET International Radar Conference*, pp 1–4, April 2009.

[8] T. Venkatamuni, L. S. Sudhakara Sarma, A. T. Kalghatgi, "Adaptive reflected power canceller for single antenna FMCW radar," *Asia Pacific Microwave Conference*, pp 1841–1844, 2009.

[9] Wei-Han Cheng, "Cancellation circuit for transmit-receive isolation," Naval Postgraduate School Master's Thesis, September 2010.

[10] D. C. Jenn, Ji Heon Ryu and R. Broadston, "Adaptive Phase Synchronization in Distributed Digital Arrays," *Conference on Adaptive Hardware and Systems*, pp 199–204, June 2010.

[11] T. H. Ang, "Conceptual design and software simulation of a wideband leakage cancellation circuit," Naval Postgraduate School Master's Thesis, December 2010.

[12] David M. Pozar, *Microwave Engineering*, 3rd ed, John Wiley & Sons, 2005.

[13] *Pasternack SMA Female Power Divider PE2014; 2–4 GHz Data sheet*, Pasternack Enterprises, Irvine, CA, Rev A.

[14] *Spectrum Microwave 6708 phase shifter Data sheet*, Spectrum Microwave, Hudson, NH.

[15] R. W. Burns, R. L. Holden and R. Tang, "Low cost Design Techniques for Semiconductor Phase Shifters," *IEEE Transactions on Microwave Theory and Techniques*, vol. MTT-22, pp 675–688, No. 6, June 1974.

[16] Soon-Young Eom, "Broadband 180^{o} Bit Phase Shifter Using a λ/2 Coupled Line and Parallel λ Stubs," *IEEE Microwave and Wireless Components Letters*, vol. 14, pp 228–230, No. 5, May 2004.

[17] Xinyi Tang and Koen Mouthaan, "Phase-Shifter Design Using Phase-Slope Alignment With Grounded Shunt λ/4 Stubs," *IEEE Transactions on Microwave Theory and Techniques*, vol. 58, pp 1573–1583, No. 6, June 2010.

[18] Warren L. Stutzman and Gary A, Thiele, *Antenna Theory and Design*, 2nd Edition, John Wiley & Sons, 1998.

[19] Richard C. Johnson and Henry Jasik, *Antenna Engineering Handbook*, 2nd Edition, McGraw Hill, ch. 43, 1984.

INITIAL DISTRIBUTION LIST

1. Defense Technical Information Center
   Ft. Belvoir, Virginia

2. Dudley Knox Library
   Naval Postgraduate School
   Monterey, California

3. Professor R. Clark Robertson
   Chairman, Department of Electrical & Computer Engineering
   Naval Postgraduate School
   Monterey, California

4. Professor David C. Jenn
   Professor, Department of Electrical & Computer Engineering
   Naval Postgraduate School
   Monterey, California

5. Professor Ric Romero
   Assistant Professor, Department of Electrical & Computer Engineering
   Monterey, California

6. Professor Tat Soon Yeo
   Director, Temasek Defence Systems Institude (TDSI)
   Nation University of Singapore
   Singapore

7. Ms Lai Poh Tan
   Senior Manager, Temasek Defence Systems Institude (TDSI)
   National University of Singapore
   Singapore

8. Mr Pek Wee Kok
   Singapore Technologies Dynamics Pte Ltd
   Singapore